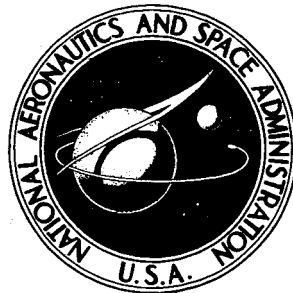


NASA TECHNICAL
REPORT



N73-16817
NASA TR R-401

NASA TR R-401

CASCO
P
FILE

MOBILITY PERFORMANCE
OF THE LUNAR ROVING VEHICLE:
TERRESTRIAL STUDIES - APOLLO 15 RESULTS

*by Nicholas C. Costes, John E. Farmer,
and Edwin B. George*

*George C. Marshall Space Flight Center
Marshall Space Flight Center, Ala. 35812*

1. Report No. NASA TR R-401	2. Government Accession No.	3. Recipient's Catalog No.	
4. Title and Subtitle Mobility Performance of the Lunar Roving Vehicle: Terrestrial Studies – Apollo 15 Results*		5. Report Date December 1972	
		6. Performing Organization Code	
7. Author(s) Nicholas C. Costes, John E. Farmer, and Edwin B. George		8. Performing Organization Report No. M451	
9. Performing Organization Name and Address George C. Marshall Space Flight Center Marshall Space Flight Center, Alabama 35812		10. Work Unit No. 914-40-00-00-00	
		11. Contract or Grant No.	
12. Sponsoring Agency Name and Address National Aeronautics and Space Administration Washington, D.C. 20546		13. Type of Report and Period Covered Technical Report	
		14. Sponsoring Agency Code	
15. Supplementary Notes Prepared by Space Sciences Laboratory and Astrionics Laboratory, Science and Engineering. *Presented to the 4th International Conference of the International Society for Terrain-Vehicle Systems, Stockholm and Kiruna, Sweden, April 24-28, 1972.			
16. Abstract <p>The constraints of the Apollo 15 mission dictated that the average and limiting performance capabilities of the first manned Lunar Roving Vehicle, when operated on the lunar surface, be known or estimated within narrow margins. For this reason, extensive studies were conducted during the year preceding the Apollo 15 launch and are described herein. The results of these studies are compared with the actual performance of the Lunar Roving Vehicle during the Apollo 15 mission. From this comparison, conclusions are drawn relating to the capabilities and limitations of current terrestrial methodology in predicting the mobility performance of lunar roving vehicles under in-situ environmental conditions, and recommendations are offered concerning the performance of surface vehicles on future missions related to lunar or planetary exploration.</p> <p style="text-align: center;">EDITOR'S NOTE</p> <p>Use of trade names or names of manufacturers in this report does not constitute an official endorsement of such products or manufacturers, either expressed or implied, by the National Aeronautics and Space Administration or any other agency of the United States Government.</p>			
17. Key Words (Suggested by Author(s)) Lunar Surface, Astronaut, Lunar Rover, Off-road Mobility, Soil Mechanics, Topography, Traverse, Wire-mesh Wheel, Wheel/Soil Interaction, Lunar Soil Simulant, Wheel Slip, Torque, Pull, Power Number, Slope, Bekker Soil Values, Rover Computer Model, Power Profile, Sinkage		18. Distribution Statement	
19. Security Classif. (of this report) Unclassified	20. Security Classif. (of this page) Unclassified	21. No. of Pages 86	22. Price* \$3.00

* For sale by the National Technical Information Service, Springfield, Virginia 22151

NOTICE

The International System of Units of measurement has been used throughout this document; however, in cases for which conversion of existing theoretical treatments based on the English system of units was not feasible, the initial units have been retained.

TABLE OF CONTENTS

	Page
INTRODUCTION	1
LRV DESCRIPTION	2
LUNAR SURFACE TRAFFICABILITY AND WHEEL-SOIL INTERACTION STUDIES BEFORE THE APOLLO 15 MISSION	9
General Considerations	9
Lunar Surface Engineering Properties/Trafficability Panel	9
Lunar Soil Mechanics Investigations	10
Lunar Surface Topographic Studies	11
Soft-Soil Steady-State Mobility Performance Design Guidelines	15
Wheel-Soil Interaction and Related Soil Mechanics Studies Under Terrestrial Gravity and Ambient Pressure Conditions	15
Wheel-Soil Interaction Tests Under 1/6-g Gravity and Low- Atmospheric Pressure Conditions	28
Soil Mechanics Tests on Lunar Soil Simulants Under Varying Gravity Conditions and Related Analyses	30
MSFC COMPUTER MODEL RELATING TO LRV MOBILITY PERFORMANCE AND POWER PROFILE ANALYSIS	30
EVALUATION OF LRV MOBILITY PERFORMANCE DURING APOLLO 15	37
Lunar Surface Topography at the Hadley-Apennine Region	37
Lunar Soil Mechanical Properties	37
LRV Mobility Performance at Hadley-Apennine	47
LRV Power Profile Analysis	55
CONCLUSIONS	68
APPENDIX – BEKKER/LLD ANALYTICAL SOIL-VEHICLE MODEL	71
REFERENCES	73

LIST OF ILLUSTRATIONS

Figure	Title	Page
1.	Lunar Roving Vehicle	3
2.	LRV subsystem components and control-and-performance-display console	4
3.	LRV wheel and fender	5
4.	Folded LRV immediately before stowage on LM descent stage of Apollo 15 spacecraft	7
5.	Comparison of gradation curves from Apollo lunar samples and terrestrial soils used as lunar soil simulants in wheel-soil interaction tests	17
6.	Apparatus for LRV wheel-soil interaction tests performed at the WES, Vicksburg, Mississippi	19
7.	LRV wheel-soil interaction tests performed at the WES on different GM wheel and tread cover designs	20
8.	Typical WES wheel-soil interaction test results [41, 42]. Experimental and theoretical relations of pull and torque coefficients versus wheel slip	21
9.	Typical WES wheel-soil interaction test results [41, 42] on LSS ₁ through LSS ₄ . Experimental and theoretical relations of power number versus pull coefficient	23
10.	Typical WES wheel-soil interaction test results [41, 42] on LSS ₁ through LSS ₄ . Experimental and theoretical relations of wheel sinkage versus wheel slip	25
11.	Typical WES wheel-soil interaction test results [43] on LSS ₁ through LSS ₅ . Effect of soil consistency and strength on mobility performance parameters	26
12.	Simplified flow diagram of MSFC-developed LRV mobility performance and power profile analysis computer program	32
13.	Performance characteristics of LRV traction-drive system components	33
14.	Effect of lunar surface roughness characteristics on energy losses in LRV dampers	35

LIST OF ILLUSTRATIONS (Concluded)

Figure	Title	Page
15.	Map of Apollo 15 landing site at Hadley-Apennine region with LRV traverses during EVAs I, II, and III	38
16.	Comparison of pre-mission estimates and post-mission assessments of slope-distributions encountered along LRV traverses during Apollo 15 mission	39
17.	Increasing levels of lunar surface roughness at Hadley-Apennine region	41
18.	Trenching operations at Station 8, end of EVA II	43
19.	Analysis of data obtained by Self-Recording Penetrometer [5]	45
20.	Apollo 15 core tubes and soil bulk density data [5]	46
21.	Variability in lunar surface hardness	48
22.	LRV wheel-soil interaction at various locations of the Hadley-Apennine region	49
23.	LRV parked along slope gradient at Station 6, Apennine Front, during EVA II	56
24.	MSFC computer model estimates on LRV maximum speeds and wheel slip at Hadley-Apennine	58
25.	MSFC computer power profile analysis results	59
26.	Power number versus pull coefficient for different LLL soil values	67

LIST OF TABLES

Table	Title	Page
1.	Estimates of Lunar Soil Density and Shear Strength Characteristics	12
2.	Physical and Mechanical Properties of Lunar Soil Simulants	18
3.	Variation in Lunar Soil Properties at Apollo 14 Site as Determined from MET Tracks	31
4.	Cone Penetration Resistance Test Results from Apollo 15 and Luna 17 Landing Sites	44
5.	Post-Mission Evaluation of LRV Performance at the Apollo 15 Site	61
6.	Comparison of Computer Program Results on LRV Energy Consumption Using Experimental Data from WES Wheel-Soil Interaction Tests and Corresponding LLL Soil Values	65
7.	Comparison of Measured and Computed LRV Energy Consumption During Apollo 15 Mission Using Spectrum of LLL Soil Values	66

ACKNOWLEDGMENTS

The success of the Lunar Roving Vehicle (LRV) program has been the result of close teamwork among a multitude of individuals and organizations. Therefore, although it would be futile to mention each person separately, the authors would like to take this opportunity to express their deep appreciation to all those in Government or non-Government service who have been members of the LRV Team.

Special thanks go to Astronauts Col. D.R. Scott and Col. J.B. Irwin for making the Rover "go" on the lunar surface and for their penetrating observations and excellent descriptions regarding the Rover's performance.

The unquestionable expertise and guiding spirit of Dr. M.G. Bekker that led to the successful development of a "moon buggy" are hereby acknowledged.

The authors take special pleasure in expressing their deep appreciation to all of the U.S. Army Engineer Waterways Experiment Station (WES) personnel who, under the general direction of Dr. D.R. Freitag,* Mr. A.J. Green, and Dr. K.-J. Melzer, participated in the LRV wheel-soil interaction tests and in real-time evaluation of the Rover's performance on the lunar surface. The multifold contributions of Mr. C.J. Nuttall, Jr., of WNRE, Inc., to the wheel-soil interaction test program and the helpful advice of Dr. I.R. Ehrlich of Stevens Institute of Technology and members of the Land Locomotion Laboratory (LLL), U.S. Army Tank Automotive Command, are greatly appreciated. The untiring efforts of Mr. T.H. Fox of the Astrionics Laboratory, NASA-Marshall Space Flight Center (MSFC), in implementing the computer program relating to the LRV mobility performance and power profile analysis mathematical model and in making significant contributions to the analyses reported in this paper are gratefully acknowledged. Many thanks go also to Mr. H. Reid, Jr., of the MSFC Astrionics Laboratory for providing the laboratory test data on the functional characteristics of the LRV traction-drive system components and to Mr. Q. Peasley of the MSFC Space Sciences Laboratory for developing the computer program relating to the analytical expressions on wheel-soil interaction, referred to in the appendix as "the Bekker/LLD soil-vehicle model."

The senior author wishes to express his appreciation to all of his colleagues from the LLL; Jet Propulsion Laboratory; NASA-Manned Spacecraft Center (MSC); University of California, Berkeley; U.S. Geological Survey; and WES, who formed the Lunar Surface Engineering Properties/Trafficability Panel during the LRV development days and, in particular, to Mr. O.H. Vaughan of the Aero-Astroynamics Laboratory, MSFC, who served as co-chairman of that panel, co-authored the section on the lunar surface trafficability model included in the MSFC Lunar Surface Environmental Design Criteria Document and, in addition, has made significant contributions to studies relating to lunar surface topography and LRV traverse analysis. Also, the assistance offered by the Simulation Branch, Mechanical and Crew Systems Integration Division, Astronautics Laboratory, MSFC; the Zero-g Test Office, Wright-Patterson Air Force Base; and the Astronaut Office and Flight Crew Support Division, MSC, in carrying out the soil mechanics tests under 1/6-g simulated gravity environment is greatly appreciated.

*Presently, Technical Director, U.S. Army Cold Regions Research and Engineering Laboratory, Hanover, New Hampshire.

ACKNOWLEDGMENTS (Concluded)

The senior author also wishes to express his appreciation to his fellow team members of the Apollo 11 Soil Mechanics Investigation, Apollo Lunar Geology Experiment, S-059, and Apollo Soil Mechanics Experiment, S-200, teams.

Finally, many thanks are due Messrs T.E. Stephens, K.M. Hinkle, and J.D. Traywick of the Marshall Center's Space Sciences Laboratory for their enthusiasm and competent handling of many LRV-related laboratory studies.

MOBILITY PERFORMANCE OF THE LUNAR ROVING VEHICLE: TERRESTRIAL STUDIES – APOLLO 15 RESULTS

INTRODUCTION

The Lunar Roving Vehicle (LRV) was developed by the National Aeronautics and Space Administration (NASA) under the technical direction of the George C. Marshall Space Flight Center (MSFC), Huntsville, Alabama. The LRV or Rover was the first manned surface vehicle to be used in lunar exploration. It was designed to transport two astronauts with their life support equipment; scientific apparatus and geological tools; lunar soil and rock samples; and television, movie, and still cameras, along geological traverses covering regions that have embraced a much greater surface area than that explored and sampled during previous manned and unmanned lunar surface missions.

Before Apollo 15, the United States had accomplished three successful manned lunar landings with a total traverse distance of approximately 7 km. The Apollo 15 landing alone resulted in scientific traverses with an overall length of 27.9 km or a distance ratio of approximately 4:1 over all three previous manned lunar missions. According to observations by members of the scientific community, this ratio approximates the ratio of the scientific returns from the Apollo 15 mission to those from the other missions. This gain in scientific returns can be mainly attributed to the augmented transportation capability furnished by the small lunar automobile, which weighs approximately 2130 N (480 lb) on earth and was designed to carry a payload of approximately 4800 N (1080 earth-pounds) on the lunar surface for maximum distances of approximately 120 km at maximum speeds of approximately 14 km/hr.

The challenge associated with the design analysis and fabrication of the LRV was

formidable. The specifications called for an electrically propelled car with a minimum weight, carrying a payload approximately twice its own weight. The vehicle should be transported to the moon in a folded configuration and should be deployed and unfolded on the lunar surface with minimum astronaut effort. The vehicle should operate in temperature extremes varying between -173 to 117°C (-279 to 243°F) over a surface of varying roughness and soft-soil consistency, having a wide range of crater and block distributions, and slopes with maximum slope angles along several vehicle lengths of approximately 25 deg. The vehicle should be designed for maximum astronaut safety and should be operative the first time it contacts the lunar surface because repairs or adjustments would be impossible during the mission. These constraints and the fact that the time available for the design, fabrication, and flight qualification of the first unit was 17 months augmented the challenge imposed on the managers, engineers, and other personnel involved at all levels in this program.

This report is divided into four major sections. The first section contains a general description of the vehicle and functional characteristics of its main component systems. In the second section, the rationale for the mobility performance design criteria set forth during the development of the vehicle is outlined and various activities are described which were sponsored or carried out by NASA before the Apollo 15 mission for the purpose of assessing the nominal and limiting mobility performance characteristics and energy consumption rate of the vehicle on the lunar surface. The third section describes the MSFC-developed LRV mobility performance and power profile analysis computer program and sources of input data. A post-mission analysis of the mobility performance of the LRV at the Hadley-Apennine region (Apollo

15 landing site) is presented in the fourth section and is based on the available quantitative and qualitative information obtained from the Apollo 15 mission and terrestrial wheel-soil interaction analytical and experimental studies.

From these analyses, comparisons are made and conclusions are drawn relative to the adequacy, advantages, and limitations of current terrestrial approaches for predicting and analyzing the mobility performance of surface vehicles in extraterrestrial environments.

LRV DESCRIPTION

The LRV was built by The Boeing Company, Aerospace Group, at its Kent Space Center near Seattle, Washington. Boeing's major subcontractor was the General Motors (GM) Delco Electronics Division Laboratories, Santa Barbara, California. Simplicity of design and operation and light weight have been the overriding features in the development and construction of the Rover. The lunar vehicle (Figs. 1 and 2) is 3.1 m (122 in.) long, slightly more than 1.83 m (72 in.) wide, 1.14 m (45 in.) high, and has a 2.29-m (90-in.) wheelbase. It weighs about 2130 N (480 lb), including tiedown and unloading systems. The Rover can carry a total weight of about 4800 N (1080 lb) including the weight of two astronauts and their Portable Life Support Systems (PLSS), which is approximately 3560 N (800 lb), plus about 1240 N (280 lb) of scientific experiments, astronaut tools, and lunar soil and rock samples.

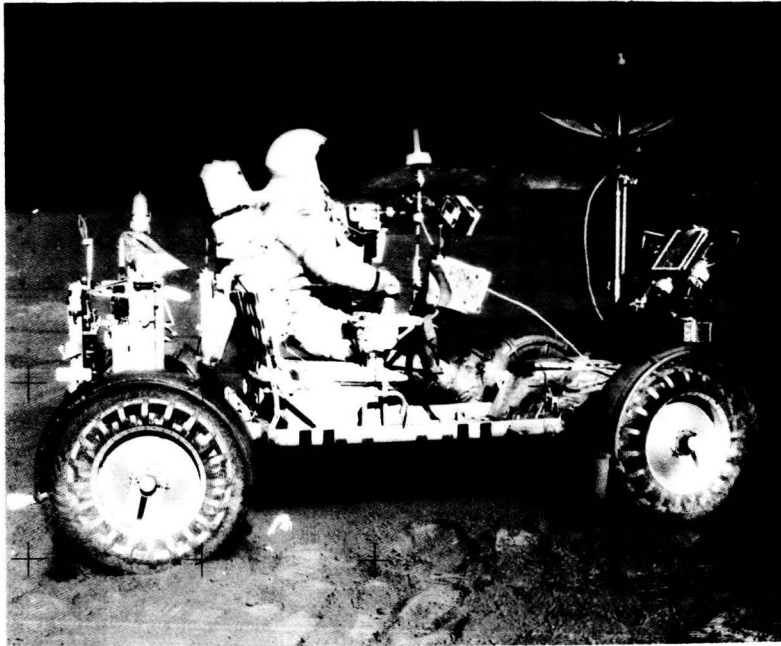
Each wheel is individually powered by an electrical motor, and the vehicle's top speed is of the order of 9 to 13 km/hr, depending upon the mean slope, roughness characteristics, obstacle distribution, and soil conditions of the lunar surface. The Rover's power comes from two nonrechargeable silver-zinc batteries. The

vehicle has two complete battery systems, each of which can provide power for operation. Instruments are used to measure the amount of discharge of electrical energy from the storage batteries. These instruments, called ampere-hour integrators, accumulate the total amount of current drawn from the batteries and relay the information to a display console (Fig. 2b) located between the seats of the LRV.

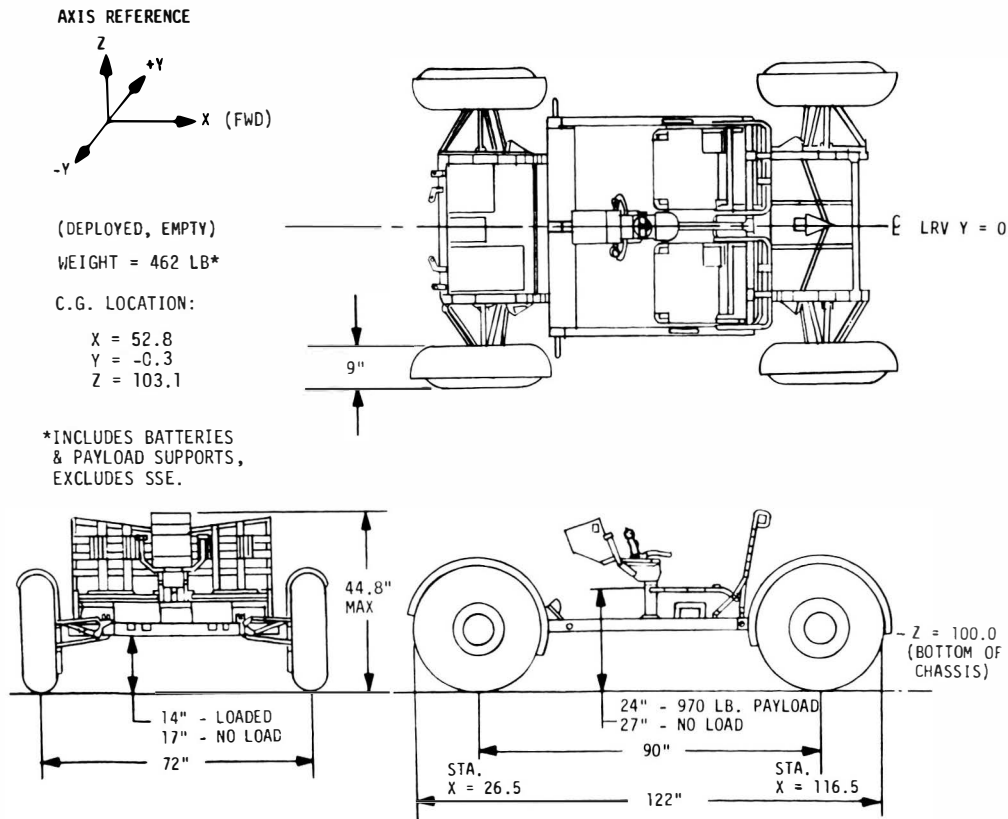
The Rover is normally steered by both front and rear wheels in a double Ackerman arrangement. Ackerman steering denotes that the inner wheel describes a smaller radius circle than the outer wheel. If one steering mechanism fails, it can be disconnected and the vehicle may complete the mission by use of the remaining system. The moon car can be operated manually by either of the astronauts using a T-shaped hand-grip control to steer the vehicle at variable speeds, forward and reverse. Maximum travel of the steering linkage results in an outer wheel angle of 22 deg and an inner wheel angle of 53 deg. Steering rate is 5.5 sec lock to lock. With both sets of wheels steerable, the vehicle has excellent responsiveness.

The wheels (Fig. 3) are woven of zinc-coated piano wire with a spun aluminum hub and a titanium bump stop. The titanium bump stop provides a stiff load path to accommodate high-impact loads. Chevron-shaped treads of titanium are riveted to the wire mesh around each wheel's outer circumference. These treads cover approximately 50 percent of the soil contacting surface. Selection of the 50-percent coverage was based on wheel-soil interaction tests performed on crushed-basalt lunar soil simulants specified by NASA. This coverage provides sufficient flotation without degrading traction. Each wheel weighs 53.3 N (12 earth-pounds).

Each Rover wheel is provided with a separate traction drive system consisting of a

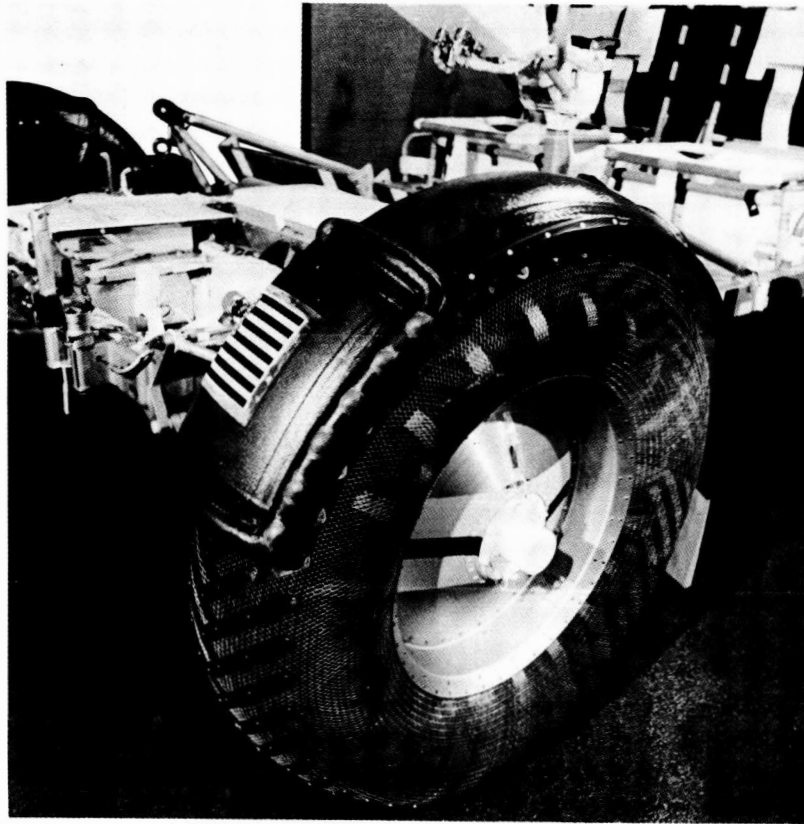


a. LRV ON LUNAR SURFACE DURING EVA I

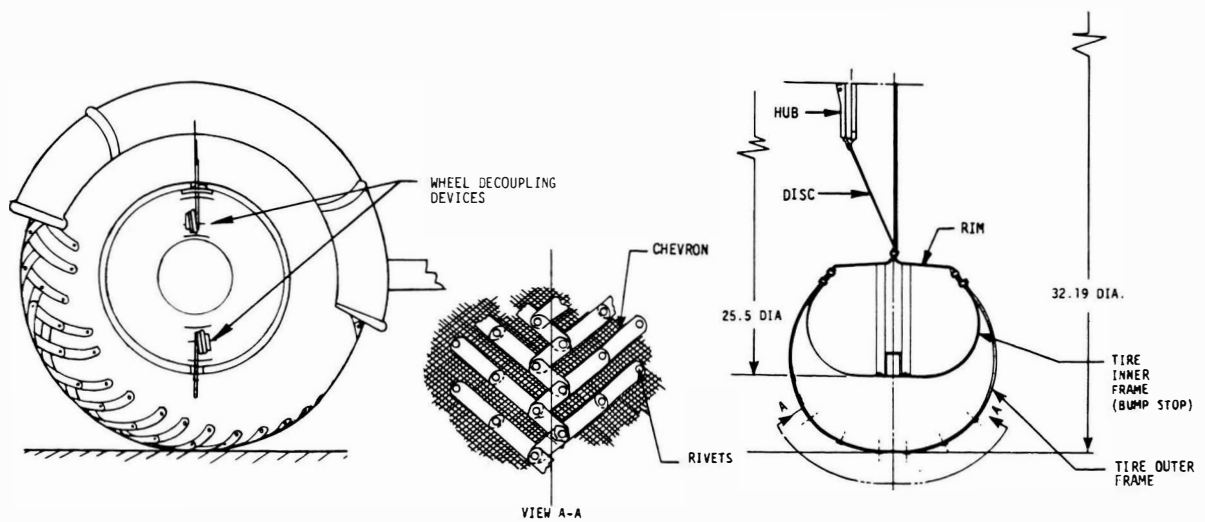


b. MOBILITY SUBSYSTEM DIMENSIONS

Figure 1. Lunar Roving Vehicle.



a. ASSEMBLED COMPONENTS. NOTE STRIPE AT THE HUB FOR LUNAR GRAND PRIX TASK.



b. WHEEL COMPONENTS (DIMENSIONS IN INCHES)

Figure 3. LRV wheel and fender.

harmonic-drive gear reduction unit, drive motor and brake assembly, and an odometer pickup which transmits to the navigation subsystem nine pulses per wheel revolution. Input torque is provided by the electrically driven motors and is transmitted to the wheels through the harmonic-drive gear reduction units. The harmonic drive reduces the motor speed by a ratio of 80:1 and allows continuous application of power to the wheels without requiring gear shifting.

Each traction drive is equipped with a mechanical brake actuated by a cable connected to a linkage in the hand controller. Braking is accomplished by moving the hand controller rearward and is aided by the 80:1 gear ratio of the harmonic drive. This operation deenergizes the drive motor and forces brake shoes against a brake drum that stops the rotation of the wheel hub. Equal braking force for the left and right wheels is effected by routing the cables through an equalizer device. Separate cables actuate the forward and rear brakes. Each wheel can be decoupled from its traction-drive system and allowed to "free wheel" about a bearing independent of the drive train. This is a reversible process and decoupling disengages the brake on the affected wheel.

The drive motors are direct-current series, brush-type motors which operate from a nominal input voltage of 36 V. Speed control for the motors is furnished by pulse-width modulation from the drive controller electronic package. Each motor is thermally monitored by an analog temperature measurement from a thermistor at the stator field which is displayed on the console. In addition, each motor contains a thermal switch which closes on increasing temperatures at 204°C (400°F) and provides a signal to the caution and warning system to actuate a warning flag.

The basic chassis is fabricated from 2219 aluminum alloy tubing and welded at the structural joints. The tubular members are

milled to minimum thickness consistent with the bending moment and shear diagrams. The chassis is suspended from each wheel by a pair of parallel triangular suspension arms connected between the Rover chassis and each traction drive. Loads are transmitted from the suspension arms to the chassis through torsion bars. In its stowed configuration, the suspension system of the Rover is rotated approximately 135 deg to allow the vehicle to be folded into a compact package (Fig. 4), which is carried in quadrant No. 1 of the cargo section (descent stage) of the Lunar Module (LM). Vertical oscillations of the chassis are attenuated by a velocity-square damper connected between the chassis and each upper suspension arm. The deflection of the suspension system and wheels combine to allow 35.6 cm (14 in.) of chassis ground clearance when the Rover is fully loaded and 43.2 cm (17 in.) when unloaded. The Rover is designed to negotiate step-like obstacles 30 cm (11.8 in.) high and can cross crevasses 70 cm (27.6 in.) wide. Slopes of the order of 20 to 23 deg can be negotiated in favorable circumstances, and the minimum turn radius is 3.05 m (10 ft).

The crew station equipment includes the seats, footrests, inboard handholds, armrests, floor panels, seat belts, fenders, and toeholds (Fig. 2).

The two seats are tubular aluminum frames spanned by nylon. They are folded flat onto the center chassis and unfolded by the astronauts after the vehicle is deployed on the lunar surface. The seat back and seat bottom are designed to support the astronauts' PLSS.

The footrests are also folded against the center chassis floor until the LRV is deployed. They are held in the stowed position by Velcro straps and lifted into position by the astronauts. Side restraints are also provided.

A pair of inboard handholds, located between the seats, constructed of 2.54-cm

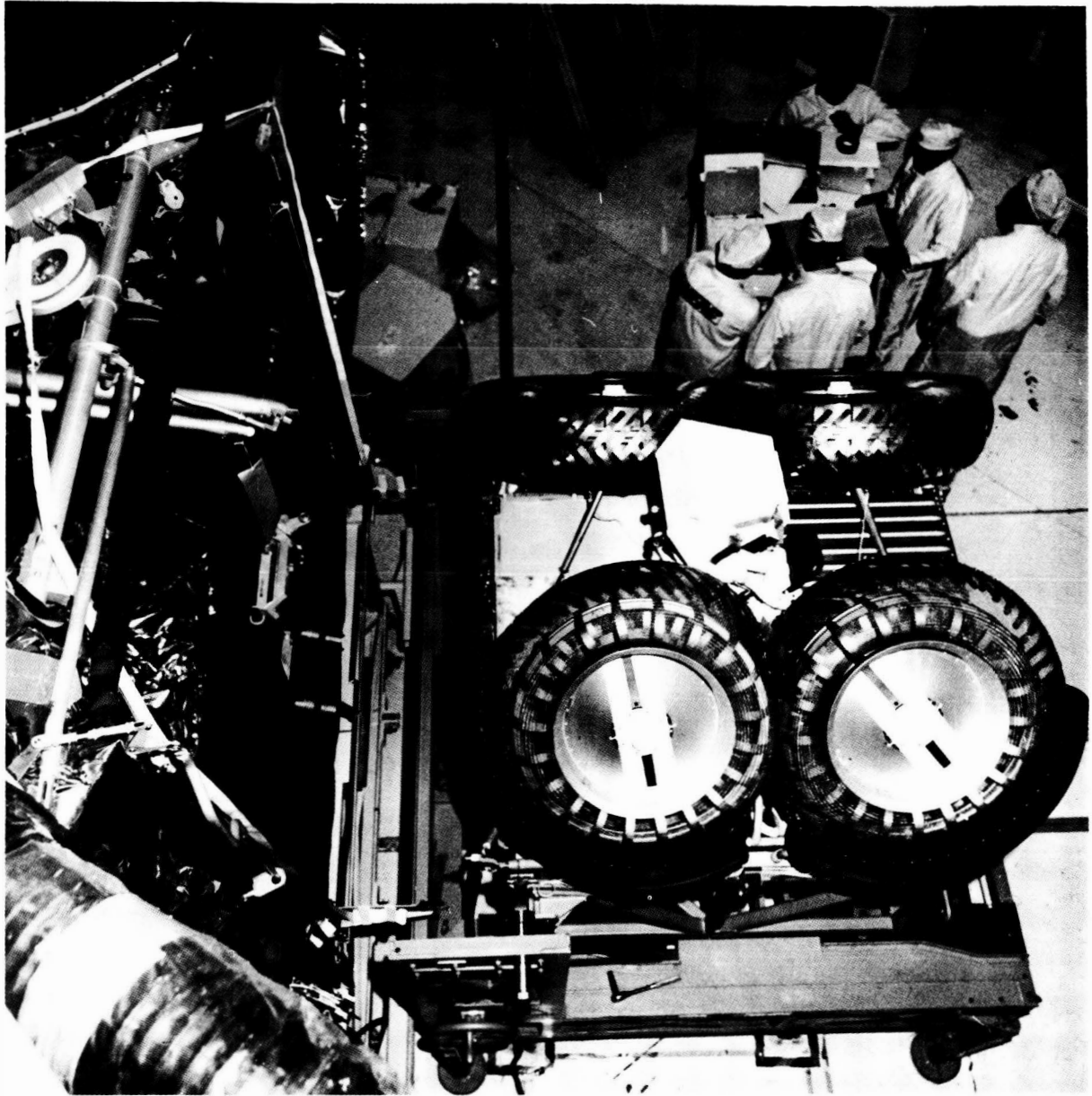


Figure 4. Folded LRV immediately before stowage on LM descent stage of Apollo 15 spacecraft.

(1-in.) aluminum tubing are used to aid the astronauts as they board the vehicle. The handholds contain receptacles for a 16-mm camera and a low-gain antenna for the Lunar Communications Relay Unit (LCRU).

The outboard handholds and center armrest provide stability and comfort for the astronauts when they are seated. The armrest, made of fiberglass, supports the astronaut's arm while he is manipulating the hand controller.

The floor panels in the crew station are made of beaded aluminum panels, which can support the full lunar weight of the astronauts when standing. The seat belts are made of nylon webbing and are designed for simple attachment and release.

Both astronauts are seated so that both front wheels are visible during normal driving. Molded fiberglass fenders protect the vehicle and astronauts from lunar dust particles which may be ejected up and forward by the wheel-soil interaction. Because of space limitations, a section of each fender is retracted while the LRV is stowed in the LM. After the vehicle is lowered to the lunar surface, the astronauts deploy the fender systems.

The driver navigates by a simple dead-reckoning navigation system that determines the direction and distance between the Rover and LM and the total distance traveled at any point during a traverse. When the lunar vehicle is out of communication with the LM, direct communication with the earth is made through the LCRU, which transmits the astronauts' voices, biomedical data, and color television. The LCRU was developed and furnished by the NASA-Manned Spacecraft Center (MSC), Houston, Texas. There is no telemetered data on performance or operation of the Rover other than pilot-monitored and reported data.

The LRV makes use of passive and semipassive thermal control measures to insure that it will not exceed operating temperature limits. Vehicle temperature constraint at liftoff is $21 \pm 3^{\circ}\text{C}$ ($70 \pm 5^{\circ}\text{F}$). Insulation and reflective coating maintain the temperature of the vehicle within tolerable limits by controlling heat loss during boost, earth orbit, translunar flight, and lunar landing. Batteries are maintained between 4 and 52°C (40 and 125°F), while thermal tolerances for other equipment vary from -34 up to 85°C (-30 to 185°F). These temperatures must be maintained through touchdown.

After touchdown, the vehicle has a semipassive thermal control system for the purpose of dissipating heat from operating equipment in the forward chassis area, maintaining the control and display console within its operating limitations, and protecting the crew station from excessive heat. This control system utilizes insulation, radiative surfaces, thermal mirrors, thermal straps, fusible-mass heat sinks, and special surface finishes.

The operating equipment in the forward chassis area includes the drive control electronics (DCE), signal processing unit (SPU), directional gyro unit (DGU), and two batteries. Passive protection is provided by a multilayered aluminized Mylar and nylon netting insulation blanket with a beta cloth (polished glass) outer layer. Aluminum thermal straps connected to the SPU and DGU transfer heat away from the electronic components and store it in the batteries and fusible-mass heat sinks. Thermal control of the DCE is accomplished with a fusible-mass heat-sink tank and a thermal radiator attached to its upper surface. At the end of the lunar sortie, the heat which has been accumulated in the batteries and heat sinks is allowed to escape through radiation. The astronauts open fiberglass dust covers to expose fused silica thermal mirrors mounted on top of the batteries, DCE, SPU, and heat sinks. The mirrors act as space radiators, thus cooling the equipment. When the batteries reach a lower operating temperature limit of approximately 7.2°C (45°F), the covers close automatically, preventing additional cooling from taking place and protecting the batteries from dust collection during a sortie.

All instruments on the vehicle's control and display console (Fig. 2b) are mounted on an aluminum plate, which is isolated from the rest of the vehicle by fiberglass mounts. The external surfaces of the console are coated with heat-resistant paint (Dow-Corning 92-007), and

the faceplate is black anodized to control the temperature and to reduce reflection.

The tubular sections of the seats, footrests, handholds, and center and aft floor panels are also anodized with an aluminum oxide, which provides a heat-reflecting and radiating surface.

Heat generated by the traction-drive assembly and damper at each wheel is radiated to space through the casting. Nitrogen at 5.2 N/cm² (7.5 psi) is hermetically sealed inside each drive assembly and aids the transmission of heat from the traction-drive motors to the outer wall.

LUNAR SURFACE TRAFFICABILITY AND WHEEL-SOIL INTERACTION STUDIES BEFORE THE APOLLO 15 MISSION

General Considerations

Because of the complex and time-consuming scientific tasks to be performed by the astronauts at each station of the planned geological traverses, the success of the Apollo 15 mission was strongly predicated upon the fulfillment of the following requirements:

1. Ability of the LRV to transfer astronauts and equipment from and to any two points A and B along the geological traverses.
2. Minimization of travel time in traversing any section A-B without hindering the stability or controllability of the vehicle, or jeopardizing in any way the safety of the astronauts.
3. Sufficient energy reserve in the LRV batteries to provide the power required for the traction-drive system, steering, navigation system, operation of the control and performance display console, starting and accelerating periods, etc.

In turn, the fulfillment of those requirements strongly depended upon the following factors: an accurate knowledge of the topography of the site (on a scale compatible with the vehicle length) and the lunar soil conditions, and the ability to predict the interaction of the vehicle with the lunar surface under the reduced 1/6-g lunar gravity environment and vacuum conditions, once the topography (i.e., the mean slope, the roughness characteristics, and the crater/block distribution along each traverse segment), as well as the lunar surface soil conditions, could be determined.

All these factors were formidable challenges to the group of engineers and other specialists, who were given the responsibility of formulating LRV design criteria and performing mobility performance analyses before the Apollo 15 mission, for the following reasons:

1. The resolution of available photographic coverage of the landing site was 20 m.
2. The site itself had never been sampled before to assess the range of lunar soil mechanical properties to be encountered along the LRV traverses.
3. The constraints imposed by the lunar environmental conditions on the mechanical behavior of the soil, as well as on the riding characteristics, maneuverability, and energy consumption of the vehicle were unknown.

These challenges were met by the following activities under the auspices of NASA.

Lunar Surface Engineering Properties/Trafficability Panel

About 1½ years before the initiation of the LRV development program, a Lunar Surface Engineering Properties/Trafficability

Panel was set up with the following explicit objectives:

1. Surveying the then state of knowledge on lunar surface mechanical properties.
2. Identifying technology gaps that would impact the potential development of an LRV (dual-mode or manned-only).
3. Recommending supporting technology studies or lunar surface experiments that would enhance the development of an LRV.
4. Formulating mobility design criteria to be incorporated in a potential contract initiation document by NASA for the development of an LRV.
5. Monitoring facets of an LRV development program relating to wheel/soil interaction, wheel design configuration, mobility performance, and power profile analysis.

This panel was chaired by the senior author and consisted of representatives from various Government organizations and universities across the United States with expertise in soil mechanics, engineering geology, and surface mobility systems.

Lunar Soil Mechanics Investigations

Soil mechanics experiments were included in the five U.S. Surveyor Spacecraft unmanned missions and in all the Apollo manned missions, up to and including Apollo 15 [1-6]. In support of the Apollo soil mechanics investigations, extensive lunar soil

simulation studies were conducted at the Geotechnical Research Laboratory of the MSFC Space Sciences Laboratory¹ [7] and at the University of California under contract to MSFC [8-10]. Parallel with these investigations, extensive analyses were performed of photographic data obtained by the five U.S. Lunar Orbiter Spacecraft missions [8, 10, 11-14] and in-place soil mechanics data obtained by the Soviet unmanned spacecraft Luna 9, Luna 13 [15], Luna 16 [16], Luna 17, and the unmanned Soviet roving vehicle Lunokhod-1 [6, 17].

As a result of these investigations, it was established that to depths of the order of 15 to 20 cm, within which the lunar soil conditions might affect the performance of the LRV, the lunar soil is characterized in general by a well-graded, slightly cohesive, granular material, with grains in the silt-to-fine-sand-size range that exhibit adhesive characteristics when in contact with other material surfaces (metallic or nonmetallic). The soil grains vary in shape from blocky angular with smooth plane surfaces to completely spherical; some of the particles are vesicular or pitted. However, no shards, needles, plates, or filaments have been observed.

The mechanical properties of lunar soils are remarkably similar to those of terrestrial granular soils of comparable gradation, although the chemical composition of the two soil types may be dissimilar. The mechanical behavior of lunar soils appears to be dominated by the particle size distribution, particle shape, and packing characteristics (density, void ratio). For a given lunar soil, the void ratio or porosity appears to be the most important single variable controlling the cohesion and the angle of internal friction of the material.

1. N.C. Costes, C.G. Hadjidakis, D.M. Holloway, J.P. Olson, and R.E. Smith, Lunar Soil Simulation Studies in Support of the Apollo 11 Mission, Internal Memo, Geotechnical Research Laboratory, Marshall Space Flight Center, Huntsville, Ala., 1969.

Lunar Surface Topographic Studies

A variety of data sources indicates that the density and strength characteristics of lunar soils may vary (1) regionally, (2) locally (within the area limits of an Apollo mission landing site), and (3) with depth. Table 1 [1-4, 6, 7, 15-33] gives an indication of the variability of lunar soil mechanical properties at the four Apollo landing sites visited to date and along the Lunokhod-1 traverses at the Mare Imbrium Luna 17 landing site.

The in-place density may be as low as 1.0 g/cm^3 at the surface in some areas. However, in other areas it may be as high as 2.0 g/cm^3 at shallow depths of a few centimeters. At depths of 10 to 20 cm, the lunar soil densities are probably greater than 1.5 g/cm^3 . The most probable values of cohesion appear to be in the range of 0.1 to 1.0 kN/m^2 (1.5×10^{-2} to $1.5 \times 10^{-1} \text{ lb/in.}^2$). The angle of internal friction appears to range between 30 and 50 deg, with the higher values associated with the lower porosities.

Data from Lunokhod-1 indicate that the strength parameters, hence, density, increase with depth. Other data indicate that the soil on the slopes is, in general, less dense and weaker than the soil covering level areas. However, in several specific cases, the reverse may be true, depending on the local geologic history and other processes that have taken place at a given locale.

Under the sponsorship of NASA, extensive studies were conducted by the U.S. Geological Survey (USGS) to ascertain the mean slope and roughness characteristics of the lunar surface at various candidate Apollo landing sites from orbital photographs with a maximum resolution of 3 to 5 m^2 ,^{3,4} [34-35]. The resolution of photographs of the Apollo 15 site was only 20 m.

From these studies, the lunar surface topography was subdivided from a trafficability point of view into four main categories – Smooth Mare, Rough Mare, Hummocky Uplands, and Rough Uplands. Each major classification is characterized by (1) a mean slope, (2) obstacle distribution, and (3) three ranges of power spectral densities related to surface roughness characteristics on a scale compatible with the vehicle wheel dimensions and ground clearance.

The information derived from these studies contributed to the design of the LRV suspension system to ensure optimum vehicle riding characteristics, stability, and maneuverability, as well as to determine the dynamic energy losses dissipated in the LRV dampers. The same information was used to assess “wander factor” associated with obstacle avoidance or vehicle velocities and

-
2. H.J. Moore, R.J. Pike, and G.E. Ulrich, Lunar Terrain and Traverse Data for LRV Design Study, U.S. Geological Survey Working Paper, Flagstaff, Ariz., 1969.
 3. R.J. Pike, Revised PSD Function Describing Major Lunar Terrain Types, U.S. Geological Survey Working Paper, 1970.
 4. R.J. Pike, Lunar Landscape Morphometry, Parts I, II, and III, U.S. Geological Survey Professional Paper (to be published).

TABLE 1. ESTIMATES OF LUNAR SOIL DENSITY AND SHEAR STRENGTH CHARACTERISTICS

a. Estimates of Lunar Soil Density

Bulk Density, ρ (g/cm ³)	Mission	Investigator
0.4		Halajian (1964) [18]
0.3		Jaffe (1964, 1965) [19, 20]
1.5	Surveyor I	Christensen et al. (1967) [21]
1.1	Surveyor V	Christensen et al. (1968) [22]
0.8	Luna XIII	Cherkasov et al. (1968) [15]
1.5	Surveyor III & VII	Scott and Roberson (1968) [1] and Scott (1968) [23]
1.54 to 1.66	Apollo 11	Costes et al. (1969) [24]
1.54 to 1.75	Apollo 11	Costes and Mitchell (1970) [25]
0.74 to >1.75	Apollo 11	Scott et al. (1971) [3]
1.81 to 1.92*	Apollo 11	Costes et al. (1971) [7]
1.6 to 2.0	Apollo 12	Scott et al. (1971) [3]
1.80 to 1.84*	Apollo 12	Costes et al. (1971) [7]
1.55 to 1.90*	Apollo 12	Houston and Mitchell (1971) [26]
1.7 to 1.9	Apollo 12	Carrier et al. (1971) [27]
1.2	Luna XVI	Vinogradov (1971) [16]
1.5 to 1.7	Lunokhod-1	Leonovich et al. (1971) [17]
1.45 to 1.6	Apollo 14	Carrier et al. (1972) [28]
1.35 to 2.15	Apollo 15	Mitchell et al. (1972) [6]

* Upper bound estimates.

TABLE 1. (Continued)

b. Estimates of Lunar Soil Cohesion and Friction Angle
Based on Pre-Apollo Data

Cohesion (kN/m ²)	Friction Angle (deg)	Basis	Investigator
0.35	33	(1) Boulder Track Analysis Orbiter Data	Nordmeyer (1967) (see Ref. 6)
0.15-15	55	(2) Surveyor I Strain Gage and TV Data	Jaffe (1967) [29]
0.13-0.4	30-40	(3) Surveyor I	Christensen et al. (1967) [21]
	>35	(4) Surveyor III, Soil Mechanics Surface Samples	Scott and Roberson (1968) [1]
Soil Slightly Weaker Than That at Surveyor I and Surveyor III Sites		(5) Surveyor V Landing Data	Christensen et al. (1968) [22]
0 10	For 45-60 0	(6) Surveyor III, Landing Data	Christensen et al. (1968) [30]
>0.07	For 35	(7) Surveyor VI, Vernier Engine Firing	Christensen et al. (1968) [31]
0.5-1.7		(8) Surveyor VI, Altitude Control Jets	
0.35-0.70	35-37	(9) Surveyor III and VII, Soil Mechanics Surface Samples	Scott and Roberson (1968) [1]
0.1	10-30	(10) Lunar Orbiter Boulder Track Records	Moore (1970) [32]
1.0	19-53	(11) Lunar Orbiter Boulder Track Records	Hovland and Mitchell (1971) [33]

TABLE 1. (Concluded)

c. Estimates of Lunar Soil Cohesion and Friction Angle Based on Apollo 11, Apollo 12, and Apollo 14 Data

Cohesion (kN/m ²)	Friction Angle (deg)	Apollo Missions	Basis	Investigator
Consistent with Lunar Soil Model From Surveyor Data		11 11	Astronaut Footprints, LM Landing Data, Crater Slope Stability	Costes et al. (1969) [24]
0.3-1.4	35-45	11	Penetrometer Tests at LRL on Bulk Soil Sample	Costes et al. (1970) [2]
0.8-2.1	37-45	11	Penetration of Core Tubes, Flagpole SWC [†] Shaft	Costes et al. (1971) [7]
Consistent with Lunar Soil Model From Surveyor Data		12	Astronaut Footprints, LM Landing Data, Crater Slope Stability	Scott et al. (1971) [3]
0.6-0.8	38-44	12	Penetration of Core Tubes, Flagpole, SWC [†] Shaft	Costes et al. (1971) [7]
<0.03-0.3	35-45	14	Soil Mechanics Trench	Mitchell et al. (1971) [4]
Soil Shear Strength Equal to or Greater Than That of Soil Model From Surveyor Data		14	Apollo Simple Penetrometer	Mitchell et al. (1971) [4]
	37-47*	14	MET Tracks	Mitchell et al. (1971) [4]

* See Table 3.

[†]SWC – Solar Wind Composition (Experiment).

accelerations/decelerations in attempting to negotiate a traverse section of given roughness.

Soft-Soil Steady-State Mobility Performance Design Guidelines

Because the NASA Request for Proposals for the development of the LRV was initiated about 1½ months after the completion of the Apollo 11 mission, the initial guidelines relative to the lunar soil properties and trafficability were based mainly on the soil mechanics data obtained from the U.S. Surveyor Spacecraft unmanned missions. From this information, the following Land Locomotion Laboratory (LLL) Soil Values were recommended for use with the analytical expressions developed by M.G. Bekker and co-workers [36-37] in preliminary LRV design studies relating to soft-soil, steady-state mobility performance on level terrain:⁵

$$k_c = 0 \text{ to } 0.4 \text{ lb/in. per inch}$$

$$k_\phi = 3.0 \text{ lb/in.}^2 \text{ per inch}$$

$$n = 1.0$$

$$K = 0.7 \pm 0.3 \text{ in.}$$

$$c = 0 \text{ to } 0.05 \text{ lb/in.}^2$$

$$\phi = 35 \pm 4 \text{ deg}$$

$$\rho = 50 \text{ to } 100 \text{ lb/ft}^3$$

$$\mu = 0.6 ,$$

in which k_c , k_ϕ , n , and K are LLL soil values; c , ϕ , and ρ are soil cohesion, angle of internal friction, and bulk density, respectively; and μ is the coefficient of friction at the interface of the LRV wheel with the lunar surface.

The MSFC Lunar Environmental Criteria Document stipulated specifically that these preliminary recommendations might be subject to change as a more comprehensive and realistic analysis of data relating to lunar soil-vehicle interaction would become available.

The lower, mid-range, and upper-bound values of the range of these soil characteristics formed three analytical soil models, designated respectively by The Boeing Company as Soil A, Soil B, and Soil C. On the basis of these models, LRV mobility performance parametric studies were performed during the initial phases of the LRV development program. The same studies also considered the following qualitative description of very fine-grained lunar soil, designated as dust:

1. Extremely fine-grained material – 10 to 15 cm (4 to 6 in.) deep.
2. Some areas with up to 10-percent magnetizable material.
3. Compactible.
4. Cohesive.

Wheel-Soil Interaction and Related Soil Mechanics Studies Under Terrestrial Gravity and Ambient Pressure Conditions

Before the development of the LRV, no actual mobility performance data existed relating to wheel-soil interaction involving extremely light wheel loads (of the order of magnitude of those exerted by the LRV under the lunar gravitational field), and fine-grained, granular, slightly cohesive soils, similar to those anticipated to be encountered on the moon. Accordingly, to gain insight into the available safety margins or potential operational problems associated with the LRV

5. Natural Environmental Design Criteria Guidelines for Use in the Design of Lunar Exploration Vehicles, Exhibit 1 of Work Statement on Request for Proposals for the Development of a Manned Lunar Roving Vehicle, NASA Marshall Space Flight Center, 1969.

performance on the moon, extensive wheel-soil interaction experimental studies were performed with single prototype-scale wheels and wheeled mobility test beds at the facilities of the U.S. Army Engineer Waterways Experiment Station (WES) [38-43]. These tests were performed on lunar soil simulants specified by MSFC and were monitored by MSFC personnel.

The specified gradation, packing characteristics, consistency, and strength characteristics for these simulants were within the ranges of the corresponding properties of the actual lunar soils as they became available from Apollo 11, Apollo 12, and Apollo 14 lunar soil mechanics data during the progress of the LRV program. During the initial phases of the LRV development program, the lunar soil simulant used in the wheel-soil interaction tests was a uniform dune sand from the Arizona desert, designated as Yuma Sand. As soon as the preliminary analysis of the earth-return soil samples from the Apollo 11 mission [24] was completed, MSFC specified a new simulant consisting of a ground-basalt from Napa, California, with a grain-size distribution similar to that of the Apollo 11 lunar soil samples. This latter lunar soil simulant was designated as LSS (WES mix) and it was placed at five different consistencies by varying its void ratio and moisture content under carefully controlled compaction procedures. The five consistencies were designated respectively as LSS₁ through LSS₅. Figure 5 shows grain-size distribution curves from the Yuma Sand, LSS (WES mix) and earth-returned lunar soil samples collected during the Apollo 11, Apollo 12, Apollo 14, and Apollo 15 missions. From these curves, it is indicated that although the LSS (WES mix) was primarily based on Apollo 11 lunar soil mechanics data, its gradation characteristics are similar to those of soil samples collected from all the Apollo missions to date.

At the request of the senior author, extensive soil mechanics tests were also

performed at the WES on both the Yuma Sand and the LSS (WES mix) to determine classical soil mechanics parameters describing the mechanical behavior of these soils at the various consistencies used as lunar soil simulants. These tests included triaxial compression tests, in-place plate shear strength tests, and stability analyses of unsupported vertical sides of excavated trenches and were supplemented with grain-size analyses and determination of the in-place moisture content, unit weight, void ratio, and relative density of the same simulants. In addition, the penetration resistance gradient of these soils was obtained with standard WES cone penetrometers, and the LLL soil values k_c , k_ϕ , n , c_b , and ϕ_b were determined using standard Bevameter plate and ring-shear apparatus. A limited amount of vane shear tests and tests using a Cohron sheargraph were also performed. The purpose of these tests was to provide information through which an LRV mobility performance analysis could be made by investigators from all available schools of thought on vehicle mobility and wheel-soil interaction. Table 2 shows the different consistencies of the lunar soil simulants used for these tests and their respective properties.

Figures 6 and 7 show respectively the WES test apparatus and various wheel and tread cover configurations used in these tests. As a result of these studies the following were accomplished:

1. Before the initiation of the LRV program, a thorough evaluation of various lunar rover wheel design concepts was made under carefully controlled laboratory conditions.
2. During the preliminary design phase of the LRV program, a thorough evaluation was made of various wheel design concepts and tread covers considered by Boeing/GM for the purpose of maximizing wheel traction at minimum energy cost.

3. The effect of soil gradation, packing characteristics, strength, and deformability on the mobility performance of LRV wheels (under wheel loads anticipated in the lunar gravity environment) was assessed directly. Such information was nonexistent and could not be extrapolated from existing experience on terrestrial mobility systems which are subjected to wheel loads much higher in magnitude than those on the LRV wheels at the lunar surface.

4. The influence of (1) vehicle velocity, (2) acceleration, (3) mode of testing consisting of constant-slip tests, programmed-slip tests with wheel angular velocity constant and carriage speed decelerating at constant rate, programmed-slip tests with carriage speed constant and wheel angular velocity accelerating at constant rate and constant/ramped-slip tests at different velocities and accelerations, and (4) sloping surfaces on the mobility performance characteristics of the selected LRV wheel was assessed.

5. Basic mobility performance characteristics (slope-climbing capability and power-consumption rate versus wheel-slip) were determined that were used as inputs to MSFC- and Boeing/GM-generated computer programs to predict the mobility performance of the LRV.

6. LRV mobility performance characteristics were established that formed baselines for monitoring, comparing, and checking parallel mobility studies, performed by GM on the same crushed-basalt lunar soil simulant.

7. Basic information on the LRV performance was obtained and potential operational problems were identified that were factored in the planning of the geological traverses and scientific tasks carried out during the Apollo 15 mission.

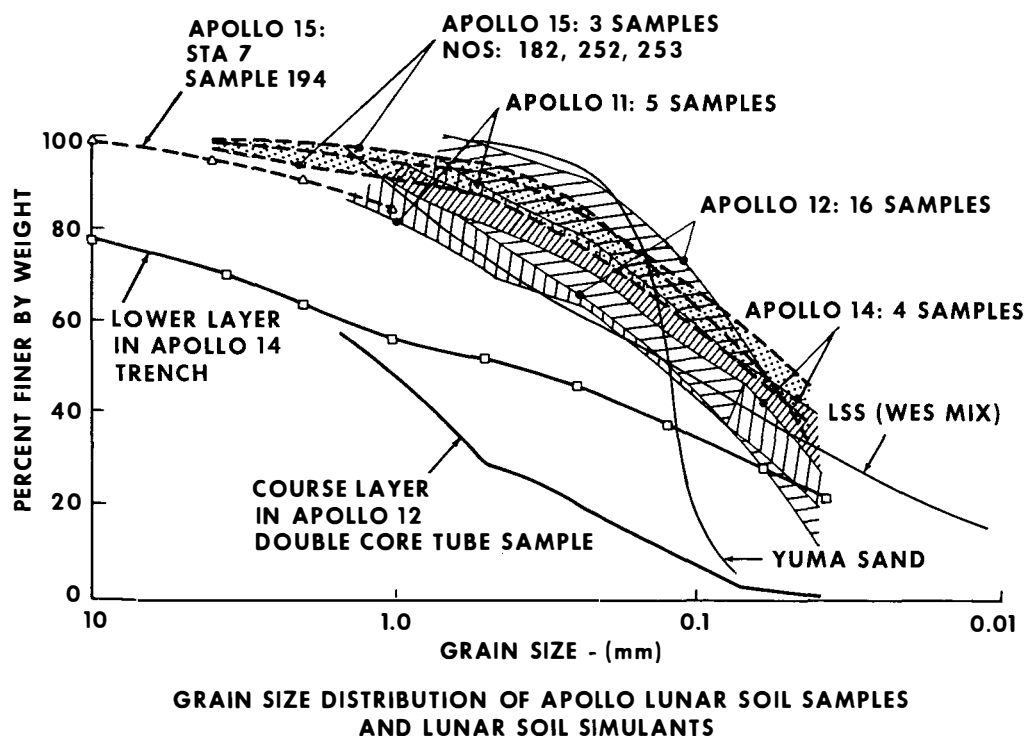


Figure 5. Comparison of gradation curves from Apollo lunar samples and terrestrial soils used as lunar soil simulants in wheel-soil interaction tests.

TABLE 2. PHYSICAL AND MECHANICAL PROPERTIES OF LUNAR SOIL SIMULANTS

Soil Condition	Yuma Sand												
	G (MN/m ³)	e	D _r (%)	ρ (g/cm ³)	ρ_L (g/cm ³)	k_c [(lb/in.) ¹⁺ⁿ]	k_ϕ [(lb/in.) ²⁺ⁿ]	n	ϕ_b (deg)	c_b (kN/m ²)	ϕ_{PL} (deg)	ϕ_T (deg)	c_{TR} (kN/m ²)
S ₁	0.54	0.77	32	1.51	1.75	0.54	6.01	0.72	13.8	1.65	29.8	37.1	0
C ₀	0.21	1.02	0	1.32	1.53	2.61	2.46	0.73	21.6	0.83	28.1	34.6	0.28
C ₁	1.26	0.94	14	1.38	1.60	0.21	8.03	0.67	23.5	0.97	29.0	36.0	0.55
C ₂	3.17	0.83	52	1.46	1.69	4.96	10.08	0.52	15.2	2.14	31.2	38.4	1.10
Crushed Basalt													
LSS ₁ – (Loose-Air Dry)	0.2	0.90	31	1.52	1.63	0.42	4.32	0.90	29.0	0.97	34.0	38.5	0
LSS ₂ – (Intermediate Density-Air Dry)	0.6	0.83	42	1.58	1.69	0.13	5.34	1.15	29.0	1.03	35.0	39.0	0.3
LSS ₃ – (Dense-Air Dry)	1.8	0.74	52	1.66	1.78	-1.58	8.83	1.48	28.8	1.03	35.5	40.0	0.6
LSS ₄ – (Loose-Moist)	1.0	0.90	31	1.52	1.63	1.76	5.04	1.18	29.0	0.83	34.0	38.5	0.8
LSS ₅ – (Dense-Moist)	6.4	0.69	59	1.71	1.83	(Not Available)				36.0	41.5	2.9	

G – Penetration resistance gradient

e – Void ratio

D_r – Relative density

ρ – Dry bulk density (specific gravity of solids: Yuma Sand – 2.67; crushed basalt – 2.89)

ρ_L – Equivalent bulk density of lunar soil (specific gravity of solids – 3.1), based on the same void ratio

k_c , k_ϕ , n – LLL soil values obtained by standard plate Bevameter tests

ϕ_b , c_b – Soil friction angle and cohesion obtained by standard Bevameter ring-shear tests

ϕ_{PL} – Soil friction angle obtained from in-place plate shear tests

ϕ_T – Soil friction angle obtained from triaxial compression tests

c_{TR} – Soil cohesion obtained from trench slope stability analysis and triaxial compression tests

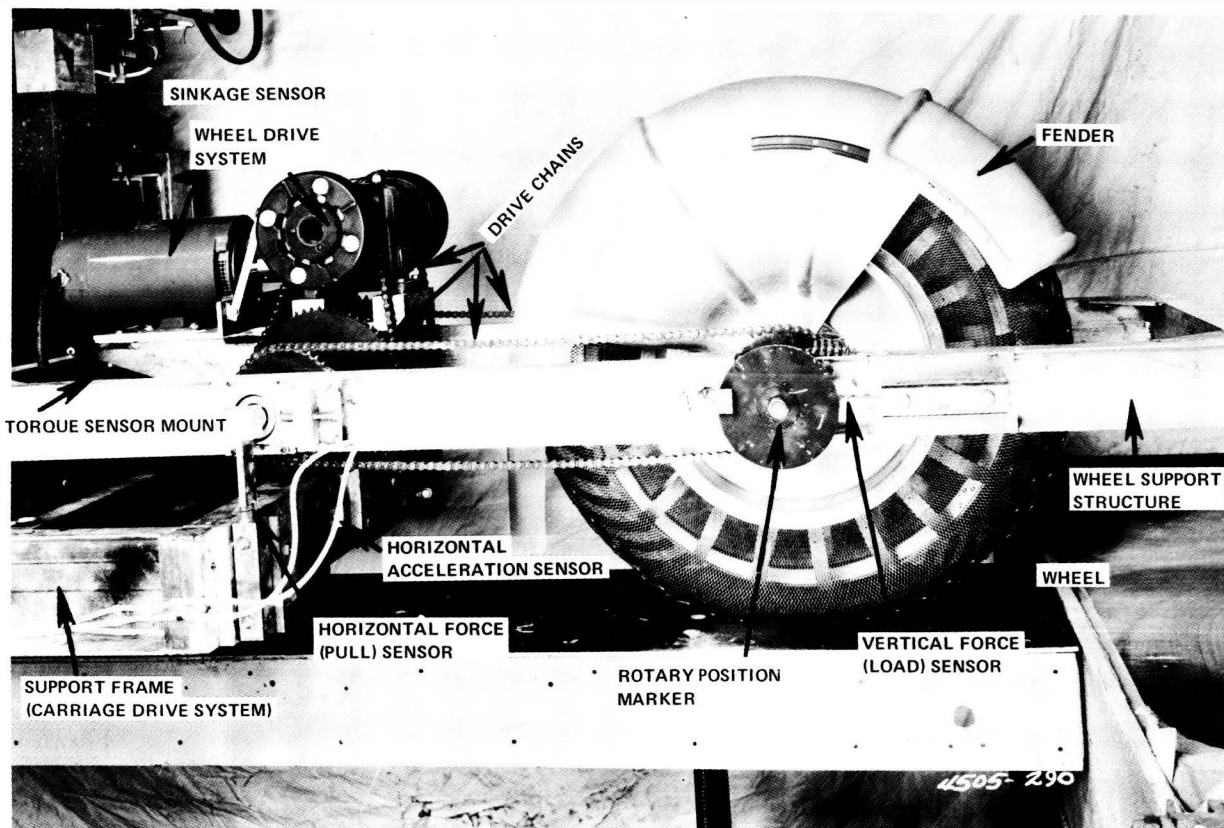


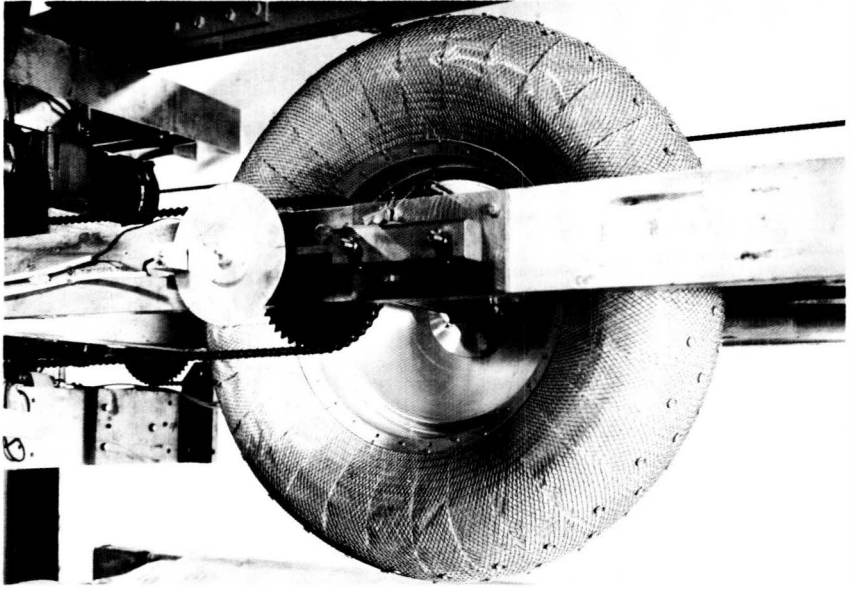
Figure 6. Apparatus for LRV wheel-soil interaction tests performed at the WES, Vicksburg, Mississippi.

Green and Melzer [41, 42] and Melzer [43] have described detailed analyses of these tests. Typical test results are shown in Figures 8 through 11. For comparison, analytical curves computed from expressions developed by Bekker and co-workers [36, 37] (see appendix) and using the LRV wheel geometry, wheel load-footprint characteristics, and average LLL soil values obtained by the WES for the same lunar soil simulants before and after each corresponding test [42] are superposed on the experimental data.

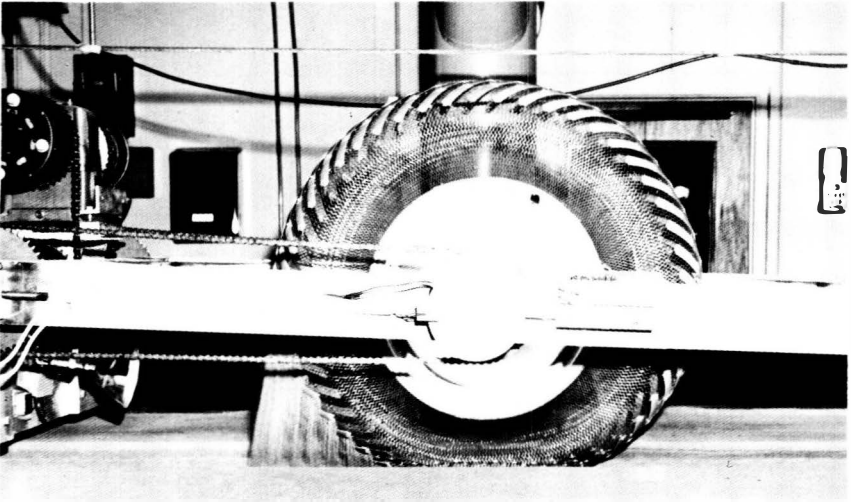
From this comparison, it is indicated that the theoretical curves tend to overestimate the mobility performance of the single wheels, as obtained from the experimental data,

although reasonably good agreement exists between the general trends of corresponding analytical and experimental data. Relative differences can be tentatively attributed to the following factors:

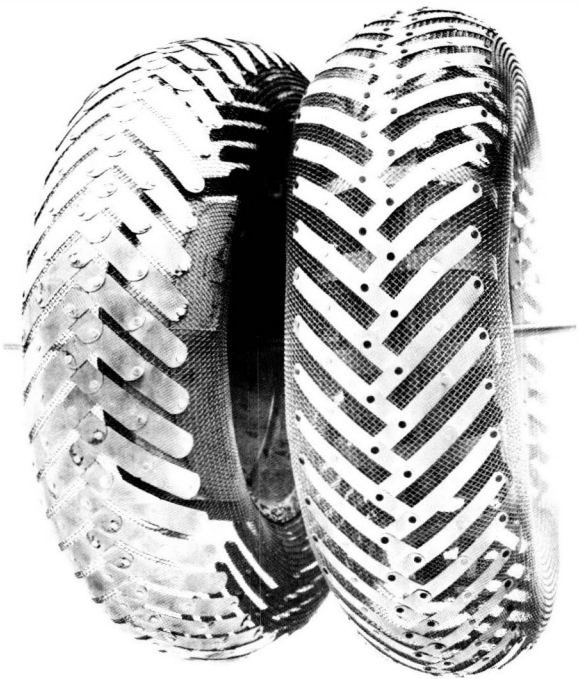
1. In addition to common criticisms regarding the lack of dimensional homogeneity and inherent limitations of the analytical expressions used in these calculations, which consist of terms representing decoupled effects of soil compressibility and shear strength/deformation characteristics on wheel performance, the analytical form of the same equations is such that the resulting calculations tend to overpredict the wheel mobility performance. For instance:



a. "CLOSED" WIRE-MESH WHEEL WITH BUTTON-TYPE GROUSERS



b. "OPEN" WIRE-MESH WHEEL WITH 50-PERCENT CHEVRON TREAD COVER DESIGNS



c. "OPEN" WIRE-MESH WITH 75-AND 50-PERCENT CHEVRON TREAD

Figure 7. LRV wheel-soil interaction tests performed at the WES on different GM wheel and tread cover designs.

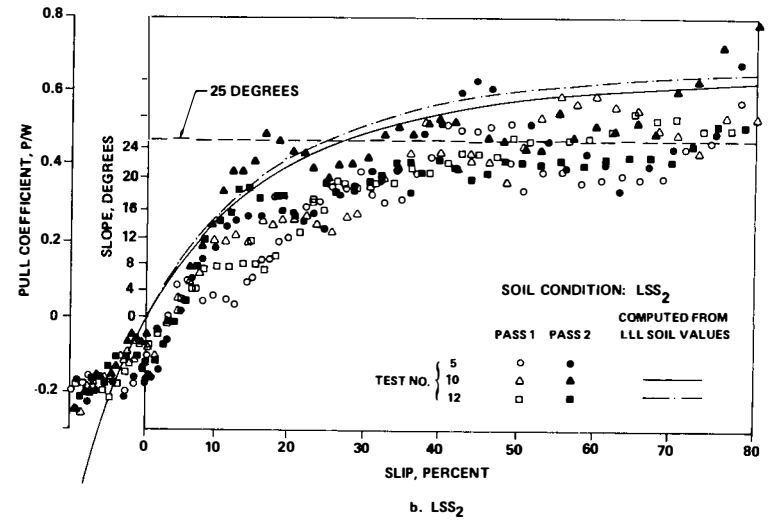
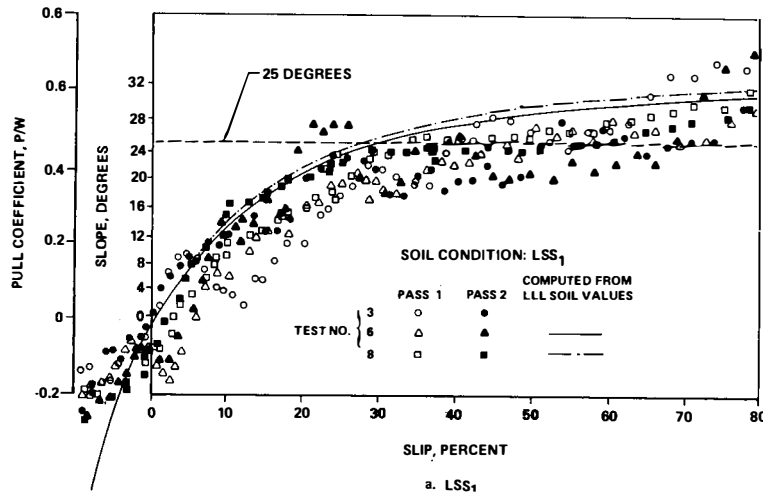
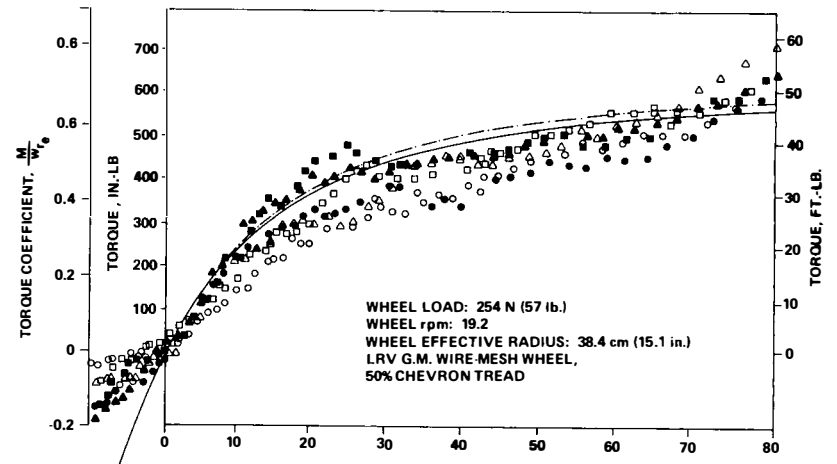
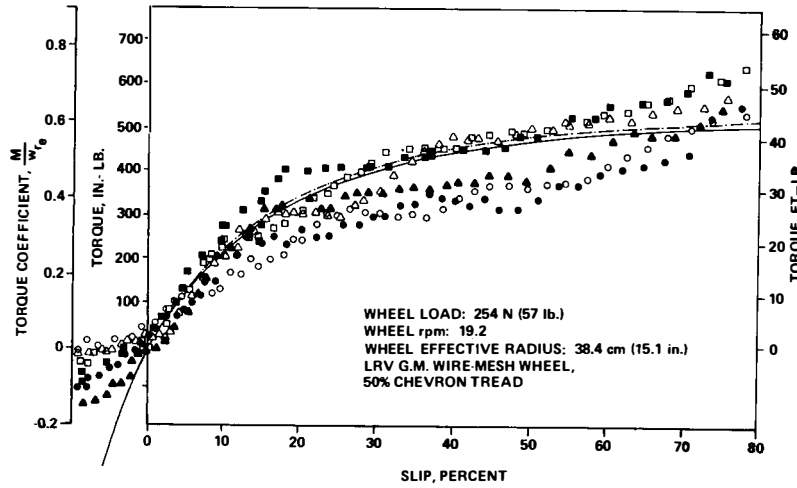
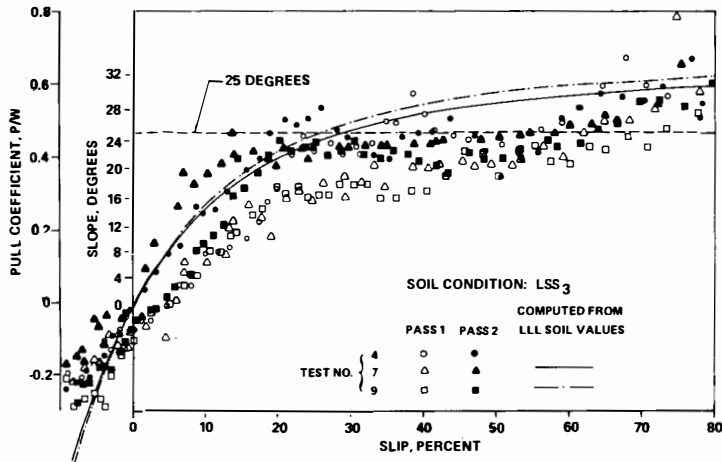
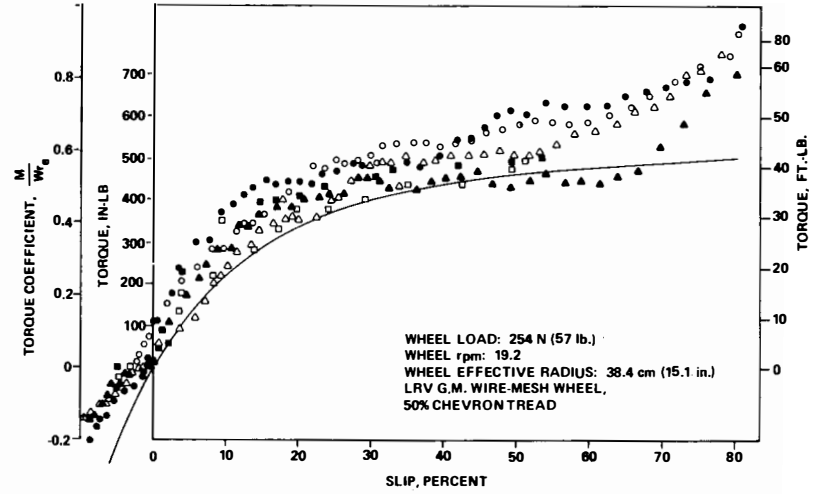
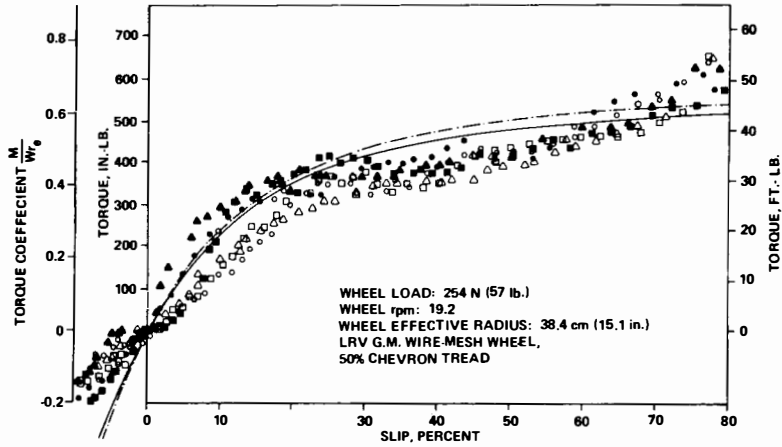
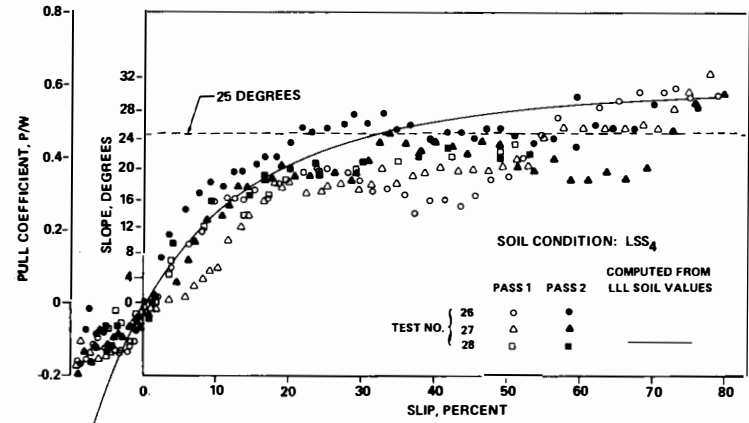


Figure 8. Typical WES wheel-soil interaction test results [41, 42].
 Experimental and theoretical relations of pull and torque coefficients versus wheel slip.

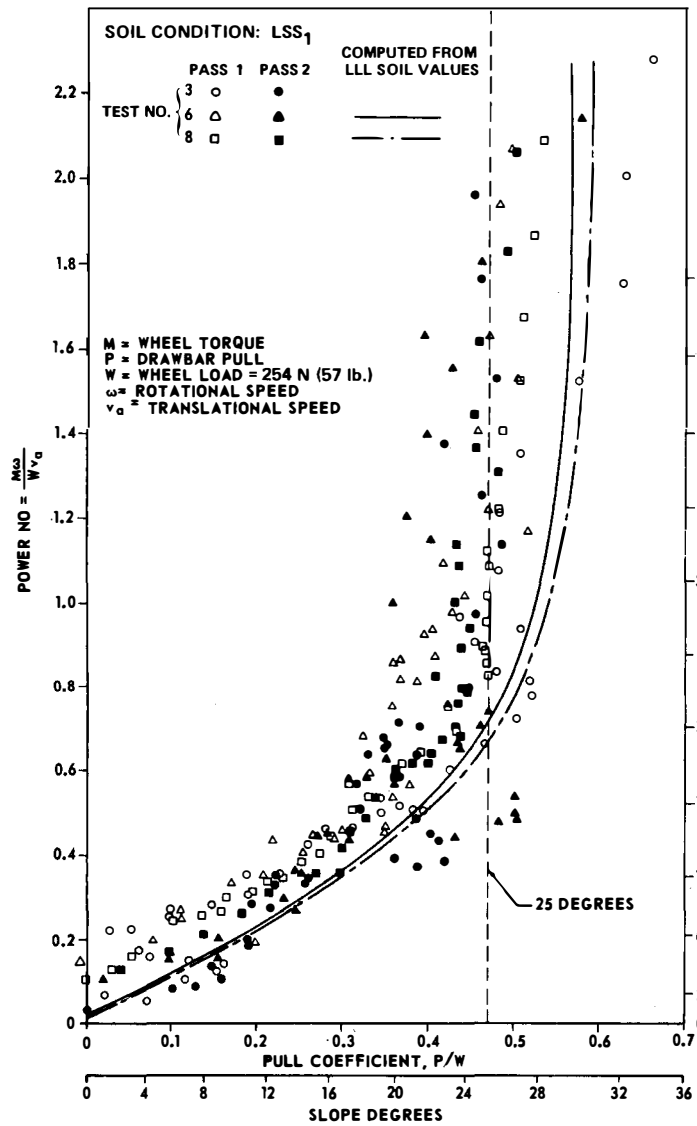


c. LSS₃

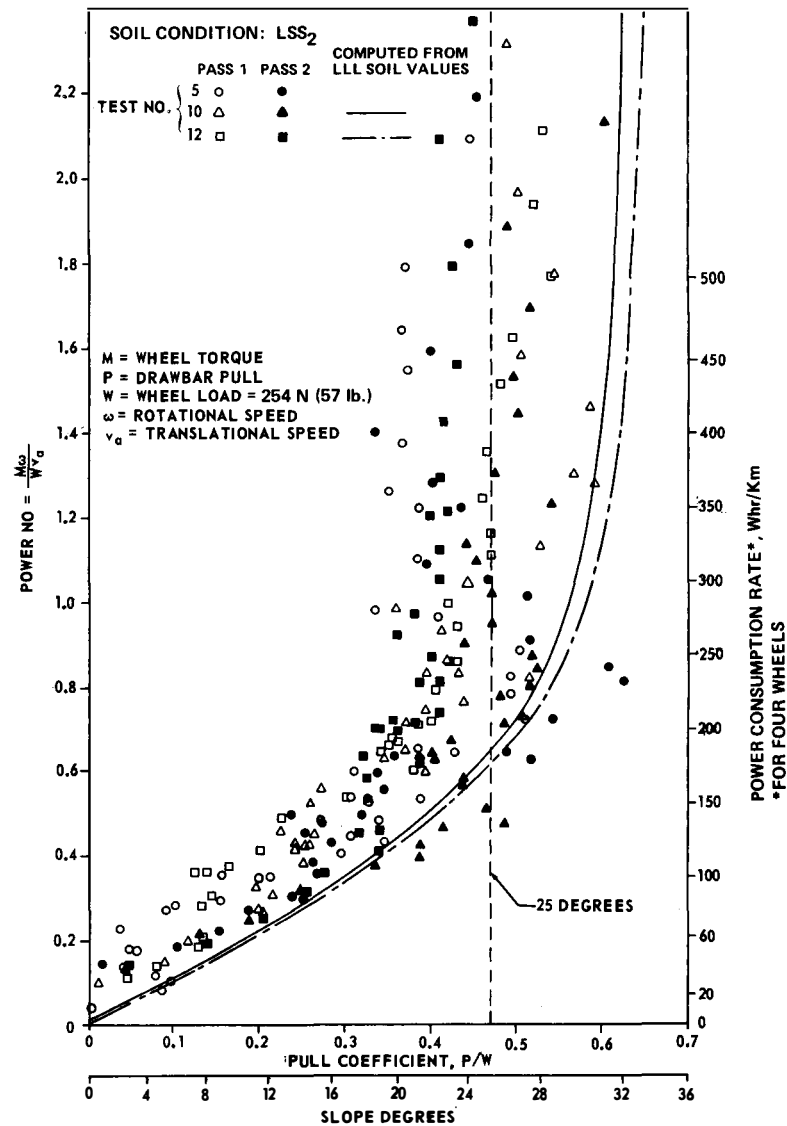


d. LSS₄

Figure 8. (Concluded).

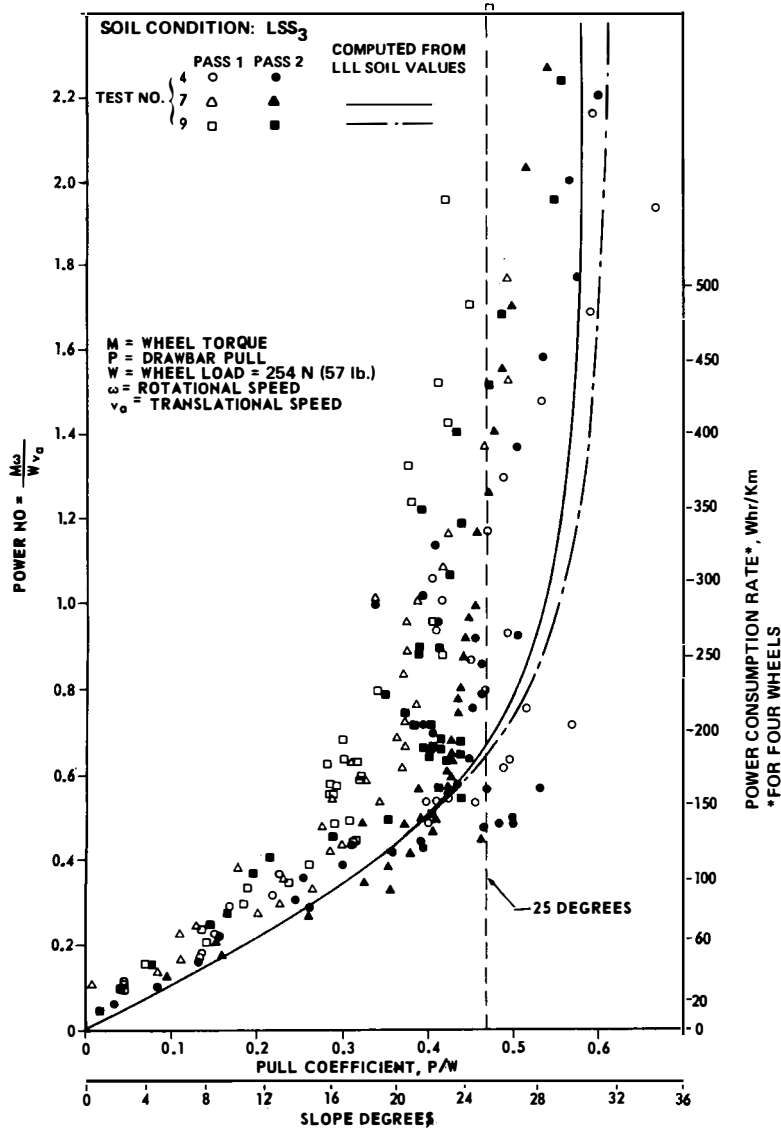


(a)

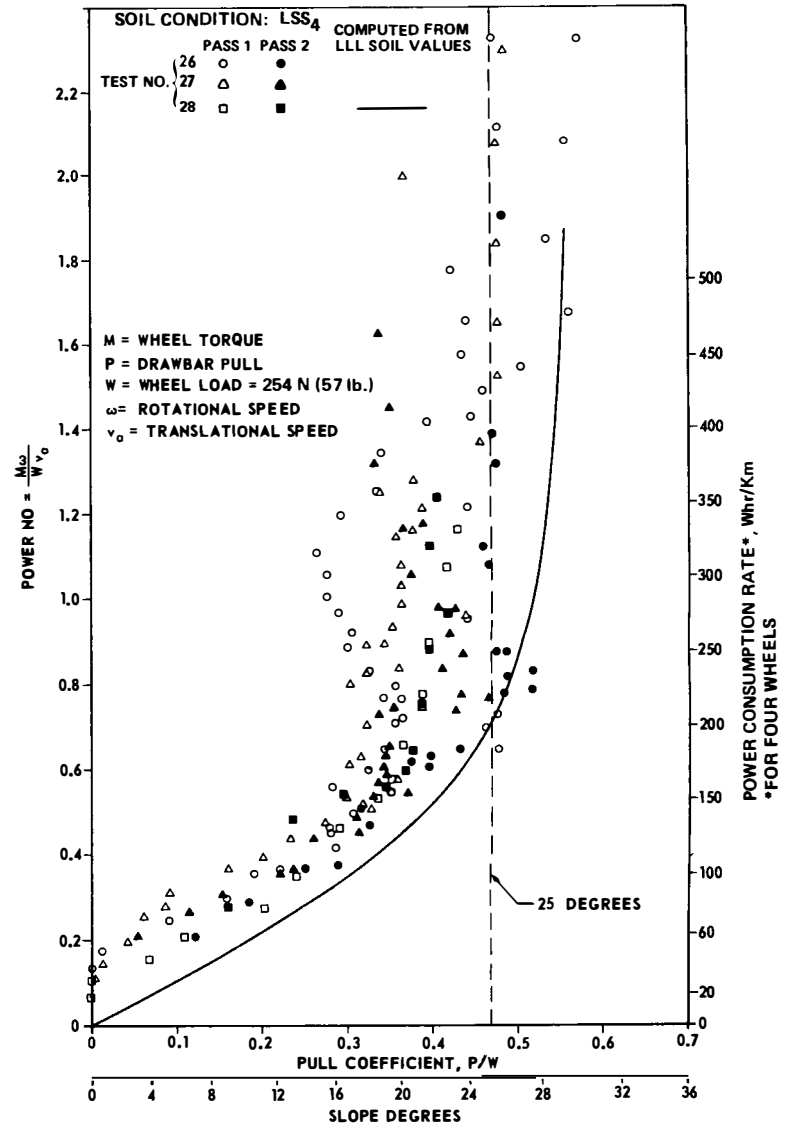


(b)

Figure 9. Typical WES wheel-soil interaction tests results [41, 42] on LSS₁ through LSS₄. Experimental and theoretical relations of power number versus pull coefficient.

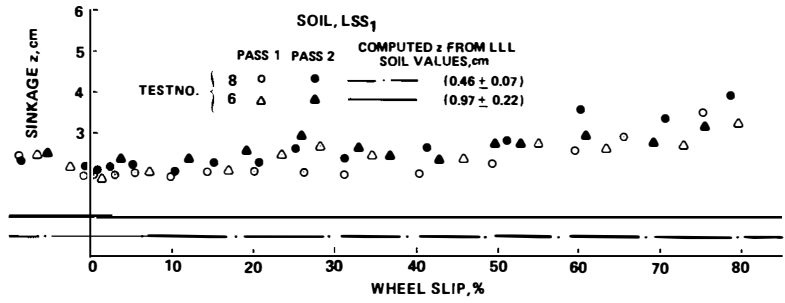


(c)

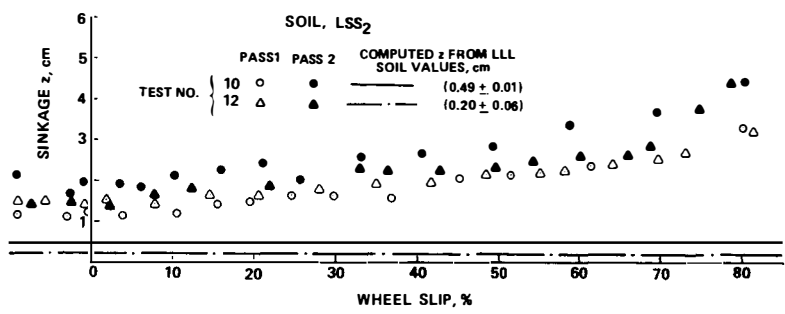


(d)

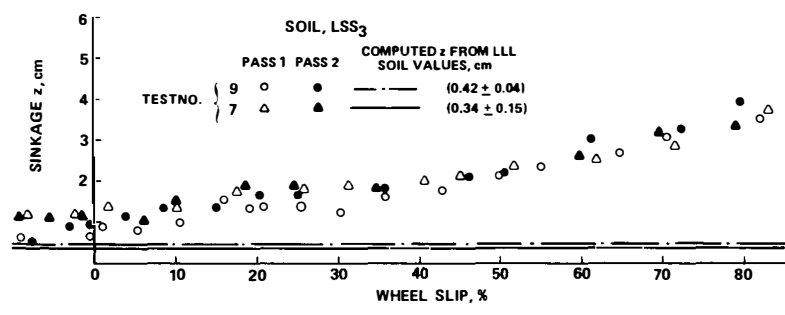
Figure 9. (Concluded)



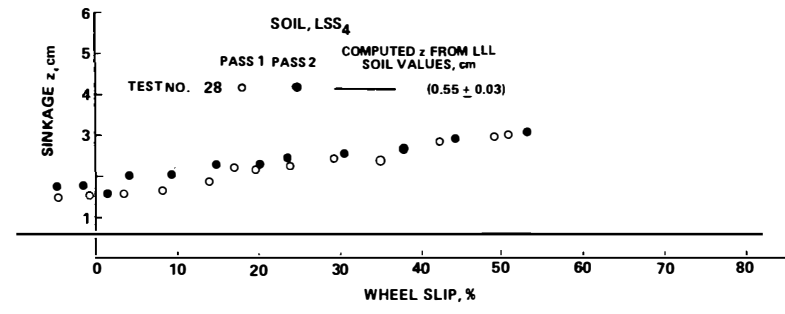
(a)



(b)



(c)



(d)

Figure 10. Typical WES wheel-soil interaction test results [41, 42] on LSS₁ through LSS₄. Experimental and theoretical relations of wheel sinkage versus wheel slip.

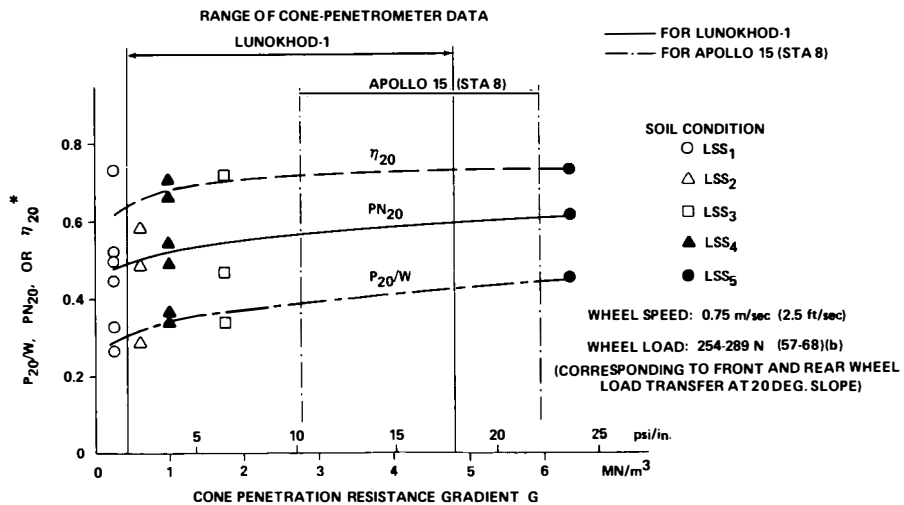
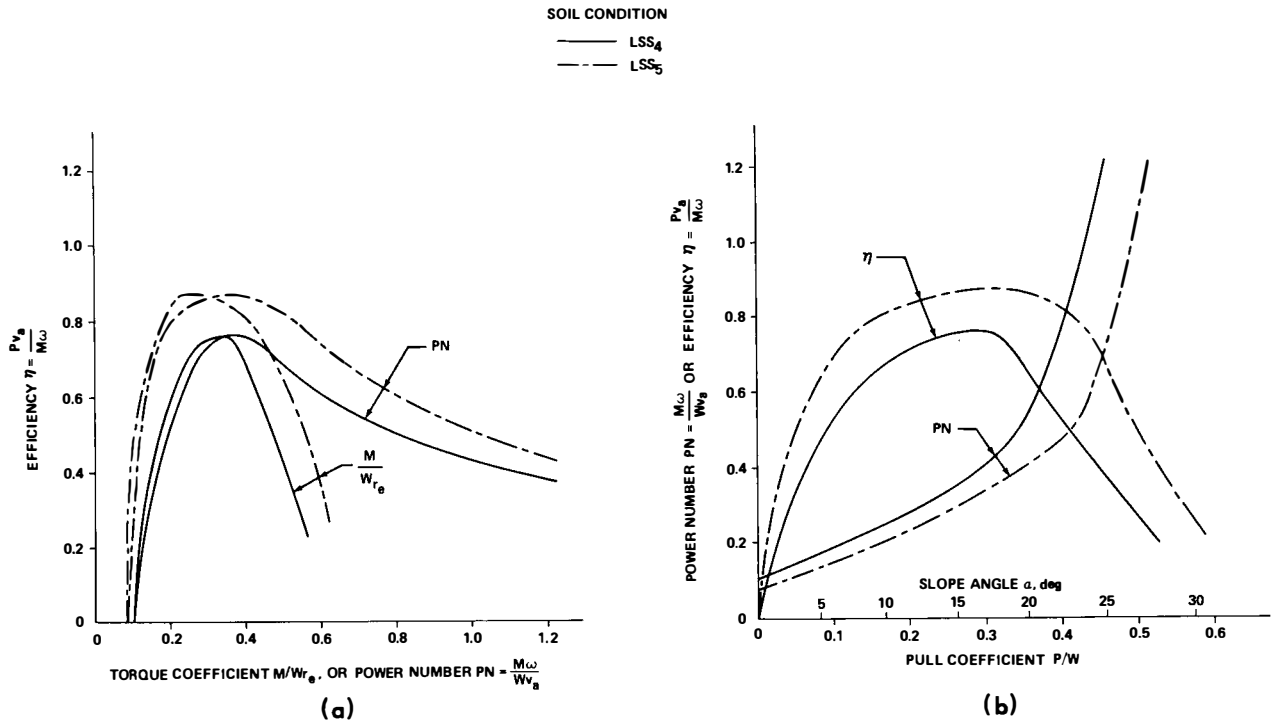


Figure 11. Typical WES wheel-soil interaction test results [43] on LSS₁ through LSS₅. Effect of soil consistency and strength on mobility performance parameters. [Note comparison between range of G values for LSS (WES mix) and G values obtained from Apollo 15 and Lunokhod-1.]

a. At zero wheel slip; the theory predicts zero energy input to the wheel, as expressed by the torque coefficient M/Wr_e and power number $M\omega/Wv_a$ [40, 41-43], whereas the actual tests indicated that zero energy input occurs usually at a negative wheel slip, defined as the towed point [40, 41-43], and at zero wheel slip a finite amount of energy is input to the wheel. In these expressions M is the applied wheel torque, W is the wheel load, ω is the wheel angular velocity, v_a is the translational speed of the carriage, and r_e is the effective radius of the wheel; the latter is defined as the average value between the radius of the undeflected wheel and the radius of the deflected wheel on hard surface under the action of load W .

b. At negative values of wheel slip, the resulting negative values of both the pull coefficient and the torque coefficient, as predicted by the theory, are unrealistically high. These theoretical trends may result in underprediction of the minimum negative slope angle at which the vehicle will coast at a given speed without requiring additional power from the batteries.

c. For a given wheel load and soil condition, the theory predicts constant wheel sinkage, whereas the actual tests have indicated that the sinkage increases monotonically with wheel slip (Fig. 10), resulting in higher energy losses than those predicted by the theory.

d. The theory is mainly applicable to relatively slow-motion, steady-state wheel-soil interaction, taking place on level soil surfaces. Accordingly, inertial effects and the development of air-pore pressures within air-dry, or slightly moist, fine-grained soil masses, caused by the dynamic wheel-soil interaction at high speeds or accelerating periods, are not accounted for, nor is the effect of slope angle on the degradation of wheel mobility performance on sloping surfaces of the same soil consistency.

2. The relative degradation of the actual wheel performance as compared with the analytical calculations may have been caused partly by the presence of air-pore pressures developed in the lunar soil simulants. The coefficient of permeability to water at 20°C of crushed-basalt simulants of grain-size distribution and packing characteristics comparable to those used in the wheel-soil interaction tests is of the order of 10^{-4} cm/sec [9], corresponding to a permeability of the order of 10^{-8} cm².

From these considerations and visual observations during testing, it is possible that the shear-strength and the compressibility of the LSS (WES mix) might have been affected adversely by the presence of air-pore pressures developed during testing, resulting in an apparent degradation of the wheel performance. On the other hand, the rate of deformation at which the LLL soil value tests were performed may not have been of sufficient magnitude to develop air-pore pressures within the soil mass. Thus, the soil values so obtained may have been representing a stronger and less compressible soil than actually developed during the wheel-soil interaction tests. In connection with these observations, it should be noted that the absence of lunar atmosphere eliminates the possibility of wheel performance degradation caused by air-pore pressures. Hence, the actual LRV performance on the lunar surface would be expected, in general, to be better than that indicated by the experimental results from the WES wheel-soil interaction tests.

The main conclusions from these studies were:

1. The 50-percent chevron-covered, wire-mesh GM wheel exhibits slightly better performance characteristics than other GM wheel configurations.

2. The maximum slope-climbing capability of the LRV wheel on the simulated lunar soils ranges between 18 and 23 deg.

3. The wheel slip at the self-propelled point on level soft-soil surface ranges between 2 and 5 percent. On sloping soft-soil surfaces, the wheel slip is expected to be higher, as indicated by the P/W-versus-slip plots in which P/W is the pull coefficient [40].

4. Within the load range 178 to 377 N (40 to 85 lb), the pull P and torque M developed as a result of the wheel/soil interaction increase linearly with the wheel load. The coefficients of proportionality for the pull-versus-load and torque-versus-load linear relationships increase with wheel slip and soil strength and do not appear to be influenced by:

a. The wheel angular velocity and the translational speed of the carriage, within the carriage speed range of 0 to 11 km/hr.

b. The wheel acceleration (or carriage deceleration), within the acceleration/deceleration range of 0.03 to 1.5 m/sec² (0.1 to 4.95 ft/sec²).

c. The wheel load, within the load range 178 to 377 N (40 to 85 lb).

d. The mode of testing, as described above.

e. The direction of chevron cover.

f. The presence or absence of fenders.

5. The stronger the soil, the higher the wheel mobility performance efficiency η , where $\eta = Pv_a/M\omega$, appears to be.

6. The maximum wheel mobility performance efficiency on level soil surfaces for soil conditions LSS₄ and LSS₅ appears to be realized at a pull coefficient ranging between 0.27 and 0.30, at a torque coefficient

ranging between 0.31 and 0.33, and at a power number ranging between 0.36 and 0.38.

7. As expected, the wheel mobility performance efficiency η for soil condition LSS₅ is higher than that realized for soil condition LSS₄. However, no conclusions can be drawn regarding the overall efficiency of the LRV on soil condition LSS₅ before obtaining actual test data, or at least performing power profile analyses on traverses of varying slope distributions.

The apparent lack of dependence of wheel performance on wheel speed and acceleration can be tentatively attributed to the combined effects of air-pore pressures developed within the soil mass and inertial effects during momentum transfer between soil particles at high-wheel velocities or accelerations, which tend to counteract each other. Again, because of the absence of lunar atmosphere and because of inertial effects associated with the dynamic interaction of the LRV wheels with the actual lunar soil, the mobility performance of the LRV on the lunar surface would, in general, be expected to be enhanced at higher speeds, contrary to the indications provided by the trends of the experimental results obtained from the WES wheel-soil interaction tests.

Wheel-Soil Interaction Tests Under 1/6-g Gravity and Low-Atmospheric Pressure Conditions

Parallel with the WES wheel-soil interaction tests which were performed under terrestrial gravity and ambient atmospheric pressure conditions, 65 wheel-soil interaction tests [44] were conducted onboard a U.S. Air Force C-135A aircraft flying parabolic trajectories at altitudes ranging between 7600 and 12 200 m (25 000 to 40 000 ft). The flight trajectories were executed in a specific manner, resulting in local accelerations which closely simulated the 1/6-g lunar gravity field.

The wheel-soil interaction tests were performed on single, prototype-scale LRV wheels with and without fenders, inside a vacuum chamber carried onboard the aircraft.

The wheel was mounted on a horizontal arm of a carousel-type mechanism, which enabled the wheel to propel itself along circular paths about a central post normal to the soil surface while rotating about its own axis. The circular track was 1.57 m (62 in.) in diameter, 58 cm (22.75 in.) wide, and contained the same crushed basalt used as a lunar soil simulant in the WES tests. The LSS was placed air-dry to a depth of about 27 cm (10.5 in.) and was filled and graded by a remotely controlled rotary tiller mounted on a horizontal arm diametrically opposite to the wheel.

The ambient pressure inside the aircraft was maintained at 24 mm Hg. During testing it was estimated that about 99 percent of the air was evacuated from the vacuum chamber as a result of pumpdown, using one of two diffusion pumps provided with the system. However, the recorded atmospheric pressure in the chamber during testing ranged between 2 and 5 mm, as contrasted with 10^{-11} mm Hg (torr), which is the order of magnitude of the actual lunar atmospheric pressure [45-47].

Test variables during these tests included:

1. Wheel revolutions per minute.
2. Wheel load normal to the soil surface, which was applied with a spring mechanism independent of the gravity field conditions.
3. Degree of vacuum.

Photographic documentation was provided by means of two cameras, one tracking the front of the wheel and the other tracking the rear. In addition, viewing ports enabled visual observations and qualitative evaluations to be made during testing.

Detailed descriptions and analyses of these tests are given by Mullis [44] and MSFC.⁶ It appears that large errors associated with the instrumentation and data acquisition system make questionable the quantitative information obtained from the wheel mobility performance. However, the following qualitative conclusions could be drawn from these tests:

1. The combined effect of reduced gravity and low-atmospheric pressure (absence of air-pore pressures) on the wheel-soil interaction enhances the mobility performance of the wheel, as was also concluded from the WES tests.

2. If considered separately, the effects of lunar gravity and atmospheric conditions on dust, generated by the ejection of fine-grained soil particles as a result of the wheel-soil interaction, tend to oppose each other. However, the combined effect of these two factors tends to reduce potential hazards caused by dust which might include the following: loss of terrain visibility caused by dust clouds while the astronauts are driving the LRV; dust contamination or damage to astronaut helmet visors, instrument panels, thermal insulation reflectors, optical surfaces, etc.

3. The proposed wheel fender and flexible flap design was adequate within the anticipated range of LRV speeds on the lunar surface.

6. MSFC Lunar Roving Vehicle Dust Profile Test Program, internal reports S&E-ASTN-TI (71-82), May 26, 1971; S&E-ASTN-TI (71-101), June 23, 1971, and S&E-ASTN-SMS (71-25), July 6, 1971, Astronautics Laboratory, Marshall Space Flight Center, Huntsville, Ala.

4. The wheel mobility performance and energy requirements were not influenced by the presence or absence of fenders, as was also concluded from the WES tests.

5. The continuous mass transfer of fine-grained soil accumulated inside and ejected through the wire-mesh wheel while the wheel was in motion did not appear to impose operational problems on the wheel mobility performance and energy requirements.

6. The probability of entrapment by the wheel woven-wire mesh and subsequent ejection of small rock particles, ranging in size between 2.5 cm (1 in.) and pea gravel, which could impair the safety of the astronauts or cause damage to instruments, equipment, wheels and/or fenders, was very small.

Soil Mechanics Tests on Lunar Soil Simulants Under Varying Gravity Conditions and Related Analyses

Cone-penetration resistance tests on Yuma Sand and crushed-basalt lunar soil simulant, similar to that used in the wheel-soil interaction tests, were also performed in a C-135A aircraft flying parabolic trajectories resulting in 1/6-, 1-, and 2-g local gravitational fields [7]. These tests were conducted under carefully controlled experimental conditions inside the pressurized cabin of the aircraft (ambient pressure, 24 mm Hg) and provided very useful quantitative information regarding the effect of gravity on the strength and deformation characteristics of simulated lunar soils.

The data from these tests were used in conjunction with bearing capacity theory and the dimensional analysis of the performance of

pneumatic tires on soft soils developed by Freitag [48] to evaluate lunar surface properties and trafficability from wheel tracks developed by the pneumatic tires of a two-wheeled, ricksha-type pushcart, designated as Modularized Equipment Transporter (MET). The MET was used during the Apollo 14 mission to carry instruments, geological tools, photographic equipment and soil/rock samples along the geologic traverses [4]. The results of this analysis are shown in Table 3. Similar analyses were performed at the Geotechnical Research Laboratory of the MSFC Space Sciences Laboratory using photographs from wheel tracks developed by the Soviet unmanned vehicle Lunokhod-1 during traverses at the Mare Imbrium landing site of the Soviet unmanned spacecraft Luna 17.⁷

From these analyses the confidence levels on the mechanical properties and trafficability of the lunar surface were increased. As a result, the specifications relating to the physical and mechanical properties of lunar soil simulants and testing procedures used in the terrestrial wheel-soil interaction simulation studies, which were conducted a few months before the Apollo 15 mission, were further refined.

MSFC COMPUTER MODEL RELATING TO LRV MOBILITY PERFORMANCE AND POWER PROFILE ANALYSIS

The initial objectives of the computer model for the LRV were twofold: (1) the prediction of energy consumed in the four traction-drive motors as a function of traverse conditions, throttle manipulation, and velocity of the vehicle and (2) the analysis of failure modes.

7. N.C. Costes, Penetration Resistance Characteristics of Lunar Soil as Determined from Lunokhod-1 Tracks, unpublished report, Geotechnical Research Laboratory, Space Sciences Laboratory, Marshall Space Flight Center, Huntsville, Ala., 1971.

TABLE 3. VARIATION IN LUNAR SOIL PROPERTIES AT APOLLO 14 SITE AS DETERMINED FROM MET TRACKS^a

Geology Traverse Stations According To Descending Geologic Age			G_L (N/cm ²)		e_L		ρ_L (g/cm ³)		ϕ_L (deg)	
Regional Geologic Feature	Traverse Location	Terrain Type	Range	Average	Range	Average	Range	Average	Range	Average
			Highly Subdued Craters	LM Site, ALSEP Site, Sta. A; B	Level, Firm	0.83-0.47	0.73	0.68-0.70	0.69	1.85-1.81
LM Site	Soft Spots and Crater Rims	0.34-0.27		0.30	0.74-0.75	0.74	1.79-1.77	1.78	39.6-38.5	39.0
Moderately Subdued Craters	A; G; B ₂	Level, Firm	2.02-0.47	0.91	0.62-0.71	0.68	1.91-1.81	1.85	47.1-41.0	43.2
	A; B ₁ ; B ₂	Soft Spots and Crater Rims	0.47-0.20	0.30	0.71-0.77	0.75	1.81-1.75	1.77	41.0-37.2	38.5
Sharp Craters	B ₃ ; C'	Level, Firm	0.83-0.34	0.65	0.68-0.74	0.70	1.85-1.79	1.83	43.4-39.6	42.1
	C'	Soft Spots and Crater Rims	0.47-0.20	0.34	0.71-0.77	0.74	1.81-1.75	1.78	41.0-37.4	39.4

a. After Ref. 4. Also to appear in the Journal of Geophysical Research, Vol. 77, No. 29, October 1972.

Previous analyses of off-the-road wheeled vehicles [36, 38, 49-57] indicated that single-wheel models were sufficient to predict the energy consumed by an actual four-wheeled vehicle; however, the inclusion of failure modes necessitated the development of a four-wheel model. The primary purpose for developing this model was to estimate the energy flow to the drive motors and their associated electronics, exclusive of navigation, steering, and other energy-consuming systems onboard the LRV.

Because of time limitations, complicated mathematical expressions were avoided. The approach taken was to test each part of the traction drive system in the laboratory and model the system based on the actual performance characteristics of each component. All major contributors to energy consumption were included, and it appears that any further additions and complications would not significantly change the final result. The suspension for each wheel was not modeled as an independent system, but was accounted for in the analysis, as will be shown later.

Until the present model was completed, the LRV performance was evaluated by models in which the vehicle was assumed to be moving at a constant speed. The energy required to accelerate the vehicle was accounted for as an add-on. This method eliminates successive iterative cycles which are active during periods of positive and negative acceleration. The assumption of a constant-velocity model also does not take into consideration the effects of rotational inertias, such as those of the wheel and the motor armature inertias, which must be overcome to accelerate the vehicle; therefore, in the model developed every effort was made to consider all significant transient effects.

A simplified block diagram of the mobility system is shown in Figure 12. The following paragraphs and associated performance diagrams explain in greater detail the functional characteristics of each component block of this diagram.

1. Torque-versus-speed characteristics of the wheel motors at different

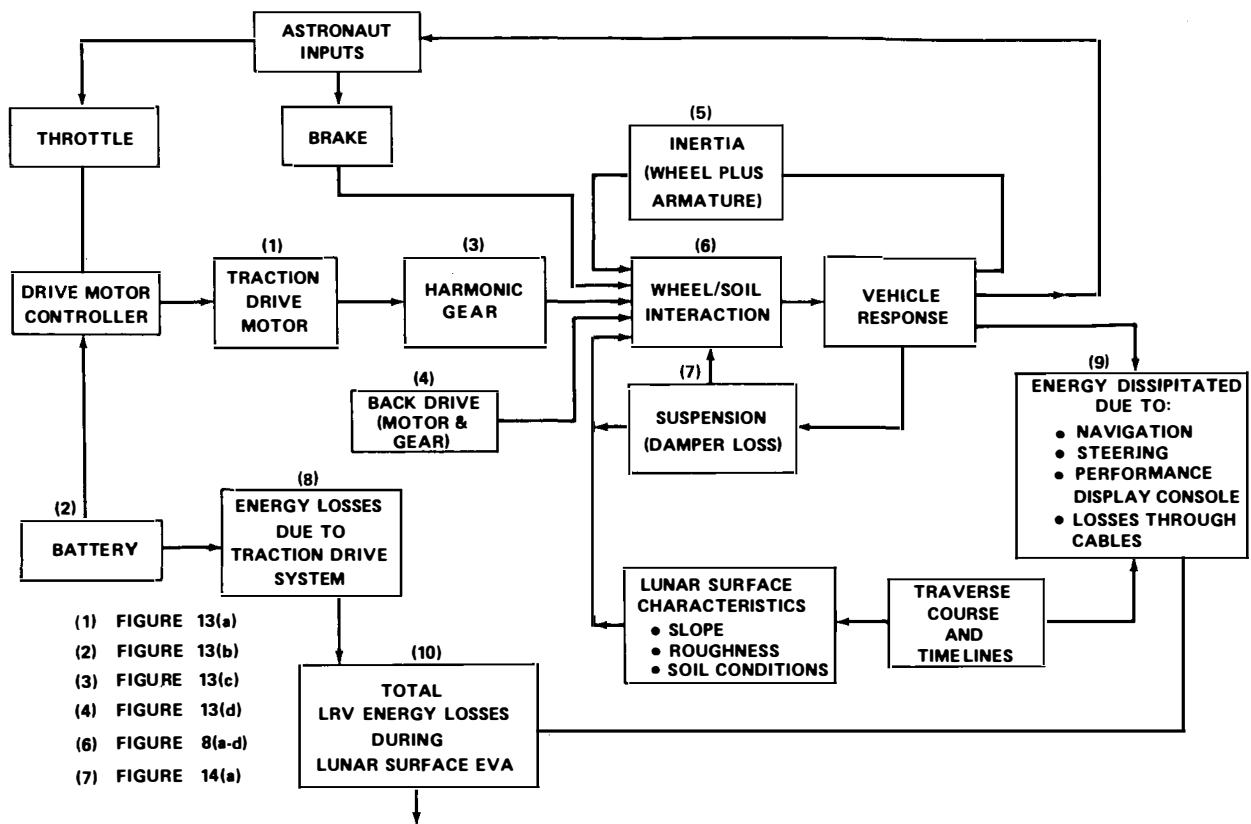


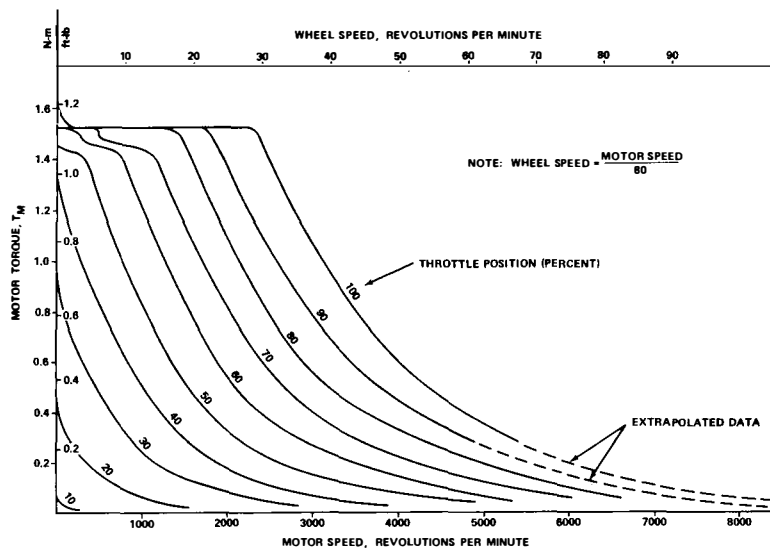
Figure 12. Simplified flow diagram of MSFC-developed LRV mobility performance and power profile analysis computer program.

throttle settings are shown in Figure 13a. These data were obtained from laboratory tests performed under constant speed conditions.

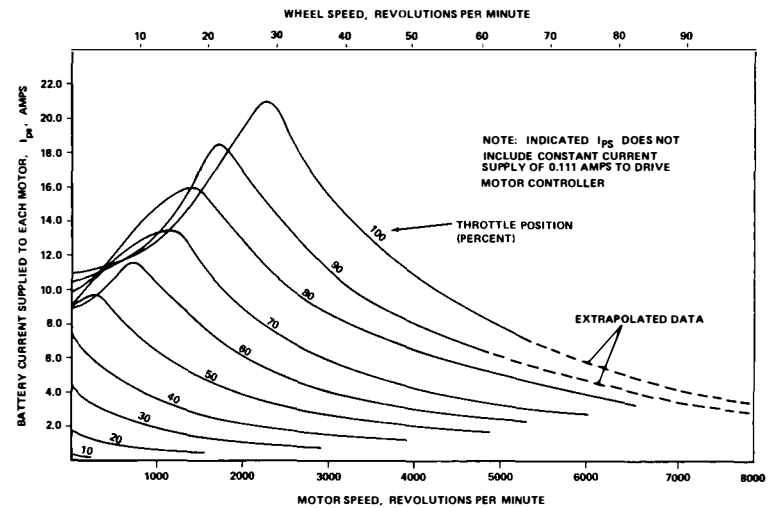
2. The energy flow from the batteries was determined in terms of supply current (I_{ps}) as a function of motor speed and throttle position (Fig. 13b). These data were obtained also from laboratory tests performed under constant speed conditions. In this connection, it should be noted that the battery "sees" only the traction drive motor and controller. All the energy flow from the batteries is consumed in developing a torque at the motor shaft. In this manner, all losses are accounted for at this point. Therefore, the problem is mainly one of determining the torque and speed requirements imposed on the motor by the astronaut, the lunar surface conditions, and the interaction of the other system components.

3. The straight-line equations shown in Figure 13c, along with the constant-speed reduction factor, completely describe the harmonic-gear torque and speed characteristics. In this analysis the characteristics of four gears were used to determine an average curve to minimize any gear-to-gear variations that might occur. The effects of speed on the gear torque characteristics were found to be small and, therefore, were ignored. As mentioned in an earlier section of this report, the harmonic gear reduces the motor speed by a constant factor of 80.

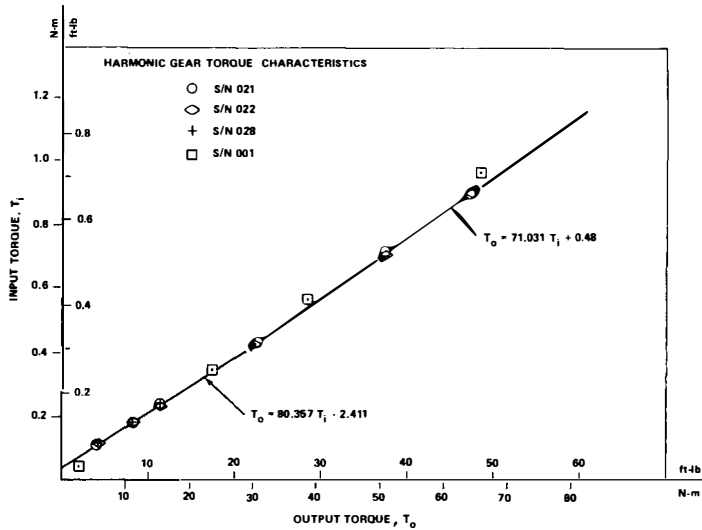
4. The term "back-drive" (block 4, Fig. 12) can be defined as the torque necessary to drive the motor when the torque is applied at the gear output shaft. This represents the resistance offered to LRV motion by an inoperative motor. As shown in Figure 13d, the back-drive is a function of wheel speed and



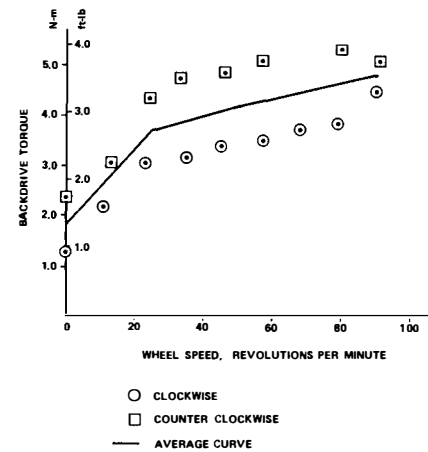
(a)



(b)



(c)



(d)

Figure 13. Performance characteristics of LRV traction-drive system components.

direction. However, it is not a major contributor to traction drive losses and its influence on energy consumption becomes apparent only when:

a. One or more motors are inoperative and must be "pulled" by the remaining motors.

b. The throttle is cycled between upper and lower bounds.

c. One attempts to determine the surface angle that will cause the LRV to move at a constant velocity with a zero throttle setting (coast angle).

5. To account for energy transfer and losses caused by the rotational inertias of the motor armature and the wheel during vehicle acceleration and deceleration, a combined inertia is used based on the rotational inertia of the wheel and the motor armature, the latter conditioned by the harmonic gear characteristics. These losses are usually small as compared with other losses incurred; however, they increase significantly with the increasing number of vehicle stops and frequency and rate of change of the throttle position.

6. Wheel/soil interaction characteristics, as discussed in the previous section, are considered in the form of torque-versus-slip and pull-versus-slip diagrams, as shown in Figure 8.

7. The damper losses are computed from the relation

$$P_d = \frac{K_r}{256} v_a^2 \quad , \quad (1)$$

in which P_d is the damper power loss (W), v_a is the vehicle speed (km/hr), K_r is a lunar surface roughness coefficient (dimensionless),

and 256 is a conversion factor. The coefficient K_r has been determined for four general types of lunar surface roughness, designated as Smooth Mare, Rough Mare, Hummocky Uplands, and Rough Uplands. Based on power spectral density estimates made by the USGS, as discussed in the previous section, the value of K_r varies between 17.5 and 300. Figure 14 shows typical damper losses as a function of vehicle speed for the four terrain types in order of increasing levels of lunar surface roughness, as well as pre-mission predictions and post-mission assessments relating to the roughness characteristics of the lunar surface encountered by the LRV during the Apollo 15 mission.

In the normal operating mode, the following steps are taken:

1. The weight supported by each wheel is calculated from prescribed slope angles and vehicle acceleration.

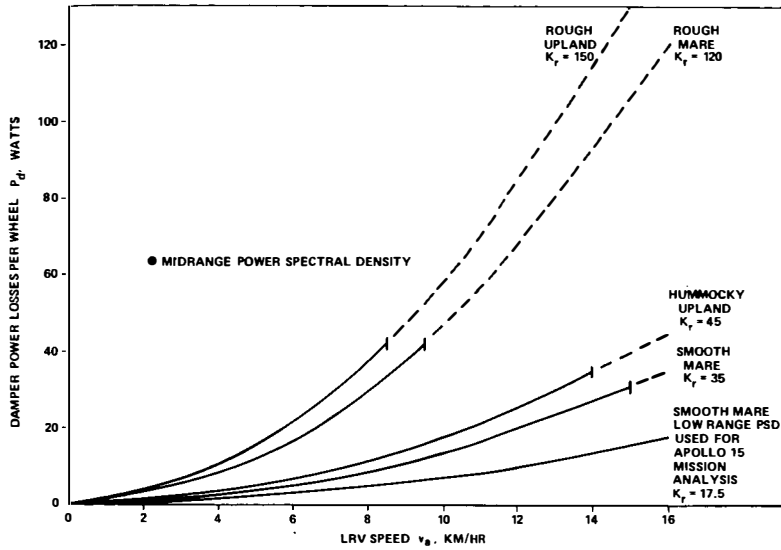
2. One of the following two criteria is considered: Either a throttle position is specified and the maximum vehicle speed compatible with that throttle setting is calculated, or a maximum vehicle speed is specified and the throttle position required to maintain this speed is determined.

3. The throttle position is used as the forcing function.

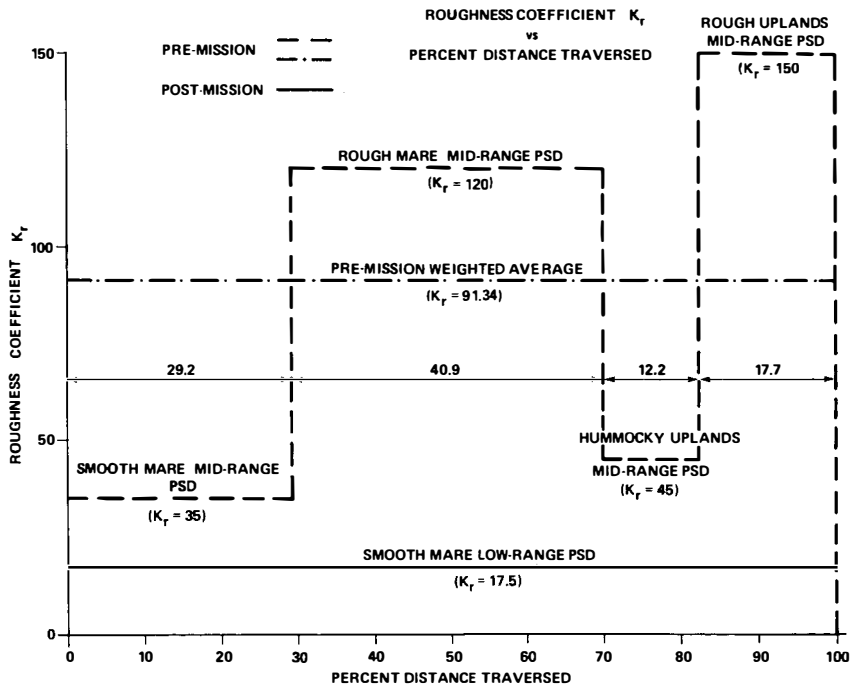
4. The motor torque is developed and transmitted to the wheel soil interface, conditioned by the characteristics of the harmonic gear and the combined inertias of the motor armature and wheel.

5. The wheel slip is determined from the torque-slip characteristics and is stored.

6. The pull developed by the wheel/soil interaction is determined from the pull-slip characteristics and the magnitude of wheel slip calculated in step 5.



a. DAMPER POWER LOSSES VERSUS LRV SPEED FOR VARIOUS ROUGHNESS COEFFICIENTS K_r



b. COMPARISON OF PRE-MISSION ESTIMATES AND POST-MISSION ASSESSMENTS OF LUNAR SURFACE ROUGHNESS AT APOLLO 15 LANDING SITE

Figure 14. Effect of lunar surface roughness characteristics on energy losses in LRV dampers.

7. The pull required at each wheel to cause vehicle motion is determined. This is accomplished by assuming that the pull-to-weight ratio (pull coefficient), after damper losses have been accounted for, is essentially equal to the tangent of the slope angle.

8. The pull developed, as determined in step 6, is compared with the pull required, as determined in step 7. If the pull developed equals the pull required, the vehicle is considered to propel itself at a constant speed. If the pull developed exceeds the pull required, the excess pull is used to calculate the rate of acceleration of the vehicle on the particular slope considered. Similarly, if the pull developed is less than the pull required, the difference between these values is used to compute the rate of deceleration of the vehicle.

9. Through successive time integrations, the vehicle acceleration or deceleration, combined with the initial speed conditions before the throttle positioning, is used to calculate the vehicle speed.

10. The vehicle speed determined in step 9 is used in conjunction with the wheel slip determined in step 5 to calculate a new wheel angular velocity, from which a new motor speed and torque are determined. Also, based on equation (1) and the lunar surface roughness characteristics prescribed on the slope considered, the vehicle speed is used to calculate damper energy losses and equivalent wheel torque accounting for these losses.

This cycle is repeated until the pull developed equals the pull required and the vehicle assumes a steady-state, constant speed for the particular throttle setting and lunar surface characteristics prescribed. If for a given throttle setting the maximum pull developed is less than the pull required, the setting is adjusted until the vehicle propels itself on the

particular lunar surface traverse segment considered or becomes immobilized in the event its limiting mobility performance capabilities cannot cope with the lunar surface conditions prescribed along the traverse path.

Through this computational process, the following quantities are obtained at the end of each traverse section:

1. Total energy used by the mobility system (W-h).
2. Energy consumption rate (W-h/km traversed).
3. Average speed (km/hr).
4. Total damper energy dissipated (W-h).
5. Average rate of damper energy dissipation (W-h/km).
6. Distance traversed (km).
7. Total time to complete the traverse (sec).

These output quantities are used in conjunction with another MSFC-developed computer program to calculate the energy dissipated in the following manner:

1. In operating the LRV navigation system and performance display console.
2. In steering the vehicle.
3. Through cable losses.

The sum of these losses and those of the traction drive system (blocks 8 and 9, Fig. 12) represents the total energy drawn from the batteries during a given traverse, as shown in block 10, Figure 12.

EVALUATION OF LRV MOBILITY PERFORMANCE DURING APOLLO 15

Lunar Surface Topography at the Hadley-Apennine Region

A map of the Apollo 15 landing site including the LRV traverses during the three periods of Extravehicular Activity (EVA) is shown in Figure 15. A comparison of pre-mission estimates and post-mission assessments of the slope distribution encountered along the LRV traverses during each of the three EVAs, as well as for the whole mission, can be made in Figure 16. The latter estimates were based on map distances corresponding to lunar surface linear segments ranging between 100 and 500 m. The topographic data used to obtain slope ranges was a 1 : 15 840 - scale topographic map compiled by NASA MSC from Orbiter V photographs with a photographic resolution of 20 m [58].

Before egressing to the lunar surface from the LM and deploying the LRV, the Apollo 15 crew visually assessed the lunar surface characteristics during a Standup EVA (SEVA). From these observations, only a small percentage of the surface appeared to be covered with fragmental debris. The crew further remarked that the gently undulating, hummocky profile of the lunar surface in the vicinity of the landing site looked very much like the Fra Mauro (Apollo 14) topography; in general, it appeared that the surface would offer no trafficability problems to the LRV. As shown by TV and surface photography, the Mare region at the site is indeed gently undulating and although abundantly cratered, a very small percentage of surface area is strewn with blocky debris. Craters near the LM, although 25 to 30 m in diameter, had smooth interiors and very small amounts of blocky ejecta, indicating that the fragmental layer was relatively thick at this site.

In terms of surface roughness, the entire area traversed by the LRV can now be classified a Smooth Mare surface; however, some photography does show blocky craters and crew comments indicate other types of long-wavelength roughness, as indicated by the series of large depressions of swales (apparently very old subdued craters), which were traversed by the LRV during EVA III. Figure 17 shows increasing levels of lunar surface roughness encountered during the Apollo 15 LRV traverses [58].

A comparison between pre-mission estimates and post-mission assessments of the lunar surface roughness characteristics in terms of power spectral density distributions can be made from the graphs shown in Figure 14b. By comparing the weighted average value of the pre-mission estimates on the roughness coefficient K_r with the current assessments, it can be seen that the power losses on the dampers may have been overestimated in pre-mission LRV power profile analyses by a factor of 5.2.

Lunar Soil Mechanical Properties

The Apollo 15 mission provided a greater opportunity for the study of the physical and mechanical properties of the lunar surface than any other previous mission. This enhancement in scientific returns resulted not only from the extended stay time and the high-mobility capability provided by the LRV but also from four new soil mechanics data sources, which became available for the first time during the Apollo program. These were:

1. The Self-Recording Penetrometer (SRP).
2. New, larger-diameter, thin-walled core tubes.
3. The LRV.
4. The Apollo Lunar Surface Drill (ALSD).

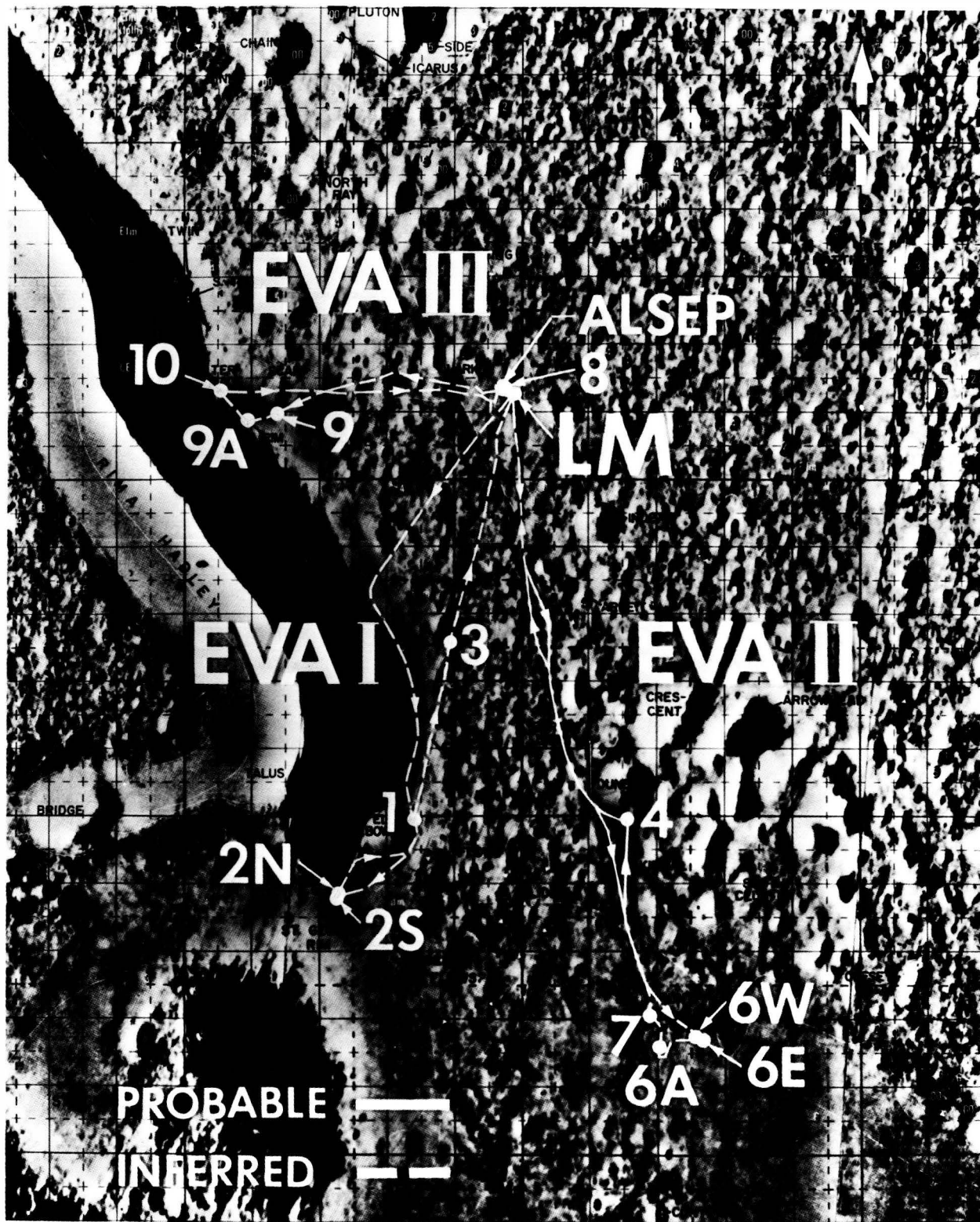


Figure 15. Map of Apollo 15 landing site at Hadley-Apennine region with LRV traverses during EVAs I, II, and III.

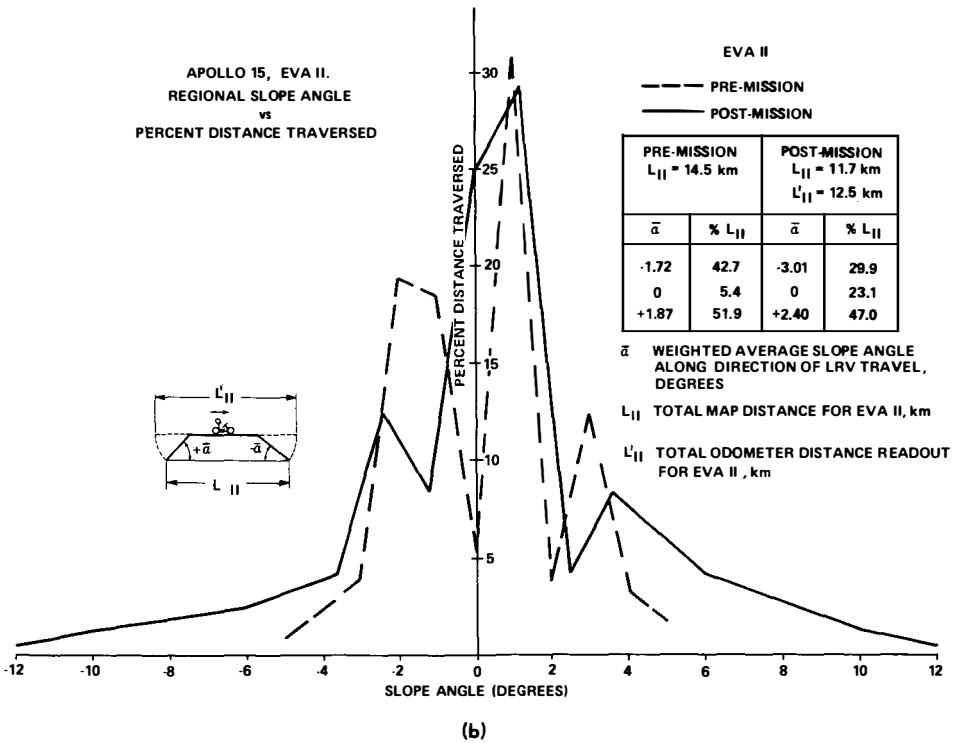
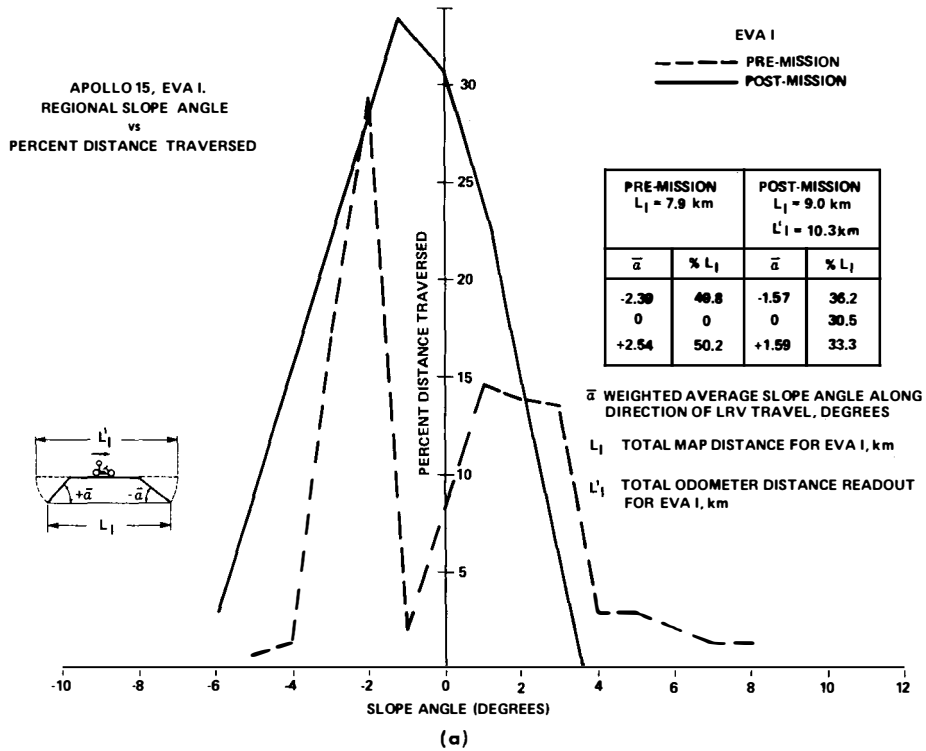
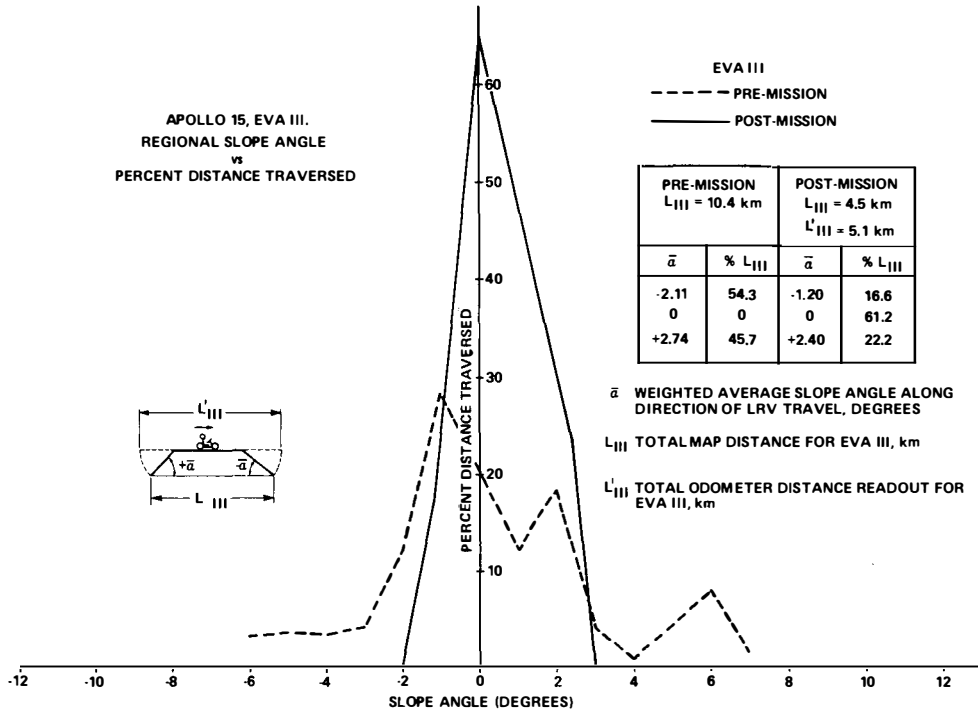
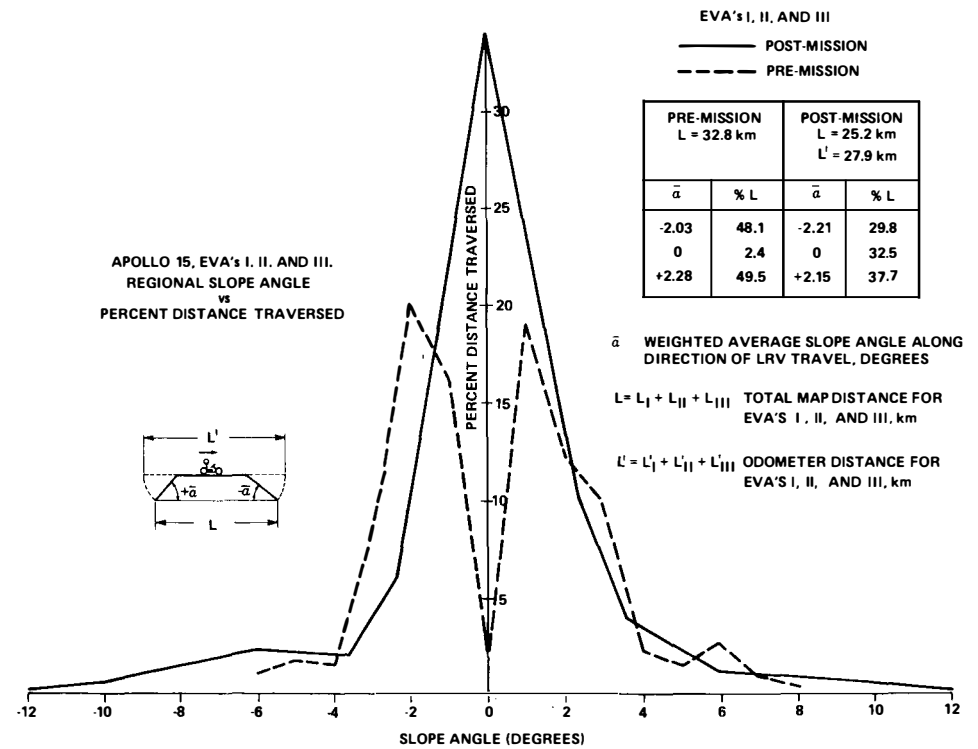


Figure 16. Comparison of pre-mission estimates and post-mission assessments of slope distributions encountered along LRV traverses during Apollo 15 mission.



(c)

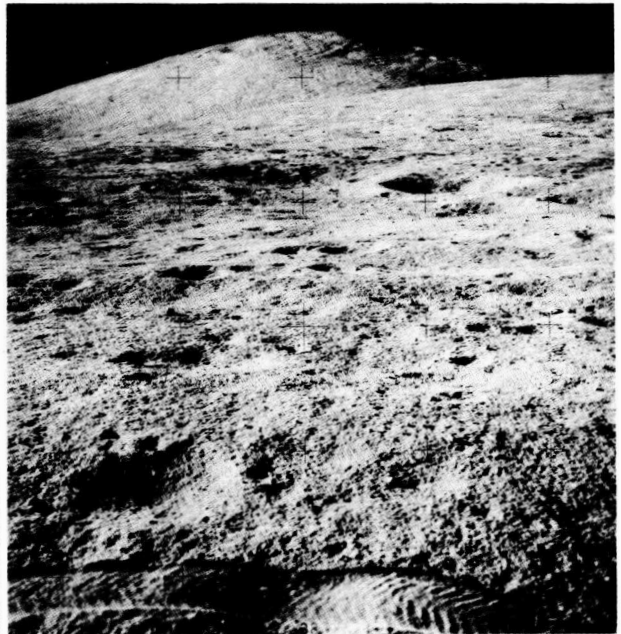


(d)

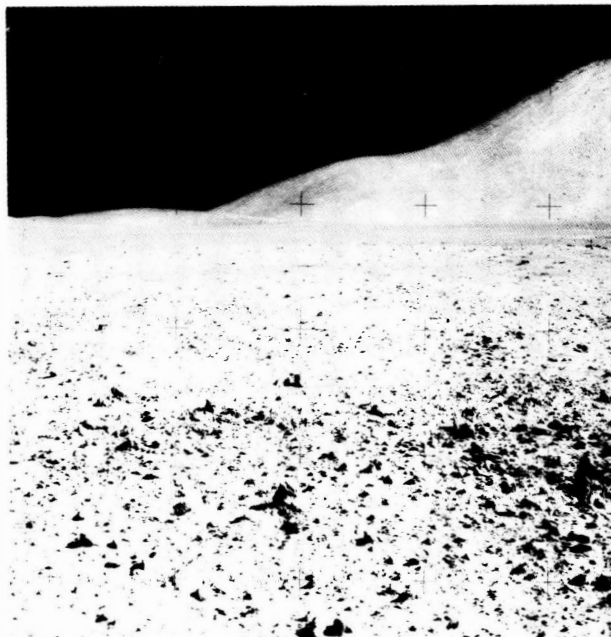
Figure 16. (Concluded).



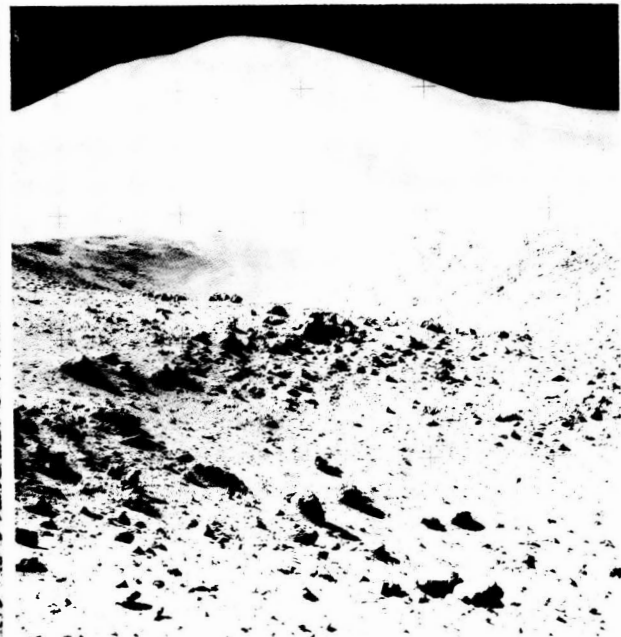
a. SMOOTH MARE, VIEWED FROM STATION 8, EVA II



b. GENTLY UNDULATING TERRAIN NEAR STATION 2, EVA I



c. SPARSE BOULDER FIELD (BOULDER SIZE
15 TO 20 CM) NEAR STATION 9, EVA III
NOTE LRV TRACKS IN THE MIDDLE OF THE PHOTO.



d. BOULDER FIELD AT THE RIM OF HADLEY RILLE

Figure 17. Increasing levels of lunar surface roughness at Hadley-Apennine region.

These data sources provided the best bases for quantitative soil mechanics analyses made thus far in the Apollo program.

The SRP (Fig. 18c) was developed at the Geotechnical Research Laboratory of the MSFC Space Science Laboratory [7] and was built and flight-qualified at MSC. The instrument can be operated by one astronaut. It weighs 23 N (5 lb) on earth, can penetrate to a maximum depth of 76 cm (30 in.) and, through a spring-loading mechanism, can apply a maximum force of 111 N (25 lb). During operation it is attached to an extension handle that can also be fitted to other hand tools used during the geological traverses. The force-penetration records are inscribed on a cylindrical drum contained in the upper housing assembly, which is returned to earth. With the present instrument configuration, force-penetration diagrams, each carried to the maximum force capacity of the loading spring, can be obtained from 24 different locations on the lunar surface during an Apollo mission. Three conical tips with a 30-deg apex and base areas of 1.29 cm² (0.2 in.²), 3.22 cm² (0.5 in.²), and 6.45 cm² (1.0 in.²) are available for attachment to the penetration shaft, as well as a 2.54-by-12.7-cm (1-by-5-in.) rectangular bearing plate.

During the Apollo 15 mission, the 3.22-cm² base area cone and the bearing plate were used for a series of four cone penetrations and two bearing plate measurements at Station 8 toward the end of EVA II. Two of the cone penetration measurements were made within and adjacent to an LRV track, and the other two were made adjacent to and at the bottom of a 30-cm deep trench with a vertical side wall (Fig. 18a, b). The trench wall was subsequently forced to failure (Fig. 18d) by loading at the top surface with the bearing plate attached to the SRP and positioned with the long side parallel to the trench wall edge at a distance of about 10 cm from the edge.

The cone penetration data are shown in Table 4 [5, 6, 17] and Figure 19a [5]. An analysis of these data, in conjunction with a slope stability analysis applied to the loading conditions that induced failure to the trench wall (Fig. 19b), indicated that the soil cohesion and friction angle at the trench location are of the order of 1.0 kN/m² (0.15 lb/in.²) and 50 deg, respectively [5, 6]. Both values are higher than the cohesion and angle of internal friction estimates made for other Apollo sites [2-4]; however, they are consistent with the very high density and relatively fine-grained consistency of the lunar soil at Station 8.

The core tubes used in the Apollo 15 mission were developed for the following purposes:

1. To reduce the amount of sample disturbance.
2. To increase the size and amount of sample recovered.
3. To facilitate the ease of sampling by the crew.

The new thin-walled tubes shown in Figure 20b [5] are made of aluminum and are 37.5 cm (14.75 in.) long. Individual tubes can be used as single units or in combination. A comparison of core tube bits used in the Apollo 15 mission with those used in previous Apollo missions is shown in Figure 20a. The larger diameter and reduced wall thickness used for the Apollo 15 core tubes resulted in the acquisition of much less disturbed samples than in previous missions. Accordingly, the densities of these samples can be considered to be more representative of the in-place density of the lunar soil than those obtained from core tube samples before the Apollo 15 mission [6].

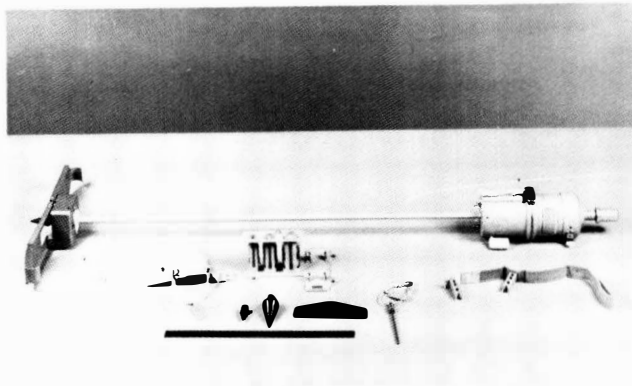
The in-place density at each of the core tube locations is determined by correcting the



a. DIGGING SOIL MECHANICS TRENCH WITH SCOOP ATTACHED TO EXTENSION HANDLE



b. EXPOSED VERTICAL SIDE OF TRENCH WALL



c. SELF-RECORDING PENETROMETER (SRP) WITH CONICAL TIP AND BEARING-PLATE ATTACHMENTS

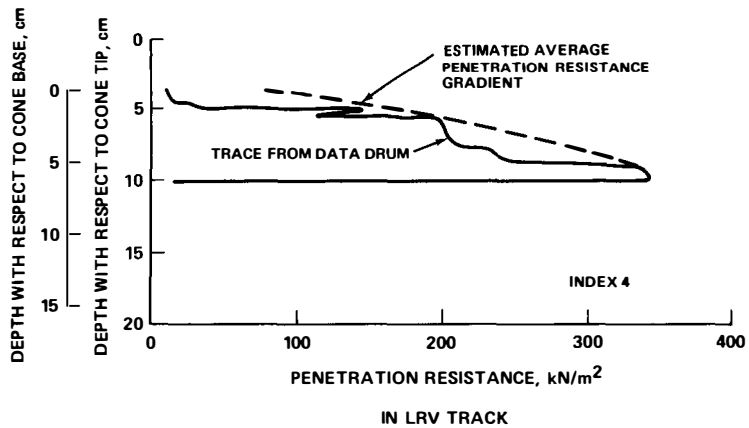
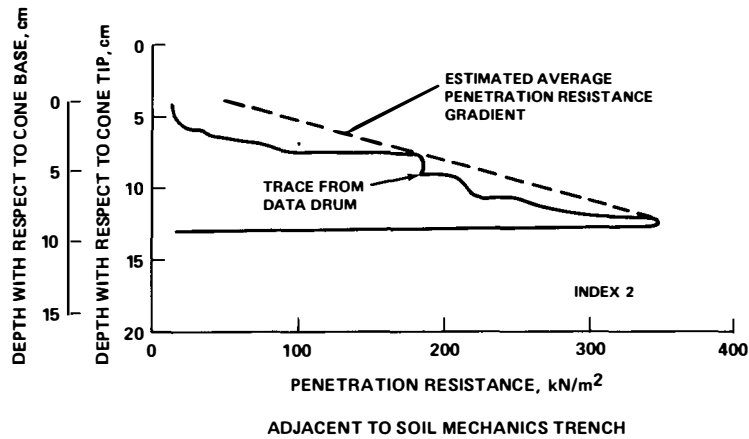


d. TRENCH AFTER COLLAPSE OF VERTICAL WALL SIDE. NOTE IMPRINT OF SRP GROUND REFERENCE PAD ADJACENT TO COLLAPSED TRENCH WALL

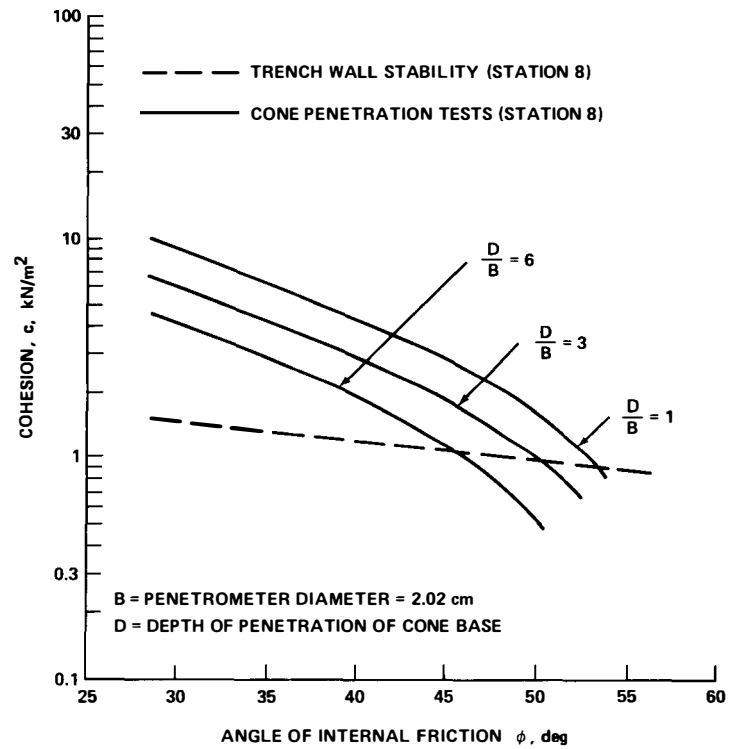
Figure 18. Trenching operations at Station 8, end of EVA II.

TABLE 4. CONE PENETRATION RESISTANCE TEST RESULTS FROM
 APOLLO 15 AND LUNA 17 LANDING SITES

Apollo 15 (Hadley-Apennine, Station 8) [Cone: 30 deg Apex; Base Area 3.23 cm ² (0.5 in. ²)]				
Location	Penetration Depth (cm)	Average Penetration Resistance Gradient		Data Source
		(MN/m ³)	(lb/in. ³)	
Adjacent to Trench	8.25	4.06	15	Mitchell et al., (1972) [5, 6]
Bottom of Trench	<10.25	>3.25	>12	
In LRV Track	5.25			
Upper 2 cm		5.97	20-24	
Lower 4 cm		4.36	16	
Adjacent to LRV Track	<11.25	2.98	>11	
Luna 17 (Mare Imbrium, Lunokhod-1 Traverses) [Cone: 60 deg Apex; Base Area 19.63 cm ² (3.04 in. ²)]				
Level Intercrater Region	0-5	0.75	2.76	Leonovich et al., (1971) [17]
	5-8	1.25	4.60	
Crater Slope	0-5	1.16	4.27	
	5-7.3	4.78	17.6	
Crater Wall	0-5	0.40	1.47	
	5-8	2.51	9.25	
Surface Sector Covered by Small Rocks	0-5	2.40	8.84	



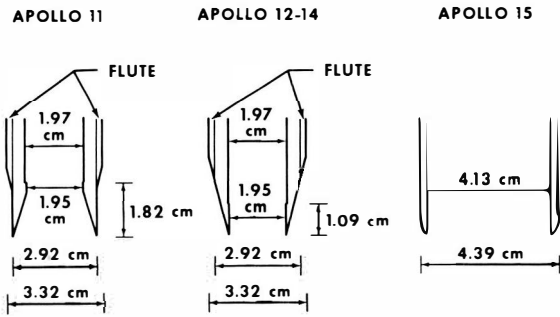
a. FORCE-PENETRATION DIAGRAMS INSCRIBED ON SRP DRUM



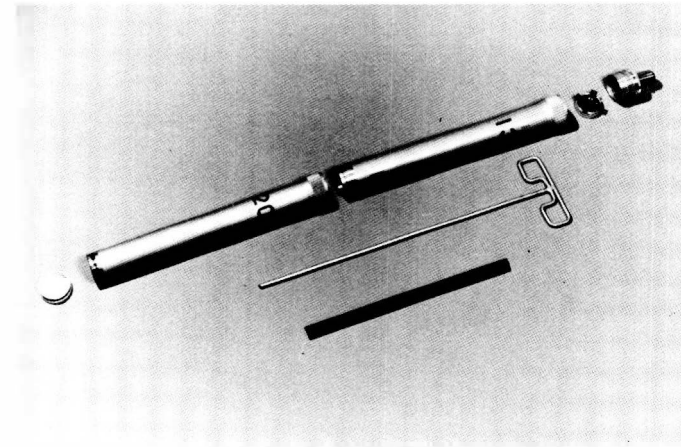
b. SOIL COHESION AND FRICTION ANGLE AT STATION 8, DETERMINED FROM TRENCH WALL STABILITY AND CONE PENETRATION RESISTANCE DATA ANALYSIS

Figure 19. Analysis of data obtained by Self-Recording Penetrometer [5].

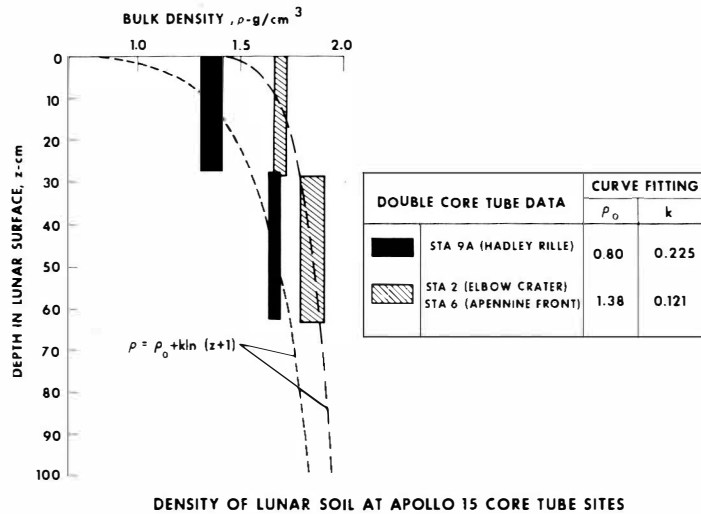
COMPARISON OF CORE TUBE BITS



(a)



(b)



(c)

APOLLO 15 MISSION SOIL CHARACTERISTICS AT STATION 8 (NEAR THE ALSEP SITE),

	POROSITY, n %	VOID RATIO e	DENSITY, ρ^* gm/cm ³	FRICTION ANGLE ϕ
RANGE	35-38	0.54-0.61	1.92-2.01	47.5-51.5
BEST ESTIMATE	36.5	0.58	1.97	49.5

*ASSUMES AVERAGE SPECIFIC GRAVITY OF SOIL GRAINS TO BE 3.1.

(d)

Figure 20. Apollo 15 core tubes and soil bulk density data [5].

bulk density in the tubes for the disturbance caused by sampling [5, 6, 26, 27]. However, since the percentage of core recoveries was high, the anticipated corrections will be very small. Accordingly, preliminary estimates of the variation of density with depth for the three Apollo 15 core tube locations have been made [6] and are shown in Figure 20c.

The in-place density at the soil mechanics trench at Station 8 has been estimated to range between 1.92 and 2.01 g/cm³, based on penetration test results and terrestrial simulations⁸ [7, 42, 59]. The corresponding values of the void ratio and angle of internal friction of the soil at the same location are shown in Figure 20d. The void ratio estimates were based on the assumption that the specific gravity of the soil particles is 3.1, i.e., that it was the same as that obtained from soil samples collected from the Apollo 11 and Apollo 12 missions.

The density of the soil samples collected with the deep drill (ALSD) stem from the same area at Station 8 near the trench has been estimated to range from 1.62 to 2.15 g/cm³ [28], with an average value of the order of 1.8 g/cm³.

From these data and visual observations, it is indicated that although the lunar surface at the Hadley-Apennine site is similar in color, texture, and general behavior to that at the previous Apollo sites, there is considerable variability in soil properties, as reflected by bulk density, strength, and compressibility, both with depth and with lateral position. Lateral variations are both regional, as characterized by conditions ranging from soft, compressible soil along the Apennine Front, to firmer, relatively incompressible soil near the rim of Hadley Rille, and local, as can be seen from the variable depth of astronaut footprints and LRV tracks (Figs. 21 and 22).

LRV Mobility Performance at Hadley-Apennine

Since the LRV had no onboard instrumentation for continuous monitoring of its performance and interaction with the lunar surface while in motion, the only quantitative data on the vehicle performance that were considered in pre-mission planning were based on the following data sources:

1. Periodic readouts by the crew of the display console indicators.
2. Crew descriptions and photographic documentation of the lunar surface conditions.
3. Photographic documentation of the vehicle's interaction with the lunar surface under controlled conditions, in conjunction with simultaneous readouts of the vehicle's speedometer and amp indicators.

The last task just listed was initiated by the authors⁹ and was designated as the Lunar Grand Prix. Its purpose was to obtain quantitative data on the torque/wheel-slip characteristics and dynamic interaction of the LRV with the lunar surface in the lunar environment.

In addition to other performance data, the Grand Prix task was anticipated to yield quantitative information that would allow a direct assessment of the following:

- a. The self-propelled point of the vehicle, defined as the wheel slip at which the net pull on the vehicle is zero.
- b. The maximum vehicle speed attained on the lunar surface.

8. Costes, Hadjidakis, Holloway, Olson, and Smith, op. cit.

9. Memo S&E-ASTR-SD-71, Jan. 12, 1971, from Director, Astrionics Laboratory, and Director, Space Sciences Laboratory, to Director, Science and Engineering, MSFC; subject: "Evaluation of the LRV Mobility Performance under in-situ Environmental Conditions."



a. NEAR RIM OF HADLEY RILLE, STATION 10, EVA III



b. SOFT RIMMED CRATER NEAR LM TRAVERSED DURING EVA I.
MOUNT HADLEY IN THE BACKGROUND



c. MARE REGION IN THE VICINITY OF THE LM LANDING SITE



d. SOFT-RIMMED CRATER NEAR ST. GEORGE CRATER, STATION 2, EVA I
HADLEY RILLE IN BACKGROUND

Figure 21. Variability in lunar surface hardness.



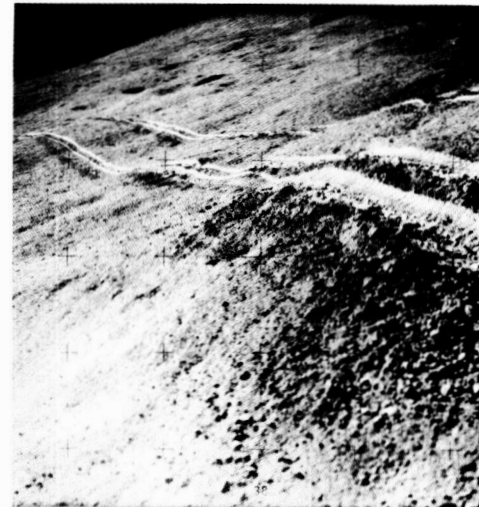
a. FIRM SOIL AT STATION 8, EVA II



b. SOFT SOIL REGION AT STATION 6A, APENNINE FRONT, DURING EVA II



c. LRV TRACKS CONTRASTED WITH ASTRONAUT BOOT PRINTS NEAR STATION 6



d. LRV WHEEL TRACKS ALONG SLOPE CONTOUR NEAR STATION 6A, APENNINE FRONT, EVA II

Figure 22. LRV wheel-soil interaction at various locations of the Hadley-Apennine region.

c. The dynamic response of the vehicle under steady-state velocity and during acceleration and deceleration periods.

d. The minimum braking distances necessary to achieve a complete stop.

e. The amount and extent of dust generated and ejected as a result of the wheel-soil interaction.

f. The validity of wheel-soil interaction inputs to the power profile computer program, independent of periodic crew observations on the lunar surface conditions and readouts on power consumption and distance traveled at different points along the traverses.

Photographic documentation for the Lunar Grand Prix was to be provided by the Data Acquisition Sequence Camera (DAC), equipped with a 10-mm lens and set at a rate of film advance of 24 frames/sec. The DAC would be operated by the LM Pilot (Astronaut J. Irwin) standing on the lunar surface and pointing the camera at an optimum phase angle (angle between the sun, the point being observed, and the observer), while the LRV would be driven by the Commander (Astronaut D. Scott) along a course normal to the line of site of the camera and at a distance of approximately 20 m from the camera position.

As shown in Figures 3 and 4, black stripes were painted diametrically across the LRV wheel hubs. Measurements of the relative angular position of these stripes in successive frames of the film taken by the DAC, which is advanced at a known fixed rate, would provide quantitative information for determining the angular velocity of the wheels. These data, combined with data on the translational speed of the vehicle obtained by measuring the relative position of the LRV with respect to fixed objects on the lunar surface shown in successive frames of the DAC film, in conjunction with the LRV speedometer readouts and estimates on the rolling radius of the LRV wheels, would provide the necessary

information for calculating the wheel slip during the Grand Prix operations.

Terrestrial simulations had indicated that very accurate estimates of wheel slip result from these measurements. Unfortunately, because of a malfunction of the film-advance mechanism of the DAC, this task, although performed at the beginning of EVA III, could not be documented. Accordingly, only visual, qualitative observations made by the crew are available.

The disappointment at the Grand Prix photographic coverage was offset by a highly informative, concise, and objective post-mission Pilot's Report, submitted by the Apollo 15 crew [60]. Following are excerpts covering aspects of the vehicle's mobility performance and interaction with the lunar surface.

The performance of the vehicle was excellent. The lunar terrain conditions in general were very hummocky, having a smooth texture and only small areas of fragmental debris. A wide variety of craters was encountered. Approximately 90 percent had smooth, subdued rims which were, in general, level with the surrounding surface. Slopes up to approximately 15 percent were encountered. The vehicle could be maneuvered through any region very effectively. The surface material varied from a thin powdered dust (which the boots would penetrate to a depth of 2 to 3 inches on the slope of the Apennine Front) to a very firm rille soil which was penetrated only a quarter inch to a half inch by the boot. In all cases, the rover's performance was changed very little.

The velocity of the rover on the level surface reached a maximum of 13 kilometers per hour. Driving

directly upslope on the soft surface material at the Apennine Front, maximum velocities of 10 kilometers per hour were maintained. Comparable velocities could be maintained obliquely on the slopes unless crater avoidance became necessary. Under these conditions, the downhill wheel tended to dig in and the speed was reduced for safety.

Acceleration was normally smooth with very little wheel slippage, although some soil could be observed impacting on the rear part of the fenders as the vehicle was accelerated with maximum throttle. During a "Lunar Grand Prix," a roostertail was noted above, behind, and over the front of the rover during the acceleration phase. This was approximately 10 feet high and went some 10 feet forward of the rover. No debris was noted forward or above the vehicle during constant velocity motion. Traction of the wire wheels was excellent uphill, downhill, and during acceleration. A speed of 10 kilometers per hour could be attained in approximately three vehicle lengths with very little wheel slip. Braking was positive except at the high speeds. At any speed under 5 kilometers per hour, braking appeared to occur in approximately the same distance as the 1-g trainer. From straight-line travel at velocities of approximately 10 kilometers per hour on a level surface, the vehicle could be stopped in a distance of approximately twice that experienced in the 1-g trainer. Braking was less effective if the vehicle was in a turn, especially at higher velocities.

Dust accumulation on the vehicle was considered minimal and only very small particulate matter accumulated over a long period of time. Larger particles appeared to be controlled very well by the fenders. The majority of the dust accumulation occurred on the lower horizontal surfaces such as floorboards, seatpans, and the rear wheel area. Soil accumulation within the wheels was not observed. Those particles which did pass through the wire seemed to come out cleanly. Dust posed no problem to visibility.

Obstacle avoidance was commensurate with speed. Lateral skidding occurred during any hardover or maximum-rate turn above 5 kilometers per hour. Associated with the lateral skidding was a loss of braking effectiveness. The suspension bottomed out approximately three times during the entire surface activity with no apparent ill effect. An angular 1-foot-high fragment was traversed by the left front wheel with no loss of controllability or steering, although the suspension did bottom out. A relatively straightline traverse was easily maintained by selection of a point on the horizon for directional control, in spite of the necessity to maneuver around the smaller subdued craters. Fragmental debris was clearly visible and easy to avoid on the surface. The small, hummocky craters were the major problem in negotiating the traverse, and the avoidance of these craters seemed necessary to prevent controllability loss and bottoming of the suspension system.

Vehicle tracks were prominent on the surface and very little variation of depth occurred when the bearing on all four wheels was equal. On steep slopes, where increased loads were carried by the downhill wheels, deeper tracks were encountered – perhaps up to an inch or two in depth. There was no noticeable effect of driving on previously deposited tracks, although these effects were not specifically investigated. The chevron tread pattern left distinct and sharp imprints. In the soft, loose soil at the Apollo lunar surface experiment package site, one occurrence of wheel spin was corrected by manually moving the rover to a new surface.

The general stability and control of the lunar roving vehicle was excellent. The vehicle was statically stable on any slopes encountered and the only problem associated with steep slopes was the tendency of the vehicle to slide downslope when both crewmen were off the vehicle. The rover is dynamically stable in roll and pitch. There was no tendency for the vehicle to roll even when travelling upslope or downslope, across contour lines or parallel to contour lines. However, qualitative evaluation indicates that roll instability would be approached on the 15-degree slopes if the vehicle were travelling a contour line with one crewmember on the downhill side. Both long- and short-period pitch motions were experienced in response to vehicle motion over the cratered, hummocky terrain, and the motion introduced by individual wheel obstacles. The long-period motion was very similar to that encountered

in the 1-g trainer, although more lightly damped. The “floating” of the crewmembers in the 1/6-g field was quite noticeable in comparison to 1-g simulations. Contributions of short-period motion of each wheel were unnoticed and it was difficult to tell how many wheels were off the ground at any one time. At one point during the “Lunar Grand Prix,” all four wheels were off the ground, although this was undetectable from the driver’s seat.

Maneuvering was quite responsive at speeds below approximately 5 kilometers per hour. At the speeds on the order of 10 kilometers per hour, response to turning was very poor until speed was reduced. The optimum technique for obstacle avoidance was to slow below 5 kilometers per hour and then apply turning correction. Hardover turns using any steering mode at 10 kilometers per hour would result in a breakout of the rear wheels and lateral skidding of the front wheels. This effect was magnified when only the rear wheels were used for steering. There was no tendency toward overturn instability due to steering or turning alone. There was one instance of breakout and lateral skidding of the rear wheels into a crater approximately 1-1/2 feet deep and 4 feet wide. This resulted in a rear wheel contacting the far wall of the crater and subsequent lateral bounce. There was no subsequent roll instability or tendency to turn over, even though visual motion cues indicated a roll instability might develop.

The response and the handling qualities of the control stick are considered adequate. The

hand controller was effective throughout the speed range, and directional control was considered excellent. Minor difficulty was experienced with feedback through the suited crewmember to the hand controller during driving. However, this feedback could be improved by a more positive method of restraint in the seat. Maximum velocity on a level surface can be maintained by leaving the control stick in any throttle position and steering with small inputs left or right. A firm grip on the handle at all times is unnecessary. Directional control response is excellent although, because of the many dynamic links between the steering mechanism and the hand on the throttle, considerable feedback through the pressure suit to the control stick exists. A light touch on the hand grip reduces the effect of this feedback. An increase in the lateral and breakout forces in the directional hand controller should minimize feedback into the steering.

Two steering modes were investigated. On the first extravehicular activity, where rear-wheel-only steering was available, the vehicle had a tendency to dig in with the front wheels and breakout with the rear wheels with large, but less than hardover, directional corrections. On the second extravehicular activity, front-wheel-only steering was attempted, but was abandoned because of the lack of rear wheel centering. Four-wheel steering was utilized for the remainder of the mission. It is felt that for the higher speeds, optimum steering would be obtained utilizing front-steering

providing the rear wheels are center-locked. For lower speeds and maximum obstacle avoidance, four-wheel steering would be optimal. Any hardover failure of the steering mechanism would be recognized immediately and could be controlled safely by maximum braking.

Forward visibility was excellent throughout the range of conditions encountered with the exception of driving toward the zero-phase direction. Washout, under these conditions, made obstacle avoidance difficult. Up-sun was comparable to cross-sun if the opaque visor on the lunar extravehicular visor assembly was lowered to a point which blocks the direct rays of the sun. In this condition, crater shadows and debris were easily seen. General lunar terrain features were detectable within 10 degrees of the zero phase region. Detection of features under high-sun conditions was somewhat more difficult because of the lack of shadows, but with constant attention, 10 to 11 kilometers per hour could be maintained. The major problem encountered was recognizing the subtle, subdued craters directly in the vehicle path. In general, 1-meter craters were not detectable until the front wheels had approached to within 2 to 3 meters.

The reverse feature of the vehicle was utilized several times, and preflight-developed techniques worked well. Only short distances were covered, and then only with a dismounted crewmember confirming the general condition of the surface to be covered.

The 1-g trainer provides adequate training for lunar roving vehicle operation on the lunar surface. Adaptation to lunar characteristics is rapid. Handling characteristics are quite natural after several minutes of driving. The major difference encountered with respect to preflight training was the necessity to pay constant attention to the lunar terrain in order to have adequate warning for obstacle avoidance if maximum average speeds were to be maintained. Handling characteristics of the actual lunar roving vehicle were similar to the 1-g trainer with two exceptions: braking requires approximately twice the distance, and steering is not responsive in the 8- to 10-kilometer range with hardover control inputs. Suspension characteristics appeared to be approximately the same between the two vehicles and the 1/6-g suspension simulation is considered to be an accurate representation with the exception of the crewmember's weight.

The navigation system is accurate and a high degree of confidence was attained in a very short time. Displays are also adequate for the lunar roving vehicle systems.

These observations made by the Apollo 15 crew on the wheel-soil interaction and vehicle performance are corroborated by numerous still photographs of the lunar surface activities and a short movie taken from the LRV while in motion during EVA II. The small amount of wheel sinkage observed is attributed to the low ground pressure exerted by the LRV wheels on the lunar surface. This low pressure resulted partly from the light wheel load, which on level terrain was of the order of 290 N (65 lb), and partly from the flexibility of the

wire-mesh wheel. The effect of differences in the relative stiffness of the LRV wheel and the sole of the astronaut boot with respect to the lunar surface soil at Station 6 on the corresponding sinkage can be seen in Figure 21c. The average unit pressure exerted on the lunar surface by each of the LRV wheels and by one astronaut boot due to the weight of the suited astronaut in lunar gravity is of the order of 7 kN/m^2 (1 lb/in.^2). However, the astronaut boot sole is much stiffer than the LRV wheel. In addition, it appears that the dynamic conditions under which the corresponding loads by the LRV wheel and the astronaut boot were transmitted to the lunar soil, and associated kinetic energy and momentum transfer, were different in the two cases.

The fact that the LRV wire-mesh wheel developed excellent traction with the lunar surface and in most cases a shallow and sharp imprint of the chevron tread was clearly discernible indicates that the soil possessed a small but finite amount of cohesion and that the amount of wheel slip was minimal. The latter observation is corroborated by the small error of traverse closure (less than 200 m in each EVA) in the odometer and navigation systems, which had been calibrated with a constant wheel-slip bias of 2.3 percent. A reported average wheel sinkage of the order of 1.25 cm (0.5 in.) at a wheel slip of 2.3 percent agrees with the data obtained from the WES wheel-soil interaction tests (Fig. 10). In general, the wheel sinkage varied between an imperceptible amount and about 5 to 7 cm (2 to 3 in.). High wheel sinkage was usually developed while the vehicle was traversing soft-rimmed, small-diameter, fresh craters.

At higher wheel slips, as was the case with the wheel spinout at Station 8 near the ALSEP¹⁰ site, the wheels dug into the lunar soil to a depth of approximately 13 cm (5 in.); i.e., down to the lower part of the wheel rim. This behavior is again in agreement with the trends of the WES wheel-soil interaction tests on lunar soil simulants. The apparent looseness of the

10. ALSEP – Apollo Lunar Surface Experiments Package.

soil at this location can be attributed either to disturbance of the soil caused by the general activities at Station 8 during the installation of the ALSEP package, which consists of a central control and communications station, a radioisotope thermoelectric generator (RTG), and scientific instruments associated with lunar surface geophysical experiments, or to local variations in the soil consistency. This is because, as discussed previously, information obtained from other sources and relating to the mechanical properties of the lunar soil at the ALSEP site indicates that the material in this area is, in general, firm.

On the basis of crew observations and photographic coverage, it appears that the Rover was operated on slopes with slope angles ranging from 0 to 12 deg. Some of the highest slopes on which the vehicle was operated were the Apennine Front near Station 6 during EVA II. One of these slopes is shown in Figure 23. The slope angle in this location is estimated to be of the order of 10 to 12 deg. Figure 21d shows the LRV tracks in the same general area (Station 6A), which were developed by the vehicle traversing along the slope contour.

Because of the vehicle's light weight and the excellent traction developed by the wire-mesh wheel on the lunar soil, its general performance while traversing either along slope gradients or slope contours was apparently very satisfactory. On the basis of the WES wheel-soil interaction tests on lunar soil simulants performed before the mission, the maximum slope angle that could be negotiated by the LRV had been estimated to be of the order of 18 to 23 deg (see, for instance, Figs. 8, 9, and 11). It appears, therefore, that the slopes that were actually negotiated at the Hadley-Apennine region represented at most 62 percent of the vehicle's estimated maximum slope-climbing capability. If the specified maximum slope of 25 deg is actually the limiting slope that can be negotiated by the LRV on the lunar surface, the slopes negotiated at the Apollo 15 site would then

represent about 46 percent of the vehicle's limiting performance capability.

In general, it can be stated that no direct quantitative information exists regarding the limiting mobility performance capabilities of the LRV at the Hadley-Apennine region because:

1. The mission profile was well within the expected capabilities of the Rover.
2. The vehicle was never operated under performance-limiting conditions or under degraded operating modes, except for a front-steering failure during EVA I.
3. The Lunar Grand Prix task could not be documented.
4. The amount of energy remaining in the LRV batteries at the end of the LRV traverses cannot be assessed because, as a result of some malfunction of the switch breaker, the batteries could not be operated to complete depletion upon the end of the mission.

LRV Power Profile Analysis

The available soil mechanics data from the Apollo 15 site, as well as from the previous three Apollo missions [4, 7] and the Mare Imbrium area at the Luna 17 landing site traversed by the Lunokhod-1 [17], indicate that the range of the average rate of the resistance to penetration of the lunar soil with depth at these sites is within the range of the penetration resistance gradient G of the lunar soil simulants used in the WES wheel-soil interaction tests. Tables 3 and 4 list the local and regional variations in the values of G for the lunar soil, obtained from the Fra Mauro site during the Apollo 14 mission, at Station 8 during the Apollo 15 mission and at various locations traversed by Lunokhod-1. As shown in Figure 11b, these ranges are encompassed by the G values characterizing the lunar soil simulants LSS_1 through LSS_5 .

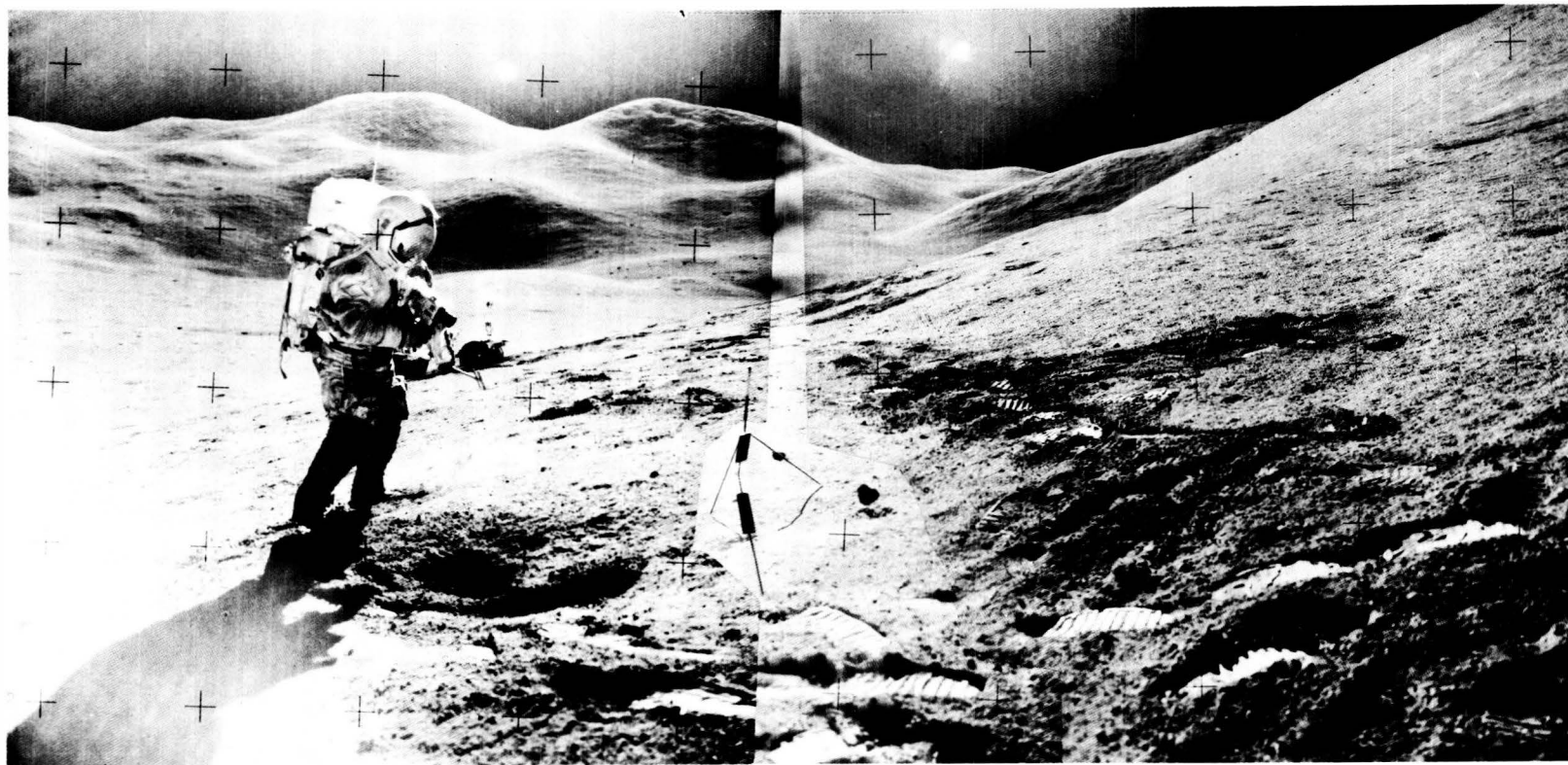


Figure 23. LRV parked along slope gradient at Station 6, Apennine Front, during EVA II.

From these considerations and because the available information indicates that the soil conditions at the Hadley-Apennine region were variable, with the density and shear strength characteristics measured at Station 8 representing upper limiting values, the post-mission LRV power profile analysis considered all data available from the WES wheel-soil interaction tests. Accordingly, computer estimates on the wheel slip and maximum speed attainable by the vehicle on a given slope at full throttle and on the LRV traction-drive system energy consumption rate (ECR) during EVA I were made on the basis of these data and post-mission assessments relating to:

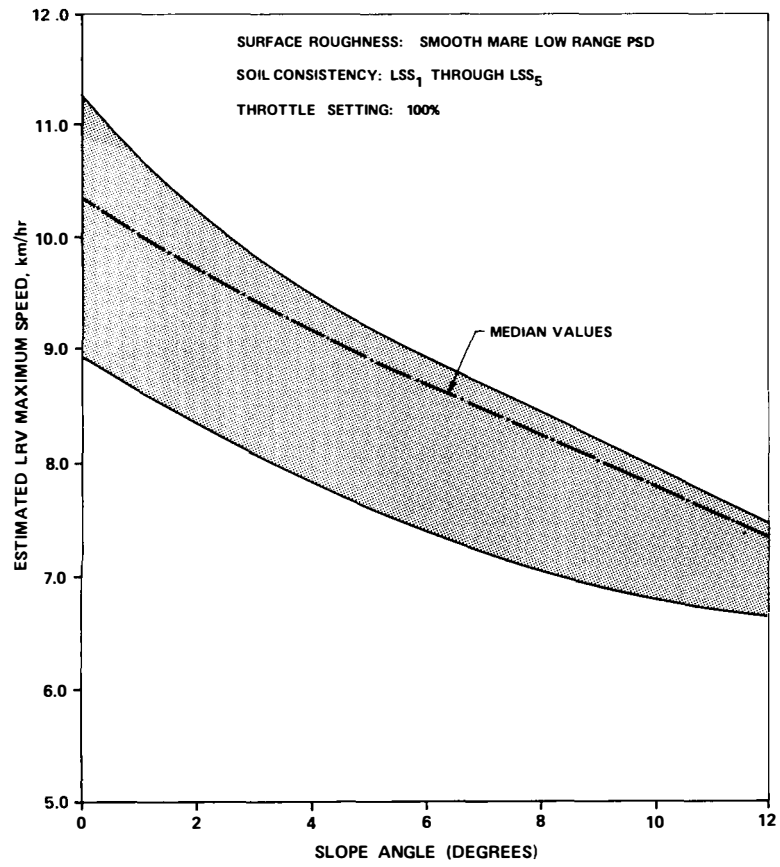
1. Slope distribution and roughness characteristics of the lunar surface.
2. The distance traversed and the average vehicle speed attained in each traverse segment of the three EVAs.
3. The driving time and time spent at stops during each of the three EVAs.
4. The average duty cycle in steering to avoid obstacles.

The results of the first two sets of calculations are shown in Figure 24. It appears that the computed wheel slip and vehicle speed values agree with observations and comments by the crew, who reported that the maximum indicated vehicle speed for comfortable riding was of the order of 6 to 7 km/hr, and at those speeds they could detect no wheel slip. In view of the calculated values of wheel slip, the latter observation is not surprising because from terrestrial experience a wheel slip of less than about 20 percent is not detectable by the vehicle driver. The indicated relatively high range of computed wheel slip at zero slope (Fig. 24b) is a result of an expected high dispersion in the experimental data at the "self-propelled point" [40], which represents conditions of incipient change in the sense of

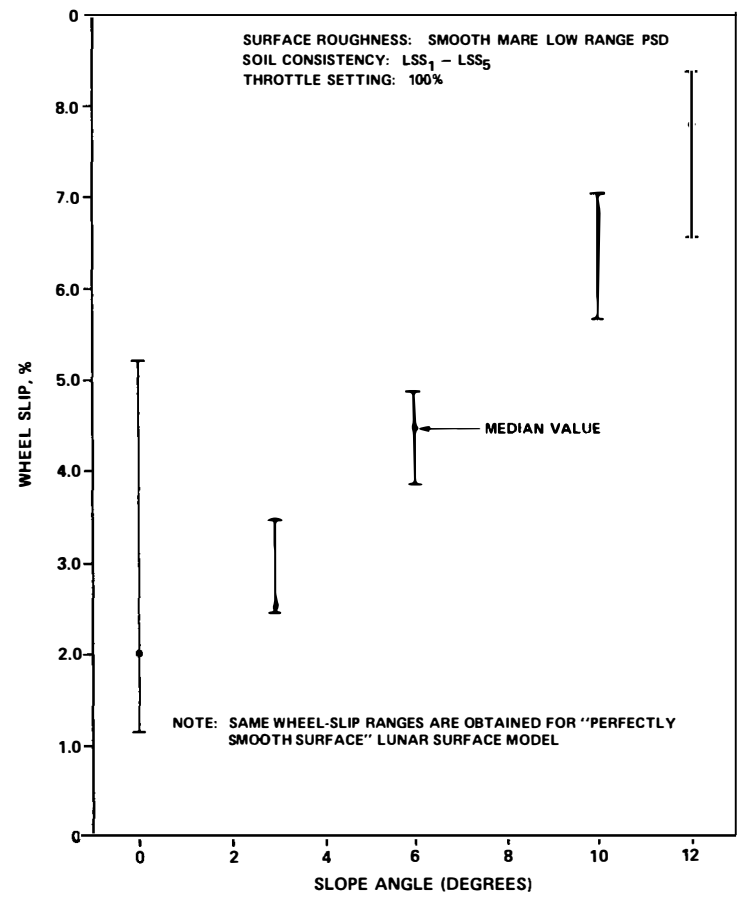
the net-pull force vector acting on the vehicle. On the other hand, the small error of closure of the LRV navigation system which, as mentioned earlier, was calibrated on the basis of a constant wheel-slip bias of 2.3, and the fact that in most cases the average mean slope angle of the lunar surface over several vehicle lengths was very close to zero agree with the computed median wheel-slip value of 2.1 at zero slope (Fig. 24b).

The results of the LRV traction-drive energy consumption rate (ECR) are shown in the form of a histogram in Figure 25a. It is interesting to note that both the ECR range and median values for soil conditions LSS₄, LSS₅, and all tests combined do not differ by a great amount. As indicated in Figure 11c, the wheel mobility performance is, in general, enhanced with increasing values of the soil penetration resistance gradient G. However, within the ranges of G and wheel loads considered, the wheel performance does not appear to be a strong function of soil consistency and strength. This latter observation is also corroborated by the crew comments in the Pilot's Report, quoted previously, that although the soil conditions at the Hadley-Apennine region were variable, no appreciable differences in the Rover mobility performance and interaction with the lunar surface were detectable throughout the Apollo 15 mission.

The apparent skewness of the ECR frequency distribution diagram for soil condition LSS₅, which was based on 15 wheel-soil interaction tests, is attributed to the relatively small number of tests available for this statistical analysis. On the other hand, the trend of the ECR histogram for soil condition LSS₄, which was based on 35 tests performed on LSS₄, tends to approach a normal (Gaussian) frequency distribution and to dominate the characteristics of the histogram for all tests combined. Although only three tests were available from each of the other soil conditions, LSS₁, LSS₂, and LSS₃, the

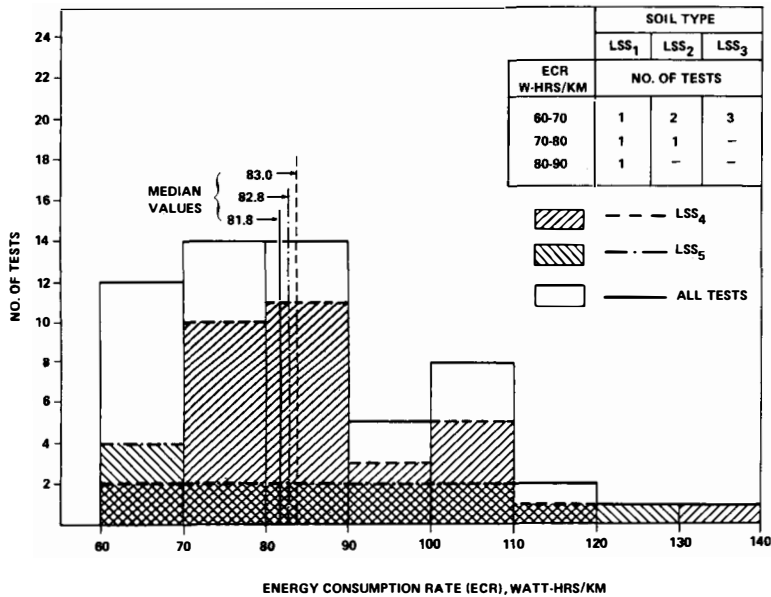


a. ESTIMATES OF MAXIMUM LRV SPEED ON SMOOTH MARE LOW-RANGE PSD LUNAR SURFACE MODEL

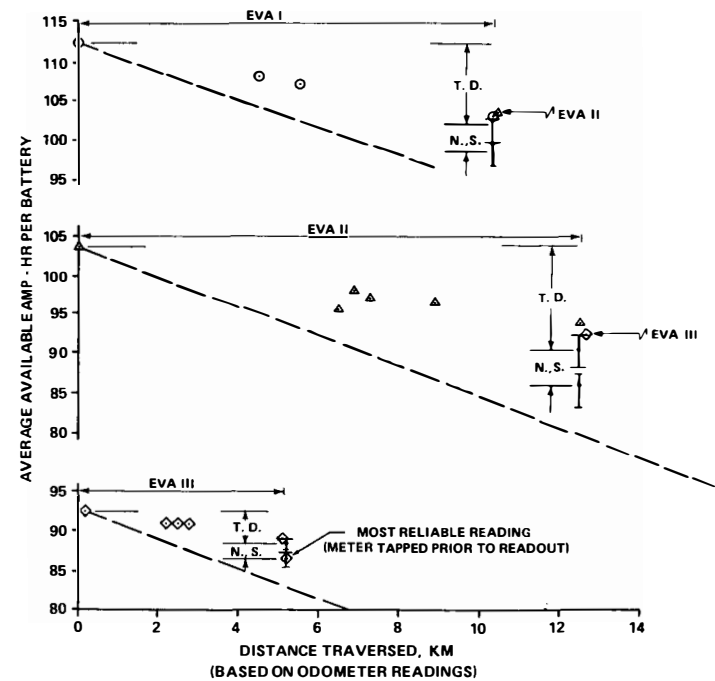
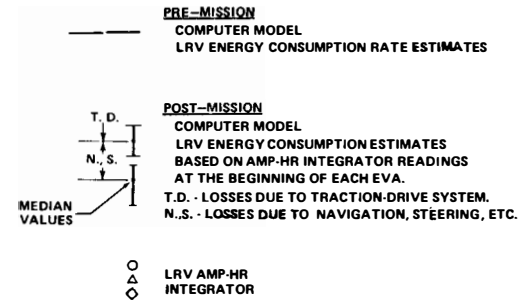


b. ESTIMATES OF LRV WHEEL SLIP VS SLOPE ANGLE UNDER FULL THROTTLE (MAX. VELOCITY) CONDITIONS

Figure 24. MSFC computer model estimates on LRV maximum speeds and wheel slip at Hadley-Apennine.



a. HISTOGRAM OF TRACTION DRIVE LOSSES FOR EVA I
BASED ON SOIL CONDITION LSS₁ - LSS₅



b. LRV ENERGY CONSUMPTION
DURING APOLLO 15 EVA'S I, II, AND III.

Figure 25. MSFC computer power profile analysis results.

histogram for all tests combined indicates a strong concentration toward the low-value ranges of the ECR spectrum.

Because of these considerations and the variability in soil conditions at the Hadley-Apennine region, calculations of the total LRV energy consumption during each of the three EVAs were based on test data from all wheel-soil interaction tests performed on soil conditions LSS₁ through LSS₃, and on tests performed on LSS₄ and LSS₅ corresponding to the lower, median, and upper LRV traction-drive ECR values during EVA I. The tacit assumption associated with this approach, that a given set of wheel-soil interaction data yielding the lowest ECR value for EVA I will also yield the lowest ECR value for EVAs II and III, is not generally correct. This is because the LRV traction-drive ECR corresponding to a given soil consistency depends also on the slope distribution and roughness characteristics of the terrain traversed, as well as on the energy dissipated in the dampers, even if one assumes that the soil conditions in all EVAs are uniform. Accordingly, the worst- or best-case soil condition for one EVA may not necessarily be in the same order when considered in conjunction with another set of topographic conditions. However, because the lunar surface topography encountered in the three EVAs did not vary appreciably with the exception of the relatively steep slopes at the Apennine Front during EVA II, the results from this analysis are not expected to vary significantly if data from other LSS₄ or LSS₅ wheel-soil interaction tests were used in the calculations.

The results from these calculations are shown in Table 5 and Figure 25b and are compared with LRV ampere-hour integrator readouts obtained during the three EVAs. As shown in Table 5 and in Figures 12 and 25b, the energy consumed by the LRV navigation system, steering, control display, and other sources not related to the traction-drive system is considered as an add-on item and is

calculated through another MSFC-developed computer program.

A comparison of the LRV ampere-hour integrator readouts with the computer results indicates that the computed values tend to overestimate the energy consumption indicated by the vehicle's onboard instruments. The median percentage deviation between the measured and computed values is of the order of 30 percent. In view of the fact that the Apollo 15 mission was the first proving ground for testing a self-propelled manned vehicle in an extraterrestrial environment, this agreement (or deviation) between computed and measured values is considered to be very satisfactory, even by terrestrial mobility standards.

The deviations between the computed and measured values of energy consumption may have been caused by the combined effect of a variety of sources, including the following:

1. Inaccuracies in the readouts of the LRV ampere-hour integrators [58]. The performance of these instruments was somewhat erratic during the mission. In some instances, no energy loss was indicated after the vehicle had traversed several kilometers and in others, energy "gains" were registered while the vehicle was parked! At the end of EVA III, there was a detectable difference in the ampere-hour reading by tapping the instrument.

2. Errors in present estimates of the regional slope distribution at the Hadley-Apennine region, which are still based on topographic maps with a 20-m resolution and still photographs obtained during the mission. To date, an analysis of photographs obtained with the Apollo 15 Orbital Science panoramic and metric mapping cameras has not increased the resolution of photographs of the Apollo 15 site to enable a better assessment of the mean regional slopes at the Hadley-Apennine region.

TABLE 5. POST-MISSION EVALUATION OF LRV PERFORMANCE AT THE APOLLO 15 SITE

a. EVA I

LRV Traverse Characteristics			Lunar Surface Characteristics						LRV Energy Consumption					
Total Distance Traversed ^a (km)	EVA Time ^b (hr)		Average LRV Speed ^c (km/hr)	Regional Mean Slope Angle α Along Direction of EVA Traverse ^d			Roughness Model	Soil Type	Computer Model Estimates of Traction Drive Losses ^h (amp-hr/km)		Computer Model Estimates of Total Energy ^j Consumed (amp-hr)		Total Energy ^k Consumed Obtained From LRV Ampere-Hour Integrator Readouts (amp-hr)	
	Driving	Stops		Mean Slope Characteristics	Up-Slope	Level			Down-Slope	Median	Range ⁱ	Median		Range ⁱ
10.3	1.08	2.80	9.5	α (deg)	+1.59	0	-1.57	SM LR ^e	LSS ₁	2.08	1.95-2.43	27.82	26.49-31.69	17.5 ^k
				Percent Distance Traversed										
								PSS ^f	(3) ^g	2.01	1.89-2.35	26.67	25.79-30.83	
								SM LR	LSS ₂	1.95	1.94-2.35	26.50	26.32-30.8	
								PSS	(3)	1.89	1.87-2.27	25.80	25.60-29.91	
								SM LR	LSS ₃	1.86	1.84-1.96	25.55	25.26-26.60	
								PSS	(3)	1.80	1.77-1.90	24.88	24.57-25.92	
								SM LR	LSS ₄	2.28	1.79-2.97	30.00	24.69-37.59	
								PSS	(32)	2.20	1.72-2.89	29.17	24.03-36.66	
								SM LR	LSS ₅	2.08	1.80-2.76	27.84	24.81-35.25	
				PSS	(11)	2.01	1.73-2.68	27.15	24.13-34.35					

a. Based on LRV odometer readings.

b. Estimated from astronaut voice transcripts.

c. Determined from LRV odometer and speedometer readouts and LRV driving time estimates.

d. Based on linear segments 100 to 500 m long, measured on topographic map compiled from Orbiter V photography (scale: 1:15840; resolution: 20 m).

e. SM LR - smooth-mare, low-range PSD.

f. PSS - perfectly smooth surface.

g. Total number of WES wheel-soil interaction tests considered in analysis.

h. On the basis of a 36 V energy source.

i. Lowest and highest estimate.

j. Including traction-drive system, navigation system, steering system, stop-and-go, and other spurious losses.

k. Based on average values at beginning and end of each EVA.

TABLE 5. (Continued)

b. EVA II

LRV Traverse Characteristics			Lunar Surface Characteristics					LRV Energy Consumption						
Total Distance Traversed ^a (km)	EVA Time ^b (hr)		Average LRV Speed ^c (km/hr)	Regional Mean Slope Angle α Along Direction of EVA Traverse ^d			Roughness Model	Soil Type	Computer Model Estimates of Traction Drive Losses ^h (amp-hr/km)		Computer Model Estimates of Total Energy ^j Consumed (amp-hr)		Total Energy ^j Consumed Obtained From LRV Ampere-Hour Integrator Readouts (amp-hr)	
	Driving	Stops		Mean Slope Characteristics	Up-Slope	Level			Down-Slope	Median	Range ⁱ	Median		Range ⁱ
12.5	1.37	2.64	9.15	α (deg)	+2.40	0	-3.01	SM LR ^e	LSS ₁	2.18	2.01-2.51	34.48	32.23-38.80	20.5 ^k
				Percent Distance Traversed	47.0	23.1	29.9	PSS ^f	(3) ^g	2.11	1.94-2.44	33.55	31.31-37.86	
								SM LR	LSS ₂	1.98	1.92-2.40	31.90	31.11-37.35	
								PSS	(3)	1.92	1.86-2.33	31.10	30.29-36.40	
								SM LR	LSS ₃	1.92	1.85-2.07	31.10	30.20-33.01	
								PSS	(3)	1.85	1.78-2.00	30.13	29.33-32.17	
								SM LR	LSS ₄	2.34	1.57-3.01	36.51	26.54-45.46	
								PSS	(32)	2.26	1.52-2.92	35.58	25.81-44.22	
								SM LR	LSS ₅	2.13	1.79-2.78	36.51	29.71-42.40	
								PSS	(11)	2.02	1.71-2.70	32.43	28.37-41.34	

a. Based on LRV odometer readings.

b. Estimated from astronaut voice transcripts.

c. Determined from LRV odometer and speedometer readouts and LRV driving time estimates.

d. Based on linear segments 100 to 500 m long, measured on topographic map compiled from Orbiter V photography (scale: 1:15840; resolution: 20 m).

e. SM LR - smooth-mare, low-range PSD.

f. PSS - perfectly smooth surface.

g. Total number of WES wheel-soil interaction tests considered in analysis.

h. On the basis of a 36 V energy source.

i. Lowest and highest estimate.

j. Including traction-drive system, navigation system, steering system, stop-and-go, and other spurious losses.

k. Based on average values at beginning and end of each EVA.

TABLE 5. (Concluded)

c. EVA III

LRV Traverse Characteristics				Lunar Surface Characteristics					LRV Energy Consumption				Total Energy ^j Consumed Obtained From LRV Ampere-Hour Integrator Readouts (amp-hr)	
Total Distance Traversed ^a (km)	EVA Time ^b (hr)		Average LRV Speed ^c (km/hr)	Regional Mean Slope Angle α Along Direction of EVA Traverse ^d				Roughness Model	Soil Type	Computer Model Estimates of Traction Drive Losses ^h (amp-hr/km)		Computer Model Estimates of Total Energy ^j Consumed (amp-hr)		
	Driving	Stops		Mean Slope Characteristics	Up-Slope	Level	Down-Slope			Median	Range ⁱ	Median		Range ⁱ
	5.1	0.58		1.37	8.75	α (deg)	+2.40			0	-1.20	SM LR ^e	LSS ₁	2.14
				Percent Distance Traversed	22.2	61.2	16.6	PSS ^f	(3) ^g	2.08	1.91-2.41	14.03	13.12-15.79	
								SM LR	LSS ₂	1.87	1.82-2.38	12.95	12.67-15.62	
								PSS	(3)	1.81	1.75-2.31	12.61	12.32-15.27	
								SM LR	LSS ₃	1.88	1.72-2.02	13.0	12.14-13.75	
								PSS	(3)	1.81	1.65-1.95	12.62	11.80-13.39	
								SM LR	LSS ₄	2.32	1.70-2.99	15.30	12.05-18.93	
								PSS	(32)	2.25	1.63-2.92	14.95	11.69-18.51	
								SM LR	LSS ₅	2.11	1.65-2.77	14.22	11.80-17.71	
								PSS	(11)	1.90	1.59-2.69	13.12	11.45-17.29	

11.4^k

- a. Based on LRV odometer readings.
- b. Estimated from astronaut voice transcripts.
- c. Determined from LRV odometer and speedometer readouts and LRV driving time estimates.
- d. Based on linear segments 100 to 500 m long, measured on topographic map compiled from Orbiter V photography (scale: 1:15840; resolution; 20 m).
- e. SM LR - smooth-mare, low-range PSD.
- f. PSS - perfectly smooth surface.
- g. Total number of WES wheel-soil interaction tests considered in analysis.
- h. On the basis of a 36 V energy source.
- i. Lowest and highest estimate.
- j. Including traction-drive system, navigation system, steering system, stop-and-go, and other spurious losses.
- k. Based on average values at beginning and end of each EVA.

3. Inaccuracies in estimating add-on energy losses caused by navigation, steering, etc., which, according to the present analysis, are as high as 30 ± 10 percent of the estimated traction-drive losses [58].

4. Higher mobility performance efficiency developed by the four-wheeled vehicle system as compared with the efficiency of a single wheel.

In spite of these error sources, the fact that (1) the computer power profile estimates consistently overestimated the energy consumption indicated by the LRV ampere-hour integrators, and (2) the WES wheel-soil interaction test results indicate that the LRV wheel mobility performance, as estimated by the analytical procedures described in the appendix and LLL soil values obtained by the WES, was consistently higher than that indicated by the corresponding wheel-soil interaction test data, prompted a comparative analysis between these two sets of input data to the MSFC power profile computer program. The results of this analysis are shown in Table 6. In all cases, it is indicated that energy consumption estimates, based on the analytical relations of pull and torque coefficients versus slip and LLL soil values, are significantly less than those estimated from the wheel-soil interaction experimental data and are closer to the LRV ampere-hour integrator readouts. The reasons for this better agreement between measured and computed LRV energy consumption estimates on the basis of LLL soil value inputs can be attributed to several compensating factors. These include the absence of lunar atmosphere and, hence, of air-pore pressures developed in the lunar soil as a result of the wheel-soil interaction; the relatively small amount of LRV wheel slip and sinkage; and the fact that the slope distributions encountered during the LRV traverses indicate, in general, a level terrain for

which the Bekker/LLD soil-vehicle model (see appendix) is mainly applicable.

Because of these observations and because the variation in lunar soil properties did not appear to influence appreciably the LRV performance, a further analytical study was made of the LRV energy consumption at the Hadley-Apennine region using a wide spectrum of LLL soil values, some of which correspond to terrestrial LSS and Yuma Sand lunar soil simulants and others to soil mechanics data obtained from the Apollo 15 mission. The results of this analysis are shown in Table 7 and are compared with the LRV ampere-hour integrator readings. The column designated as Percent Deviation per km refers to the energy consumption entries for the whole mission and lists root-mean-square values of deviation between measured and calculated energy consumption rates. The results of these calculations indicate the following:

1. Large variations in LLL soil values do not appear to influence appreciably the energy consumption results, the percent deviation per kilometer for the whole Apollo mission varying between 11.4 and 16.0 percent. However, there is a tendency for low energy consumption values to be associated with high values of the soil deformation modulus $k = (k_c/b) + k_\phi$ and exponent n . The soil shear strength characteristics as expressed by the coefficients c_b and ϕ_b do not appear to influence the calculations.

2. As expected, the best- or worst-case soil condition for one EVA is not the best or worst case for other EVAs.

3. The percent deviation per kilometer, which is associated with the soil condition resulting in energy consumption estimates that are closest to the total amount

TABLE 6. COMPARISON OF COMPUTER PROGRAM RESULTS ON LRV ENERGY CONSUMPTION USING EXPERIMENTAL DATA FROM WES WHEEL-SOIL INTERACTION TESTS AND CORRESPONDING LLL SOIL VALUES

		EVA I		EVA II		EVA III		Total for EVAs I, II, III	
		LRV amp-hr Integrator Readings							
		17.5		20.5		11.4		49.4	
		Computer Results							
Soil	Test No.	WES	LLL	WES	LLL	WES	LLL	WES	LLL
LSS ₁	6	24.8	23.3	33.0	30.3	13.8	13.6	71.4	67.2
	8	28.5	18.4	37.6	27.7	15.8	12.6	81.9	58.7
LSS ₂	10	23.5	18.2	30.6	27.8	12.4	12.5	66.5	58.5
	12	23.3	17.9	29.9	27.3	12.2	12.3	65.4	57.5
LSS ₃	7	22.5	18.0	29.4	27.4	12.5	12.2	64.4	57.6
	9	23.5	18.1	31.3	27.5	13.2	12.4	68.0	58.0
LSS ₄	28	23.8	18.0	36.4	27.5	15.0	12.2	75.2	57.7

of energy consumed by the LRV during the three EVAs (in this case soil C₀), is not necessarily the minimum.

4. On the basis of the minimum percent deviation per kilometer for all EVAs, the best soil model considered in this analysis is Soil B, i.e., the average soil model that had been tentatively recommended for LRV mobility design analysis in the MSFC Lunar Environment Design Criteria Document.¹¹ This conclusion is somewhat ironic – although it came as a pleasant surprise to the senior author, who had co-authored the section on the lunar soil trafficability characteristics appearing in that document – because it indicates that after all of the extensive efforts expended in LRV wheel-soil interaction

studies, the first guess turned out to be the best guess.

To explore further the influence of soil characteristics on vehicle performance, the power number-versus-pull coefficient relations were computed for a number of the cases listed in Table 7. The results of this analysis are plotted in Figure 26. The cases indicated as S₁’, C₀’, C₁’ and C₂’, are identical to cases 9 (S₁), 13 (C₀), 8 (C₁), and 4 (C₂) listed in Table 7 except that the value of the soil-slip coefficient K is set equal to 1.7.

If the pull coefficient P/W is considered to be a measure of the tangent of the slope angle that can be negotiated by the vehicle, the trends of these plots indicate that,

11. Natural Environmental Design Criteria Guidelines for Use in the Design of Lunar Exploration Vehicles, op. cit.

TABLE 7. COMPARISON OF MEASURED AND COMPUTED LRV ENERGY CONSUMPTION DURING APOLLO 15 MISSION USING SPECTRUM OF LLL SOIL VALUES

Case No.	Soil Type	LLL Soil Values						LRV Load vs Wheel Footprint Characteristics				EVA I	EVA II	EVA III	Total	Percent Deviation per km
												LRV amp-hr Integrator Readings				
		c_b (lb/in. ²)	ϕ_b (deg)	k_c (lb/in.) ¹⁺ⁿ	k_ϕ (lb/in.) ²⁺ⁿ	n	K (in.)	W (lb)	A (in. ²)	b (in.)	ℓ (in.)	17.5	20.5	11.4	49.4	
												Computer Estimates Using LLL Soil Values				
1	A15-10	0.15	50.0	0.0	15.0	4.24	1.0	63.5	80.0	8.0	12.0	14.09	20.25	9.02	43.36	16.02
2	A15-11	0.60	21.0	0.0	15.0	4.24	1.0	63.5	80.0	8.0	12.0	14.09	20.25	9.02	43.36	16.02
3	A15-12	0.15	50.0	0.0	15.0	0.72	0.7	63.5	80.0	8.00	12.0	14.09	20.38	9.03	43.50	15.98
4	C ₂	0.31	15.2	4.96	10.08	0.52	1.0	58.5	66.0	7.82	10.4	14.11	20.39	9.06	43.56	15.83
5	A15-2	0.15	50.0	0.0	15.0	1.0	1.0	63.5	80.0	8.00	12.0	14.18	20.50	9.09	43.77	15.56
6	A15-3	0.60	21.0	0.0	15.0	1.0	1.0	63.5	80.0	8.00	12.0	14.18	20.50	9.09	43.77	15.56
7	LSS ₂ -12	0.24	26.0	2.64	5.44	0.72	1.0	57.0	62.0	6.85	11.0	14.32	20.88	9.05	44.25	15.41
8	C ₁	0.14	23.5	0.21	8.03	0.67	1.0	58.5	66.0	7.82	10.4	14.22	20.43	9.13	43.78	15.33
9	S ₁	0.24	13.8	0.54	6.01	0.72	1.0	58.5	66.0	7.82	10.4	14.35	20.76	9.06	44.17	15.29
10	A15-5	0.15	50.0	0.0	15.0	1.0	0.7	63.5	80.0	12.00	12.0	14.27	20.75	9.13	44.15	15.23
11	LSS ₄ -28	0.11	27.8	1.60	9.89	1.14	1.0	57.0	62.0	6.85	11.0	14.40	20.88	9.09	44.37	15.09
12	LSS ₃ -7	0.14	27.5	-0.615	10.70	1.20	1.0	57.0	62.0	6.85	11.0	14.41	20.88	9.10	44.39	15.03
13	C ₀	0.12	21.6	2.61	2.46	0.73	1.0	58.5	66.0	7.82	10.4	14.89	23.09	9.59	47.57	14.51
14	LSS ₃ -9	0.10	31.0	-1.06	9.89	1.31	1.0	57.0	62.0	6.85	11.0	14.52	21.00	9.21	44.73	14.44
15	LSS ₃ -15	0.20	27.0	-0.67	8.86	1.32	1.0	57.0	62.0	6.85	11.0	14.52	21.13	9.26	44.91	14.32
16	A15-6	0.15	50.0	0.00	15.0	0.72	1.0	63.5	80.0	8.00	12.0	14.63	21.25	9.31	45.19	13.95
17	A15-7	0.60	21.0	0.00	15.0	0.72	1.0	63.5	80.0	8.00	12.0	14.63	21.25	9.31	45.19	13.95
18	A15-8	0.15	50.0	0.00	15.0	0.72	0.7	63.5	80.0	8.00	12.0	14.58	21.25	9.36	45.19	13.90
19	LSS ₂ -14	0.14	28.8	2.94	2.82	0.67	1.0	57.0	62.0	6.85	11.0	14.63	21.25	9.36	45.24	13.79
20	LSS ₂ -10	0.18	27.5	-0.16	5.68	1.10	1.0	57.0	62.0	6.85	11.0	14.63	21.25	9.36	45.24	13.79
21	A15-9	0.15	50.0	0.00	15.0	4.24	0.7	63.5	80.0	8.00	12.0	14.63	21.25	9.36	45.24	13.79
22	LSS ₃ ^a	0.15	28.8	-1.58	8.83	1.48	1.0	57.0	62.0	6.85	11.0	14.63	21.25	9.36	45.24	13.79
23	LSS ₁ ^a	0.14	29.0	0.42	4.32	0.90	1.0	57.0	62.0	6.85	11.0	14.63	21.13	9.41	45.17	13.56
24	A15-4	0.15	50.0	0.0	2.00	1.00	1.0	63.5	80.0	8.00	12.0	19.78	23.88	10.48	54.14	13.46
25	LSS ₁ -8	0.065	31.8	2.80	3.60	0.86	1.0	57.0	62.0	6.85	11.0	14.73	21.13	9.41	45.27	13.33
26	LSS ₂ ^a	0.15	29.0	0.13	5.34	1.15	1.0	57.0	62.0	6.85	11.0	14.73	21.25	9.46	45.44	13.22
27	LSS ₄ ^a	0.12	29.0	1.76	5.04	1.18	1.0	57.0	62.0	6.85	11.0	14.73	21.25	9.46	45.44	13.22
28	LSS ₁ -6	0.13	28.2	1.08	2.70	1.10	1.0	57.0	62.0	6.85	11.0	19.67	23.75	10.48	53.90	12.96
29	Soil A ₁	0.00	31.0	0.00	3.00	1.00	1.0	57.0	62.0	6.85	11.0	19.57	23.63	10.38	53.58	12.67
30	Soil A	0.00	31.0	0.00	3.00	1.00	0.4	57.0	62.0	6.85	11.0	19.51	23.38	10.38	53.27	12.57
31	Soil C ₁	0.05	39.0	0.40	3.00	1.00	0.4	57.0	62.0	6.85	11.0	19.47	23.36	10.38	53.48	12.50
32	A15-1	0.15	40.0	0.0	2.00	1.00	1.0	63.5	80.0	6.85	11.0	19.47	23.25	10.38	53.10	11.65
33	Soil C	0.05	39.0	0.40	3.00	1.00	1.0	57.0	62.0	6.85	11.0	19.49	23.13	10.38	53.00	11.43
34	Soil B	0.025	35.0	0.20	3.00	1.00	0.7	57.0	62.0	6.85	11.0	19.46	23.13	10.36	52.95	11.41

a. Average of all tests performed with soil type indicated.

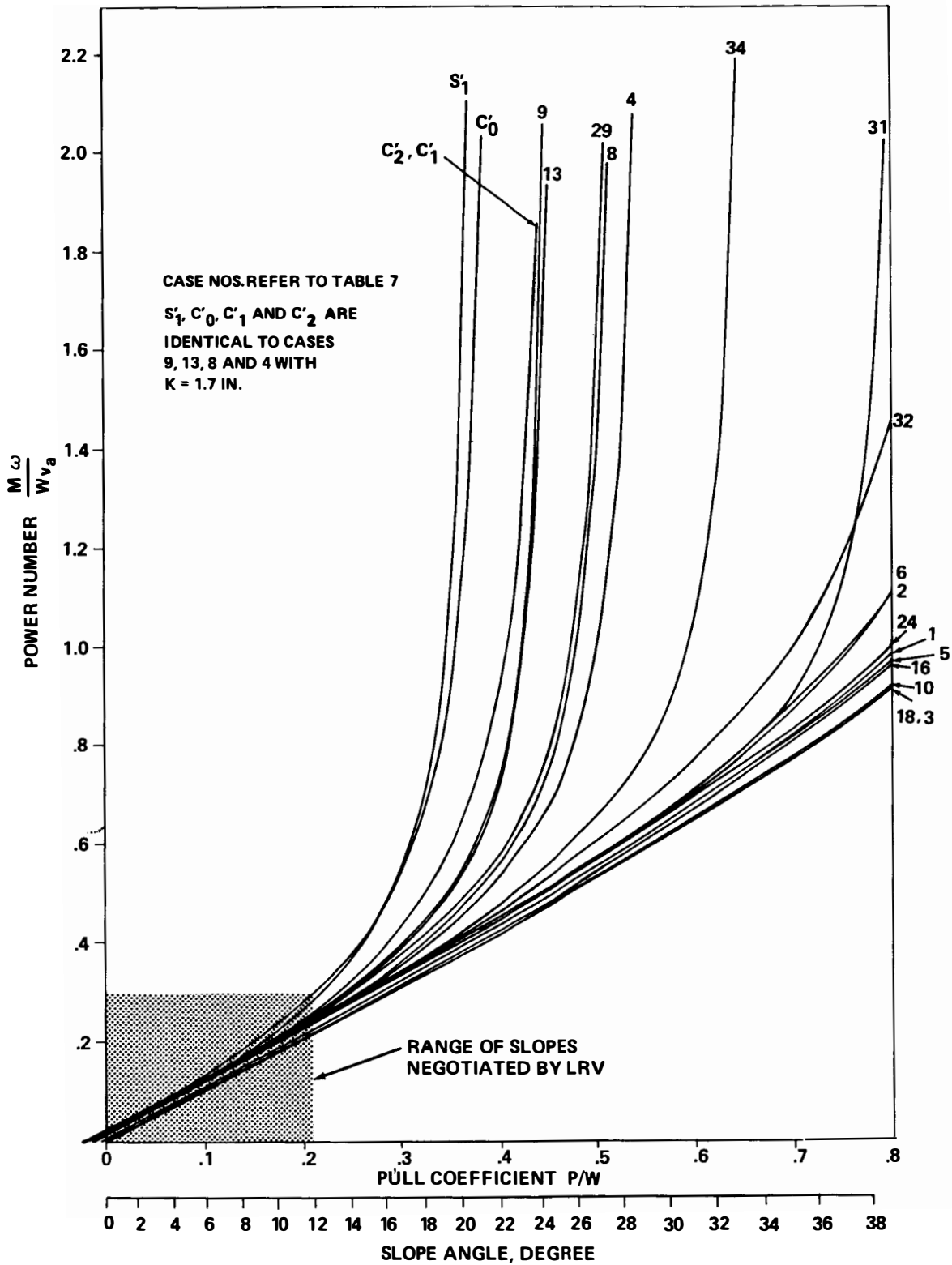


Figure 26. Power number versus pull coefficient for different LLL soil values.

within the range of slopes negotiated by the LRV at the Hadley-Apennine region, the soil conditions have very little influence on the energy consumed by the vehicle.

The same plots indicate further that the LLL soil value that has the greatest influence on the maximum slope-climbing capability of the vehicle is the soil-slip coefficient K . The higher the value of K , the lower appears to be the maximum value of P/W at which the PN versus P/W curves bend sharply upward. Although the general trend of these curves is not expected to change, it should be noted that these inferences are made from PN versus P/W diagrams that, in most cases, are obtained from wheel-soil interaction tests performed on level soil surfaces. The wheel-soil interaction on slopes is currently investigated through constant-slip and constant-pull wheel model tests performed under controlled laboratory conditions at the Geotechnical Research Laboratory of the MSFC Space Sciences Laboratory. Preliminary test results indicate good agreement between PN versus P/W relations obtained from constant-slip tests on level surfaces and constant-pull (free-surge) tests on slopes, and also between the maximum slope-climbing capability predicted from tests on level surfaces and actual wheel immobilization on slopes.

CONCLUSIONS

1. The mobility performance of the Lunar Roving Vehicle on the lunar surface was very satisfactory. The vehicle met with ease all the demands placed upon it by the Apollo 15 mission. This augmented transportation capability, which was provided for the first time in the Apollo program, enhanced the scientific returns from the Apollo 15 mission by a very significant amount.

2. No direct quantitative information exists regarding the Rover's

limiting mobility performance characteristics at the Hadley-Apennine region. This is because very little direct quantitative information on the vehicle's interaction with the lunar surface is available and because the mission profile was well within the expected capabilities of the Rover, which was never operated under performance-limiting conditions or degraded operating modes, except for a front-steering failure during EVA I.

3. Quantitative measurements of the soil mechanical properties at the Apollo 15 site indicate that the soil conditions at the Hadley-Apennine region were variable on a regional basis, ranging from soft, compressible at the Apennine Front to firm, incompressible along the rim of the Hadley Rille; at the Mare Region near the LM landing site; and at Station 8. Local variations in soil properties were also observed, the soft material usually existing at the rims of small-diameter fresh craters. This variability in lunar soil properties did not appear to have materially influenced the performance of the Rover.

4. Qualitative observations on the interaction of the vehicle with the lunar surface agree with pre-mission estimates on the vehicle's behavior, based on wheel-soil interaction tests performed on lunar soil simulants under terrestrial and $1/6$ -g gravity conditions simulated onboard a C-135A aircraft.

5. Post-mission power profile analyses based on updated information regarding the slope distribution and roughness characteristics of the lunar surface at the Hadley-Apennine region and experimental data obtained from wheel-soil interaction tests performed at the facilities of the U.S. Army Engineer Waterways Experiment Station resulted in energy consumption estimates that tend to overestimate the LRV energy consumption indicated by the vehicle's ampere-hour integrators. The median deviation between computed and measured energy

consumption is of the order of 30 percent. Although the level of agreement between the computed and measured energy losses is considered to be very satisfactory, there are various uncertainties and error sources that may account for these discrepancies. These include:

a. Errors in the ampere-hour integrator readouts.

b. Errors in post-mission estimates of the slope distribution at the Hadley-Apennine region.

c. Errors in estimating the energy consumed by the navigation system, steering, control and display console and other components, or activities not related to the traction-drive system.

d. LRV mobility performance enhancement caused by the absence of lunar atmosphere and, hence, of air-pore pressures developed in the lunar soil as a result of the wheel-soil interaction.

6. Power profile analyses using the Bekker/LLD vehicle-soil model (see appendix) and LLL soil values obtained by the WES before and after wheel-soil interaction tests are in closer agreement with the measured energy consumption than analyses performed on the basis of the experimental results obtained from the same wheel-soil interaction tests. The same vehicle-soil model tends to overpredict the mobility performance of the LRV wheel during the wheel-soil interaction tests. These differences between the analytical and the experimental results in terrestrial wheel testing and the better agreement between the analytical results and the actual performance of the LRV on the lunar surface can be attributed to various compensating factors, including:

a. The absence of air-pore pressures within the lunar soil.

b. The absence of steep-slope traverse segments during the EVAs.

c. The relatively small amount of LRV wheel slip and sinkage at the Hadley-Apennine region.

d. The higher mobility performance efficiency developed by the four-wheeled mobility vehicle system as compared with the efficiency of a single wheel.

7. Power-profile analyses using the Bekker/LLD vehicle-soil model and a wide spectrum of LLL soil values indicate that the soil model which yields energy consumption estimates with the least percent deviation per kilometer from the measured LRV energy consumption is Soil B, which was set forth in the MSFC Lunar Environmental Criteria for LRV design analysis. This model had been based on soil mechanics data obtained from the U.S. Surveyor spacecraft unmanned missions.

8. The power profile analyses described herein in items 5 and 7 indicate that within the range of slopes negotiated by the LRV during the Apollo mission, variations in the lunar soil properties did not influence significantly the vehicle's performance. This conclusion is corroborated by actual real-time observations made by the Apollo 15 astronauts and by the WES wheel-soil interaction test results.

9. A parametric analysis of the power-number-versus-pull coefficient, using the Bekker/LLD vehicle-soil model and a wide spectrum of LLL soil values in conjunction with LRV wheel geometry and load ranges, indicates that for P/W values corresponding to the maximum slopes angles traversed by the LRV, variations in the LLL soil values have very little influence on the calculated power consumption rates. In addition, from the same analysis it is indicated that the most significant LLL soil value affecting the maximum

slope-climbing capability of the vehicle is the soil slip coefficient K. This latter conclusion should be considered tentative pending the results of actual wheel slope-climbing capability tests currently performed at the MSFC Geotechnical Research Laboratory under controlled laboratory conditions.

George C. Marshall Space Flight Center
National Aeronautics and Space Administration
Marshall Space Flight Center, Alabama, 35812, March 1, 1972
914-40-00-00-00

APPENDIX

BEKKER/LLD ANALYTICAL SOIL-VEHICLE MODEL

The analytical curves shown in Figures 8 through 10 have been computed on the basis of the following relations associated with a soil-vehicle model referred to by Rula and Nuttall [61] as the "Bekker/LLD soil-vehicle model C_w ," which is mainly applicable to wheels with flexible tires interacting with soft soils. These relations have been developed by Bekker and co-workers (see, for instance, References 36 and 37) at the U.S. Army Tank Automotive Command (USATACOM) Land Locomotion Division (LLD) referred to in previous sections of this report as the Land Locomotion Laboratory (LLL).

Wheel Sinkage (in.)

$$z = \left(\frac{W}{Ak} \right)^{1/n} \quad (A-1)$$

Gross Tractive Effort (lb)

$$H = (Ac_b + W \tan \phi_b) \left[1 - \frac{K}{sl} \left(1 - e^{-sl/K} \right) \right] \quad (A-2)$$

Compaction Resistance (lb)

$$R_c = \left(\frac{bk}{n+1} \right) z^{n+1} \quad (A-3)$$

Total Motion Resistance (lb)

$$R_T = R_c \quad ,$$

in which

- W = wheel load (lb),
 - A = wheel footprint area (in.²),
 - k = $(k_c/b) + k_\phi$ = soil consistency [(lb/in.)ⁿ⁺²],
 - k_c = cohesive modulus of soil deformation [(lb/in.)ⁿ⁺¹],
 - k_ϕ = frictional modulus of soil deformation [(lb/in.)ⁿ⁺²],
 - n = exponent of soil deformation (dimensionless),
 - c_b = coefficient of cohesion (lb/in.²),
 - ϕ_b = measure of the soil's angle of internal friction (deg),
 - K = coefficient of soil slip (in.),
 - s = wheel slip (dimensionless),
 - l = tire chord length of ground contact (in.),
- and
- b = tire width of ground contact (in.).

The soil values k_ϕ , k_c , and n for the LSS cases considered in Figures 8 through 10 were obtained from Bevameter plate tests and the soil values c_b and ϕ_b for the same cases from Bevameter ring-shear tests performed at the WES. The coefficient of soil slip K was assumed in all of these cases to be equal to 1

in. Finally, the quantities b , l , and A were measured from LRV wheel footprints developed at a given wheel load W .

The net pull P was considered to be equal to

$$P = H - R_c \quad , \quad (A-4)$$

in which H and R_c are given by equations (A-2) and (A-3). Hence, the pull coefficient P/W was determined from

$$\frac{P}{W} = \frac{1}{W} (H - R_c) \quad . \quad (A-5)$$

The torque coefficient M/Wr_e was considered to be equal to

$$\frac{M}{Wr_e} = \frac{H}{W} \quad . \quad (A-6)$$

Using relations (A-5) and (A-6), a computer program was developed, accepting as input quantities the LLL soil values and the wheel load/footprint relations for the LRV wheel and the lunar soil simulants used. This program yields the following quantities as functions of wheel slip, which can be used directly as input data to the MSFC LRV Mobility Performance

and Power Profile Analysis computer program described in the text:

$$\text{Pull coefficient } \frac{P}{W} \quad ,$$

$\text{Arc tan } (P/W)$, assumed to give an indication of the slope angle that can be negotiated by the vehicle, and

$$\text{Torque coefficient } \frac{M}{Wr_e} \quad .$$

The same program also yields the following mobility performance parameters, which can be used for a comparative analysis of wheel-soil performance:

Power No.,

$$PN = \frac{M\omega}{Wv_a} = \frac{M}{Wr_e(1-s)}$$

and

Wheel mobility efficiency,

$$\eta = \frac{Pv_a}{M\omega} = \frac{\text{Pull Coeff.}}{PN} \quad ,$$

in which r_e , ω , and v_a are the effective radius of the wheel, the wheel angular velocity, and the wheel translational speed, respectively.

REFERENCES

1. Scott, R.F.; and Roberson, F.I.: Soil Mechanics Surface Sampler, Surveyor Project Final Report, Part II: Science Results. Technical Report No. 32-1265, Jet Propulsion Laboratory, Pasadena, Calif., June 14, 1968, pp. 195-206.
2. Costes, N.C.; Carrier, W.D.; Mitchell, J.K.; and Scott, R.F.: Apollo 11: Soil Mechanics Results. Journal of the Soil Mechanics and Foundations Division, Proceedings of the ASCE, Vol. 96, No. SM6, 1970, pp. 2045-2080.
3. Scott, R.F.; Carrier, W.D. III; Costes, N.C.; and Mitchell, J.K.: Apollo 12 Soil Mechanics Investigation. Geotechnique, Vol. 21, No. 1, March 1971, pp. 1-14.
4. Mitchell, J.K.; Bromwell, L.G.; Carrier, W.D.; Costes, N.C.; and Scott, R.F.: Soil Mechanics Experiment. Apollo 14 Preliminary Science Report, Sec. 4, NASA SP-272, 1971.
5. Mitchell, J.K.; Bromwell, L.G.; Carrier, W.D.; Costes, N.C.; Houston, W.N.; and Scott, R.F.: Soil Mechanics Experiment. Apollo 15 Preliminary Science Report, Ch. 7, NASA SP-289, 1972.
6. Mitchell, J.K.; Scott, R.F.; Houston, W.N.; Costes, N.C.; Carrier, W.D.; and Bromwell, L.G.: Mechanical Properties of Lunar Soil: Density, Porosity, Cohesion, and Angle of Internal Friction. Proceedings of the Third Lunar Science Conference, Jan. 10-13, 1972, Houston, Tex., Lunar Science Institute Contract No. 88, 1972.
7. Costes, N.C.; Cohron, G.T.; and Moss, D.C.: Cone Penetration Resistance Test – An Approach to Evaluating the In-Place Strength and Packing Characteristics of Lunar Soils. Proceedings of the Second Lunar Science Conference, Vol. 3, MIT Press, 1971, pp. 1973-1987.
8. Mitchell, J.K.; Carmichael, I.S.E.; Goodman, R.E.; Frisch, J.; Witherspoon, P.A.; and Heuzé, F.E.: Materials Studies Related to Lunar Surface Exploration. Final Report, NASA Contract NSR 05-003-189, University of California, Berkeley, 1969.
9. Mitchell, J.K.; Goodman, R.E.; Houston, W.N.; and Witherspoon, P.A.: Lunar Surface Engineering Properties Experiment Definition. Final Report, Contract NAS8-21432, University of California, Berkeley, January 1970.
10. Mitchell, J.K.; Houston, W.N.; Vinson, J.S.; Durgunoglou, T.; Namiq, L.I., et al.: Lunar Surface Engineering Properties Experiment Definition. Final Report, Contract NAS8-21432, University of California, Berkeley, June 1970.
11. Preliminary Terrain Evaluation and Apollo Landing Site Analysis Based on Lunar Orbiter I Photography. Report No. LWP-323, Lunar Orbiter Photo Data Screening Group, Langley Research Center, NASA, Langley Station, Hampton, Va., 1966.

REFERENCES (Continued)

12. Preliminary Geologic Evaluation and Apollo Landing Analysis of Areas Photographed by Lunar Orbiter II. Report No. LWP-363, Lunar Orbiter Photo Data Screening Group, Langley Research Center, NASA, Langley Station, Hampton, Va., 1967.
13. Preliminary Geologic Evaluation and Apollo Landing Analysis of Areas Photographed by Lunar Orbiter III. Report No. LWP-407, Lunar Orbiter Photo Data Screening Group, Langley Research Center, NASA, Langley Station, Hampton, Va., 1967.
14. A Preliminary Geologic Evaluation of Areas Photographed by Lunar Orbiter V Including an Apollo Landing Analysis of One of the Areas. Report No. LWP-506, Lunar Orbiter Photo Data Screening Group, Langley Research Center, NASA, Langley Station, Hampton, Va., 1968.
15. Cherkasov, I.I.; Vakhnin, V.M.; Kemurjian, A.L.; Mikhailov, L.N.; Mikheyev, V.V.; Musatov, A.A.; Smorodinov, M.I.; and Shvarev, V.V.: Determination of the Physical and Mechanical Properties of the Lunar Surface Layer by Means of Luna 13 Automatic Station. Moon and Planets II, A. Dollfus, ed., North Holland Publishing Co., Amsterdam, 1968, pp. 70-76.
16. Vinogradov, A.P.: Preliminary Data on Lunar Ground Brought to Earth by Automatic Probe "Luna-16." Proceedings of the Second Lunar Science Conference, Vol. 1, MIT Press, 1971, pp. 1-16.
17. Leonovich, A.K.; Gromon, V.V.; Rybakov, A.V.; Petrov, V.K.; Pavlov, P.S.; Cherkasov, I.I.; and Shvarev, V.V.: Studies of Lunar Ground Mechanical Properties with the Self-Propelled "Lunokhod-1." Ch. 8, Peredvizhnaya Laboratoriya na Lune Lunokhod-1, 1971, pp. 120-135.
18. Halajian, J.D.: The Case for a Cohesive Lunar Surface Model. Report ADR 04-40-64.2, Grumman Research Dept., Grumman Aircraft Engineering Corp., Bethpage, N.Y., June 1964.
19. Jaffe, L.D.: Depth and Strength of Lunar Dust. Transactions, American Geophysical Union, Vol. 45, 1964, p. 628.
20. Jaffe, L.D.: Strength of the Lunar Dust. Journal of Geophysical Research, Vol. 70, No. 24, 1965, pp. 6139-6146.
21. Christensen, E.M.; Batterson, S.A.; Benson, H.E.; Chandler, C.E.; Jones, R.H.; Scott, R.F.; Shipley, E.N.; Sperling, F.B.; and Sutton, G.H.: Lunar Surface Mechanical Properties - Surveyor I. Journal of Geophysical Research, Vol. 72, No. 2, 1967, pp. 801-813.
22. Christensen, E.M.; Batterson, S.A.; Benson, H.E.; Choate, R.; Hutton, R.E.; Jaffe, L.D.; Jones, R.H.; Ko, H.Y.; Schmidt, F.N.; Scott, R.F.; Spencer, R.L.; and Sutton, G.H.: Lunar Surface Mechanical Properties. Journal of Geophysical Research, Vol. 73, No. 22, 1968, pp. 7169-7192.

REFERENCES (Continued)

23. Scott, R.F.: The Density of Lunar Surface Soil. *Journal of Geophysical Research*, Vol. 73, No. 16, 1968, pp. 5469-5471.
24. Costes, N.C.; Carrier, W.D.; Mitchell, J.K.; and Scott, R.F.: Apollo 11 Soil Mechanics Investigation. Apollo 11 Preliminary Science Report, Sec. 4, NASA SP-214, 1969.
25. Costes, N.C.; and Mitchell, J.K.: Apollo 11 Soil Mechanics Investigation. Proceedings of the Apollo 11 Science Conference, *Geochim et Cosmochim. Acta*, Suppl. 1, Vol. 2, Pergamon Press, 1970, pp. 2025-2044.
26. Houston, W.N.; and Mitchell, J.K.: Lunar Core Tube Sampling. Proceedings of the Second Lunar Science Conference, Vol. 3, MIT Press, 1971, pp. 1953-1958.
27. Carrier, W.D. III; Johnson, S.W.; Werner, R.A.; and Schmidt, R.: Disturbance in Samples Recovered with the Apollo Core Tubes. Proceedings of the Second Lunar Science Conference, Vol. 3, MIT Press, 1971, pp. 1959-1972.
28. Carrier, W.D. III; Johnson, S.W.; Lisimaco, H.C.; and Schmidt, R.: Core Sample Depth Relationships: Apollo 14 and 15. Proceedings of the Third Lunar Science Conference, Jan. 10-13, 1972, Houston, Tex., Lunar Science Institute Contract No. 88, 1972.
29. Jaffe, L.D.: Surface Structure and Mechanical Properties of the Lunar Maria. *Journal of Geophysical Research*, Vol. 72, No. 6, 1967.
30. Christensen, E.M.; Batterson, S.A.; Benson, H.E.; Choate, R.; Jaffe, L.D.; Jones, R.H.; Ko, H.Y.; Spencer, R.L.; Sperling, F.B.; and Sutton, G.H.: Lunar Surface Mechanical Properties at the Landing Site of Surveyor III. *Journal of Geophysical Research*, Vol. 73, No. 12, 1968, pp. 4081-4094.
31. Christensen, E.M.; Batterson, S.A.; Benson, H.E.; Choate, R.; Hutton, R.E.; Jaffe, L.D.; Jones, R.H.; Ko, H.Y.; Schmidt, F.N.; Scott, R.F.; Spencer, R.L.; Sperling, F.B.; and Sutton, G.H.: Lunar Surface Mechanical Properties. Surveyor VI, A Preliminary Report, NASA SP-166, 1968, pp. 41-95.
32. Moore, H.J.: Estimates of the Mechanical Properties of Lunar Surface Using Tracks and Secondary Impact Craters Produced by Blocks and Boulders. Interagency Report: Astrogeology 22, U.S. Department of Interior, Geological Survey, 1970.
33. Hovland, H.J.; and Mitchell, J.K.: Mechanics of Rolling Sphere-Soil Slope Interaction. Final Report, Vol. II of IV, Contract NAS8-21432, Space Science Laboratory, University of California, Berkeley, 1971.
34. Rosema, W.J.: The Use of Spectral Analysis in Describing Lunar Surface Roughness. U.S. Geological Survey Professional Paper No. 650D, Geological Survey Research, 1969, pp. 180-188.

REFERENCES (Continued)

35. Rowan, L.C.; McCauley, J.F.; and Holm, E.A.: Lunar Terrain Mapping and Relative Roughness Analysis. U.S. Geological Survey Professional Paper No. 599G, 1971.
36. Bekker, M.G.: Introduction to Terrain-Vehicle Systems. The University of Michigan Press, Ann Arbor, Mich., 1969.
37. Janosi, Z.: An Analysis of Pneumatic Tire Performance on Deformable Soils. Mechanics of Soil-Vehicle Systems, Proceedings of the 1st International Conference on the Mechanics of Soil-Vehicle Systems, Edizioni Minerva Technica, Torino, Italy, 1961.
38. Freitag, D.R.; Green, A.J.; and Melzer, K.-J.: Performance Evaluation of Wheels for Lunar Vehicles. Technical Report No. M-70-2, U.S. Army Engineer Waterways Experiment Station, Vicksburg, Miss., 1970.
39. Freitag, D.R.; Green, A.J.; and Melzer, K.-J.: Performance Evaluation of Wheels for Lunar Vehicles (Summary Report). Miscellaneous Paper No. M-70-4, U.S. Army Engineer Waterways Experiment Station, Vicksburg, Miss., 1970.
40. Freitag, D.R.; Green, A.J.; Melzer, K.-J.; and Costes, N.C.: Wheels for Lunar Vehicles. Proceedings of the Off-Road Mobility Symposium, International Society for Terrain Vehicle Systems (ISTVS) – TRW Systems, El Segundo, Calif., 1970.
41. Green, A.J.; and Melzer, K.-J.: The Performance of Two Boeing-GM Wheels (GM VII and GM VIII) for the Manned Lunar Rover Vehicle. Miscellaneous Paper No. M-71-3, U.S. Army Engineer Waterways Experiment Station, Vicksburg, Miss., 1971.
42. Green, A.J.; and Melzer, K.-J.: Performance of the Boeing LRV Wheels in a Lunar Soil Simulant; Effect of Wheel Design and Soil. Technical Report No. M-71-10, Report 1, U.S. Army Engineer Waterways Experiment Station, Vicksburg, Miss., 1971.
43. Melzer, K.-J.: Performance of the Boeing LRV Wheels in a Lunar Soil Simulant. Technical Report No. M-71-10, Report 2, U.S. Army Engineer Waterways Experiment Station, Vicksburg, Miss., 1972.
44. Mullis, C.H.: A Study and Analysis of the MSFC Lunar Roving Vehicle Dust Profile Test Program. Final Report, Contract NAS8-26715, University of Alabama, University, Ala., 1971.
45. Johnson, F.S.; Evans, D.E.; and Carroll, J.M.: Cold-Cathode-Gage Experiment (Lunar Atmosphere Detector). Apollo 12 Preliminary Science Report, Sec. 7, NASA SP-235, 1970.
46. Johnson, F.S.; Evans, D.E.; and Carroll, J.M.: Cold-Cathode-Gage Experiment (Lunar Atmosphere Detector). Apollo 14 Preliminary Science Report, Sec. 9, NASA SP-272, 1971.

REFERENCES (Continued)

47. Johnson, F.S.; Evans, D.E.; and Carroll, J.M.: Cold-Cathode-Gage Experiment (Lunar Atmosphere Detector). Apollo 15 Preliminary Science Report, Sec. 13, NASA SP-289, 1972.
48. Freitag, D.R.: A Dimensional Analysis of the Performance of Pneumatic Tires on Soft Soils. Technical Report No. 3-688, U.S. Army Engineer Waterways Experiment Station, Vicksburg, Miss., August 1965.
49. Nuttall, C.J. Jr.: Ground Crawling: 1966 – The State of the Art of Designing Off-Road Vehicles. USAE WES Contract Report No. 3-162, U.S. Army Engineer Waterways Experiment Station, Vicksburg, Miss., 1967.
50. Schuring, D.J.; Southwell, P.H.; and Sidall, J.N.: The Energy Loss of a Wheel. Proceedings of the 2nd International Conference of the International Society for Terrain Vehicle Systems, Quebec City, Quebec, Aug. 29-Sept. 2, 1966, University of Toronto Press, Toronto, Ontario, Canada, 1966, pp. 391-424.
51. Ehrlich, I.R.; Markow, E.G.; and Dowd, R.E.: Mobility of Terrain Vehicle Systems Optimization of Design and Performance. SAE Paper No. SP-261, Society of Automotive Engineers, New York, N.Y., 1965.
52. Bekker, M.G.: Theory of Land Locomotion. Second ed., the University of Michigan Press, Ann Arbor, Mich., 1962.
53. Bekker, M.G.: Off-Road Locomotion: Research and Development in Terramechanics. The University of Michigan Press, Ann Arbor, Mich., 1960.
54. Bekker, M.G.: Off Road Locomotion on the Moon and On Earth. Automobilitismo & Automobilitismo Industriale, January 1966 (also reproduced by Journal of Terramechanics, No. 3, 1966).
55. Wong, R.: Vehicle Design and System Integration, Dual-Mode Manned/Automated Lunar Roving Vehicle Design Definition Study, Vol. II. Contract NAS8-24528, Bendix Systems Div., Bendix Corp., Ann Arbor, Mich., 1970.
56. Pavlics F.: Locomotion Energy Requirements for Lunar Surface Vehicles. SAE Paper No. 660149, Society of Automotive Engineers, New York, N.Y., 1966.
57. Pavlics, F.; and Becker, M.G.: Surveyor Lunar Roving Vehicle. Mobility Analysis, Final Report No. PR 64-26, GM DRL, General Motors Corp., Santa Barbara, Calif., 1964.
58. AS-510 Apollo 15 Mission. Saturn V Launch Vehicle Flight Evaluation Report, MPR-SAT-FE-71-2, Marshall Space Flight Center, NASA, Huntsville, Ala., November 1971.

REFERENCES (Concluded)

59. Houston, W.N.; and Namiq, L.I.: Penetration Resistance of Lunar Soils. *Journal of Terramechanics*, Vol. 8, No. 1, 1971, pp. 59-69.
60. Apollo 15 Mission Report. Report No. MSC-05161, Manned Spacecraft Center, NASA, Houston, Tex., 1971.
61. Rula, A.A.; and Nuttall, C.J. Jr.; An Analysis of Ground Mobility Models – ANAMOB. Technical Report No. M-71-4, U.S. Army Engineer Waterways Experiment Station, Vicksburg, Miss., 1971.